UPC CTTC

Numerical simulation of flames using flamelet models

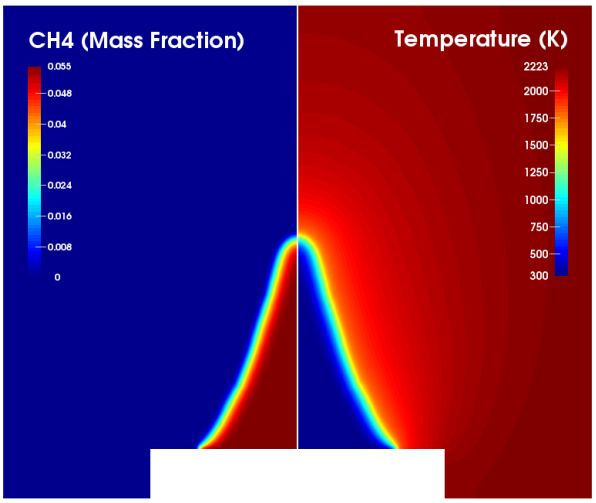

Centre Tecnològic de Transferència de Calor
Departament de Màquines i Motors Tèrmics
Universitat Politècnica de Catalunya

Shamshad Ahmad
Doctoral Thesis

Numerical simulation of flames using flamelet models

Shamshad Ahmad

TESI DOCTORAL

presentada al

Departament de Màquines i Motors T‘ermics
E.T.S.E.I.A.T.
Universitat Politècnica de Catalunya (UPC)

per a l'obtenció del grau de

Doctor per la Universitat Politècnica de Catalunya

Terrassa, April, 2017

Numerical simulation of flames using flamelet models

Shamshad Ahmad

Directors de la Tesi

Dr. Assensi Oliva Llena
Dr. Jordi Ventosa Molina

Tribunal Qualificador

Dr. José Fernández Seara
Universidad de Vigo

Dr. Maria Manuela Prieto González
Universidad de Oviedo

Dr. Joaquim Rigola Serrano
Universidad Politécnica de Catalunya

This thesis is dedicated to my Lovely Pakistan

Hats of to the people, who did not win the Pakistan just behind closed doors and through idle talking. They won through their blood, sweat of their youth, and countless sacrifices. We can never forget you and your purpose to see Pakistan a sacred place of brotherhood nourished by faith, discipline, and unity. InShaa-Allah, we will always be committed with your aims to make Pakistan a place of love, peace and prosperity.

May Pakistan Live Long!

Acknowledgements

First of all, I would like to thank Prof. Assensi Oliva Llena my supervisor and director of the Heat and Mass Transfer Technology Center (CTTC), for giving me the opportunity for doing a Ph.D. in this department. Prof. Assensi has created a good research environment. CTTC is a good place for the international students to carry out their research. I will remember your support and cooperation regarding all kinds of administrative issues as an international student.

Undoubtedly, I want to thank my adviser, Dr. Jordi Ventosa Molina. I was lucky to have a great visionary in all matters of learning. Dr. Jordi is pragmatic, rigorous, honest, and he seems to be able to solve problems with positivity. He was always available and willing to discuss issues and very supportive when things did not go as hoped. He taught me how science works, how to write papers, how to see bad results as opportunities. Dr. Jordi always gave me the freedom to pursue interesting avenues of inquiry but also keeping me on track. I never forget his follow up during my research. His advice during these years has helped me out of seemingly dead ends, and I have certainly learned a lot from our conversations. It has been a pleasure working with Dr. Jordi and I look forward to fruitful collaborations in the near future.

I would thank Prof. Carlos David Pérez-Segarra for his technical support and scientific skills to refine our research work.

I would thank all researchers and the staff in the CTTC. Especially Jordi Chiva who taught me programming language and improves my programming skills. Also, my thanks are due to Dr. F. Xavier Trias Miquel and Jordi Muela. I learned a lot of skills during my training period.

I want to thank Dr. Deniz for his support in administrative matters during academic tenure.

I would also like to express my sincere thanks to my friend Nacho for sharing his time and moral support. I will remember your companionship as a discovery during my stay in Spain.

Here, I would give my gratitude to my dearest friends Ahsan and Javid, whose friendship is my whole life's asset. I do respect of your trust, loyalty, understanding, compassion, acceptance, forgiveness, and appreciation in fact all expression of true friendship. Javid, I can never pay back, the care you gave to my family in my absence. I am fortunate to have friend like you.

I wish to express my heartfelt thanks to the higher management of my institute. Especially, my bosses Mr. Irfan Ali Khan, Mr. Ghulam Ahmad Muslim who gave me an opportunity to continue my higher study abroad. Furthermore, I would thanks to Dr. Farhad Ali for his support and visionary scientific discussions during his services.

Financial assistance of the Higher Education Commission (HEC), the government of Pakistan is gratefully acknowledged.

In the end, my identity, my family: no acknowledgment could express my heartiest gratitude and a deep sense of honor to my loving parents, for their love and support, encouragement and unceasing prayers, without which the present destination would have been just a dream. Thank you both for always believing me.

I would like to thank my two little stars that shine in my heart, my dearest sons, Muhammad Ahmad Mirza and Rafay Ahmad Mirza for the laughter and motivation gifted to me with your cute and tender voice whenever I felt sorrow in this difficult time. Thanks for making me a successful father after bearing the pain of many days, nights, and weekends apart from me.

Words are lacking to express a word of thanks to my wife Fatima, who taught me the true values and identity of the strong relationships in this painful distance. Thank you, I will never forget your contribution. I feel pleasure in transcribing my hearted thanks to my mother-in-law and father-in-law for taking care of my children in this period.

Thanks to my brothers, sisters, and sister-in-law to keep praying for my success. I especially want to pay honor to my dear brother Fayyaz Ahmad. You are a big educational motivation and inspiration of our family, and I always followed your footsteps. Thanks to my sisters, your existence gave me positivity, humbleness, and strength of self-correction. I am incomplete without the love and warmth of you all. I would like to express very special thanks to my sister Samina and Brother-in-law M. Asif to visit me and share my loneliness and to keeping me smiling.

I owe so much to my whole family for their undying support, their unwavering belief that I can achieve so much. Their prayers, affection, and cooperation can never be paid back. May Allah bless all the above people with a long happy life! (Ameen)

Shamshad Ahmad

Abstract

The thesis topic is located in the domain of numerical simulation of laminar flames. The principal aim of the presented research is the study of numerical techniques for the multidimensional simulation of flames with low computational costs. Present work is divided into three parts: First part is related to the development of a C++ simulation code for 1D laminar premixed flames. In the second part, a new technique to account for differential diffusion effects is proposed, which is based on tabulated chemistry methods. The third part focuses on the analysis of partially premixed flames.

A dedicated one-dimensional flame code is discussed for the simulation of complex/detailed chemistry and diffusion processes in premixed laminar flames. This code is written in C++ and is able to use different diffusion models (Fickian, Hirschfelder and Curtiss). The code yields accurate solutions of the major parameters as well as pollutant formation, both in the flame zone as well as downstream in the post-flame region. Results prove the accuracy of the code when compared to experimental data.

Following, a new technique is proposed to include differential diffusion effects into flamelet models. This approach is developed in the context of tabulated chemistry methods.The technique is based on correcting the progress-variable of flamelet models. The main feature of the proposed technique is the use of only one progress variable equation (1D manifold) without requiring a second parameter. This correction technique allows including detailed chemistry effects at low-cost in numerical simulation of multidimensional flames. A series of simulations are carried out for various flames. The results are excellently matched with full model solutions/detailed chemistry solutions.

The flamelet solutions databases, namely premixed and non-premixed, are further tested for partially premixed flames. This study is based on the investigation of partially premixed flame using single mode flamelet database solutions. For the verification of database solutions, finite rate chemistry simulations are also carried out to solve partially premixed flames. 3D jet coflow simulations are performed for three different level of premixing and results are compared with experimental data. The results show good agreement along with capabilities and limitations of flamelet databases solutions.

Contents

1

Introduction

1.1 Motivation to study combustion

Combustion is one of the oldest branches of science. Indeed, from the very beginning of human kind. From its early use, combustion was used as source of light and heat. With the passage of time its applications evolved according to human necessities. Nowadays, it is an emerging science due to the continuous increase of energy demands in this high-tech world. How important combustion in this scenario is, may be realized from the fact that 80 % of energy comes from combustion. If we further classify the sources of combustion, then 80 % of world energy infrastructure produces the energy by combustion of liquids, solids, and gaseous fossils. Other energy sources belong to nuclear energy or renewable energies, which still account for less than 20 % of the total energy consumption [15]. If we suppress the role of combustion, the whole society would probably clap tomorrow. In this perspective, combustion and its control are essential to our existence on this planet. In fact, combustion has provided substantial support for the world energy system. Still, there is plenty of room for research and development in this field as the technology demands evolve and change with the passage of time.

In spite of the considerable advantages that combustion has given to our quality of life, it also has a dark face. There are a lot of challenges associated with conservation of energy; the problem of global climate change and environmental concerns. The issue related to combustion is environmental pollution. The major pollutants produced by combustion are unburned and partially burned hydrocarbons, nitrogen oxides (NO and NO_2), carbon monoxide, sulfur oxides and particulate matter in various forms. Primary pollution concerns relate to specific health hazards, smogs, acid rain, global warming. Considering the importance of combustion in our society, we should be able to use it without increasing emissions and without wasting fossil fuel.

Having briefly reviewed the advantages and disadvantages of combustion, in the following, we have a look on the scientific background of combustion. The first steps were taken in the experiments by Le Chatelier dating from 1883. In the late nine-

teenth and early twentieth century, the theoretical study of combustion science was introduced (Arrhenius 1883, Burke-Schumann 1928). Arrhenius proposed his empirical formulas for the temperature dependence of chemical reactions velocities. Burke-Schumann presented their theoretical studies about the height and shape of the diffusion flames. Nowadays, the theoretical study of combustion science is well founded, at least for laminar gas-phase combustion process [9, 16, 17].

Regarding the side effect of combustion, deep scientific studies are very important to control combustion. Nowadays much attention is being paid to efficiency, process control, and pollution. This is investigated by scientists of all kinds of background: chemists, mathematicians, physicists, and engineers. Much of the scientific research in the field of combustion concerns the study of the detailed structure of the combustion. It is believed that global aspects like efficiency, control, and pollution can be estimated when the combustion process is understood on a molecular scale.

From a chemical point of view, combustion is associated with fast chemical reactions that proceed with a large conversion of chemical energy to sensible heat. This process consists of thousands of elementary consecutive, competitive, and opposing steps, the so-called chain-reactions. Chemical kinetics describes these reactive systems. Thus, this theory has a fundamental importance in combustion science. In sequences of chemical reactions, heat is released and the temperature raised. This temperature increase is transferred to the surroundings by conduction, convection, and radiation.

For example, this complex physical and chemical process are best understood by analyzing in a burning candle. Heat transfer from the flame, by conduction and radiation, forms a pool of the melted wax at the top of the candle. The melting front moves steadily down the candle as the flame consumes the wax. The melted wax ascends through the wick by capillary action and vaporizes from the heat of the flame, which is transferred primarily by conduction. Then, a complex system of reactions takes place, producing the hot gasses together with the surrounding air that raises over the flame. The origin of the color of the dark-blue region at the base shows the presence of the immediate product species from the excited CH radicals in the reaction zone [18, 19]. In certain flames, like in candle's flame, there is also an important emission of yellow light. This light is emitted by soot, which are particles of slightly hydro-generated carbon [20].

Flames can be classified into two major categories: premixed and diffusion flame. Additionally, due to the nature of fluid flow, flames have two flow regimes namely, laminar and turbulent. The candle flame is also a good example to explain these classifications. In the candle flame, it can be distinguished two main regions, an inner one containing a deficit of gases and an outer containing oxidizer gases. The chemical reactions take place between both regions that are separated by a thin zone. It means that chemical reaction appear as soon as fuel and oxidizer get in contact. In other

words, the combustion is controlled by the rate of mixing. This flame structure is defined as diffusion (or non-premixed) flames. For example, diesel engines or rocket engines are typical cases of non-premixed combustion. On the other hand, when fuel and oxidizer are mixed before reacting, it is known as premixed flames e.g. spark-ignited gasoline engines or domestic kitchen burners, etc.

The second classification is based on the flow structure of the flames. It is differentiated between laminar and turbulent flames, which is mainly controlled by input fuel and oxidizer flow rates. Both types of flames are commonly used in industrial applications.

1.2 Outline of the thesis

The thesis has been organized in four chapters. In the introduction, the mathematical formulation and models are adopted for the numerical study of laminar premixed flames. In this chapter, the main parameters to describe combustion are introduced. Reported models and theory is based on low-mach flow laminar cases.

Next, chapter two is focused on the development of a 1D numerical simulation code. All the development procedure is described in detail, step by step. The validation and verification of a C++ code are also reported in the same chapter.

The third chapter is about a new proposed correction technique. This chapter contains all the mathematical basis and explanation about the proposed technique. This work is reported in the context of low-cost computational solutions of multidimensional flame. For further verification of the correction technique, a multidimensional flame solutions are presented at the end of the chapter.

The final chapter is concerned with partially premixed flames. A 3D coflow partially premixed flame has studied using two flamelet databases. To check the capabilities of both premixed and non-premixed databases various ranges of premixing are studied. Finally, concluding remarks on results and limitation of databases are detailed.

1.3 Reactive flows

Reactive flow can be described through a set of balance equations of continuum mechanics such as mass, momentum, energy and species. All these equations are associated with various controlling or primitive parameters e.g. the mass density ρ, the velocity components u_i, temperature T and species mass fraction Y_k, etc. To begin with, all key terms to describe a combustion process are presented in this chapter.

Combustion is an exothermic process. Thus, it is necessary to define all thermodynamical and related quantities.

1.3.1 Mixture composition description

First of all, species are characterized through their mass fractions Y_k for $k = 1, 2, ..., N_s$, where N_s denote the number of species involved in the combustion process. Mass and molar fractions are defined as

$$Y_k = \frac{m_k}{m} \quad , \quad X_k = \frac{n_k}{n} \tag{1.1}$$

where m_k and n_k are molar mass and number of moles of the k^{th} species in a given volume V. The total mass and number of moles of gas in the volume are m and n, respectively. The mass density and molar weight of fluid contained in a homogeneous control volume are given by

$$\rho = \frac{m}{V} \quad , \quad W = \frac{m}{n}. \tag{1.2}$$

By definition, the summation over the total number of species N_s of molar and mass fractions must be equal to unity

$$\sum_{k=1}^{k} X_k = 1 \quad , \quad \sum_{k=1}^{k} Y_k = 1. \tag{1.3}$$

Lastly, both mass and molar fractions are related through

$$\text{mass fraction :} \qquad Y_k = \frac{W_k}{W} X_k \tag{1.4}$$

$$\text{mixture molar weight :} \qquad W = \sum_{k=1}^{N_s} X_k W_k \quad or \quad \frac{1}{W} = \sum_{k=1}^{N_s} \frac{Y_k}{W_k} \tag{1.5}$$

$$\text{mole concentration :} \qquad [X_k] = \rho \frac{W}{W_k} Y_k. \tag{1.6}$$

where W_k is the molar mass of species.

1.3.2 Thermo-chemistry

To thermally characterize the flow, the equation of state and the enthalpy are used

Equation of state

For an ideal gas, the equation of the state is

$$P_0 = \rho r T \quad \text{with} \quad r = \frac{R}{W} = \rho T R \sum_{k=1}^{N_s} \frac{Y_k}{W_k}. \tag{1.7}$$

where R=8.314 $[J.K^{-1}.mol^{-1}]$ is ideal the gas constant.

Species enthalpy

For reacting flows, there are multiple possibilities to represent the enthalpy, h_k. The enthalpy of species is defined with respect to a reference temperature T_0

$$h_k = h_{s,k} + \triangle h^0_{f,k} \tag{1.8}$$

where $\triangle h^0_{f,k}$ is the species standard enthalpy of formation at any reference temperature T_0 and $h_{s,k}$ the sensible enthalpy. T_0 may be taken as 0 K, as done by Reynolds and Perkins [1]. However, formation enthalpies at 0 K are difficult to obtain. Commonly, $T_0 = 298.15K$ is used. The specific heat capacity at constant pressure $c_{p,k} = \left(\frac{\partial h_k}{\partial T}\right)_p$ is introduced to compute $h_{s,k}$

$$h_{s,k} = \int_{T_0}^{T} c_{pk}(T)dT. \tag{1.9}$$

Therefore, sensible enthalpy $h_{s,k}$ is zero at $T = T_0$ for all substances. Furthermore, $c_{p,k}$ is related to the ideal gas constant through Mayer's relation

$$c_{p,k} = c_{v,k} + \frac{R}{W_k}. \tag{1.10}$$

where $c_{v,k} = \left(\frac{\partial e_k}{\partial T}\right)_v$ is specific heat capacity at constant volume. The enthalpy of the mixture of N_s species can be described as

$$h = \sum_{k=1}^{N_s} h_k Y_k. \tag{1.11}$$

Introducing Eq. (1.8) into the last equation, it can be rewritten as

$$\begin{aligned} h &= \sum_{k=1}^{N_s} \left(h_{s,k} + \triangle h^0_{f,k}\right) = \sum_{k=1}^{N_s} \left(\int_{T_0}^{T} c_{p,k}(T)dT + \triangle h^0_{f,k}\right) \\ &= \int_{T_0}^{T} c_p(T)dT + \sum_{k=1}^{N_s} \triangle h^0_{f,k}. \end{aligned} \tag{1.12}$$

The specific heat capacity at constant pressure c_p of mixture is composed of N_s species is

$$c_p = \sum_{k=1}^{N_s} c_{p,k} Y_k. \tag{1.13}$$

1.3.3 Chemical Kinetics

Chemical kinetics is the study of chemical reactions. All chemical reactions, take place at a definite rate and depend on the defined conditions of the system. Chemical reactions appear as a rearrangement of atoms that are balanced in equations. A rate of reaction may be expressed as the rate of decrease or increase of the concentration of a reactants or product.

In general, any chemical reaction can be expressed as

$$\begin{gathered}\nu_1^{'}\mathcal{M}_1 + \nu_2^{'}\mathcal{M}_2 + ... + \nu_{N_s}^{'}\mathcal{M}_{N_s} \rightleftarrows \nu_1^{''}\mathcal{M}_1 + \nu_2^{''}\mathcal{M}_2 + ... + \nu_{N_s}^{''}\mathcal{M}_{N_s} \\ or \\ \sum_{k=1}^{N_s}\nu_k^{'}\mathcal{M}_k \rightleftarrows \sum_{k=1}^{N_s}\nu_k^{''}\mathcal{M}_k\end{gathered} \tag{1.14}$$

where N_s is number of species and $\nu^{'}$ and $\nu^{''}$ are stoichiometric coefficients of reactants and products respectively. $\mathcal{M}$ is representation of species involved in chemical reaction. A complete chemical mechanism may be composed of one to hundreds of thousands of elementary chemical reactions. Furthermore, the same species may appear with different stoichiometric coefficients in different reactions. So that, a more compact and more general notations for Eq. (1.14) can be used

$$\sum_{k=1}^{N_s}\nu_{kj}^{'}\mathcal{M}_k \rightleftarrows \sum_{k=1}^{N_s}\nu_{kj}^{''}\mathcal{M}_k \quad ; \quad j = 1, 2, ..., M. \tag{1.15}$$

where j denotes the reaction being considered and M is number of reactions involved in chemical process. In any chemical process, mass conservation must be satisfied i.e.

$$\sum_{k=1}^{N_s}\nu_{kj}^{'}W_k = \sum_{k=1}^{N_s}\nu_{kj}^{''}W_k \quad or \quad \sum_{k=1}^{N_s}\nu_{kj}W_k = 0 \quad ; \quad j = 1, 2, ..., M \tag{1.16}$$

where $\nu_{kj} = \nu_{kj}^{'} - \nu_{kj}^{''}$.

The rates of progress for each equation involved in the system are given by the relation

$$\omega_{kj} = W_k\nu_{kj}\mathfrak{R}_j.$$

where $\mathfrak{R}_j$ is the rate of progress of k^{th} species in j^{th} reaction. It is proportional to the product of concentrations of the reacting species

$$\mathfrak{R}_j = K_{fj}\prod_{k=1}^{N_s}[X_k]^{\nu_{kj}^{'}} - K_{rj}\prod_{k=1}^{N_s}[X_k]^{\nu_{kj}^{''}}. \tag{1.17}$$

where K_j is a constant of proportionality, which is called specific reaction rate coefficient. Sub-indexes 'f' and 'r' denote forward and backward reactions,respectively. Finally, the reaction rate $\dot{\omega}_k$ of k^{th} species is evaluated as

$$\dot{\omega}_k = \sum_{j=1}^{M} \omega_{kj} = W_k \sum_{j=1}^{M} \nu_{kj} \mathfrak{R}_j. \tag{1.18}$$

Additionally, the sum of all chemical reaction rates of all species must satisfy mass conservation

$$\sum_{k=1}^{N_s} \dot{\omega}_k = 0. \tag{1.19}$$

There remains to evaluate the specific coefficients K_{fj} and K_{rj} in Eq. (1.17), which stand for forward and backward reactions constants. These coefficients are key in combustion modeling to calculate the rate of progress. In 1883, Arrhenius [2] established the theory, where only molecules that possess an energy greater than a certain threshold energy will react, namely an activation energy E. Molecules acquire the additional energy necessary from collisions induced by the thermal condition that exists in a mixture. These high-energy activated molecules lead to products. The theory of Arrhenius provides the temperature dependency of K_j's. Arrhenius principle can be expressed as

$$K_j = Z_{AB,j} \exp\left(\frac{-E_{aj}}{RT}\right) \quad or \quad K_j = Z_{AB,j} \exp\left(\frac{-T_{aj}}{T}\right). \tag{1.20}$$

where Z_{AB} is gas kinetic collision frequency in a reaction of species A and B. The term 'exp $\left(\frac{-E_{aj}}{RT}\right)$' is the Boltzmann factor, which represents the collision energy of molecules which are greater than the activation energy E_{aj}. The gas kinetic collision frequency may feature a temperature dependency [3].

$$Z_{AB,j} = A_j T^{\beta j} \tag{1.21}$$

For the calculation of the progress rate for each species, the pre-exponential constant A_j, the temperature exponent βj and activation energy E_{aj} are required. These values are provided by chemical mechanisms. With the mathematical description of the chemical reaction, a new question is posed: which species and reactions are important? Which ones have to be the part of the chemical scheme or mechanism for reacting flow applications? In fact, the answer is challenging. Therefore, a lot of work has been done on creating chemical mechanisms. In reacting flow problems, the solution always depends on the provided data of the chemical mechanisms. In the literature, different kinds of detailed and reduced chemical mechanisms can be found. For example, the GRI3.0 [4], Mueller [5] and Smooke [6] are very common and will be used throughout this thesis.

1.4 Combustion modelling

In this section, the set of transport equations to describe a chemically reacting flow are presented. The well-known Navier-Stokes equations are used to describe the combustion process. Due to the significant density changes, incompressible formulations are unsuitable to describe the flow behavior. In the current study flow velocities are much smaller than the speed of sound. Thus, a low Mach formulation is considered. As in the case of non-reacting flows, five unknowns are needed to solve the concerned system (density, pressure and velocity) and additionally the temperature. Furthermore, for reacting cases, the system have N_s more unknowns because the fluid composition must be tracked. Consequently, more modeling and computational efforts are required to solve such kind of systems.

1.4.1 Mass balance

Like in non-reacting flows, mass is not created nor destroyed. Thus the mass conservation equation is

$$\frac{\partial \rho}{\partial t} + \frac{\partial}{\partial x_j}(\rho u_j) = 0 \tag{1.22}$$

where t represents time, ρ the fluid density and u the fluid velocity.

1.4.2 Momentum balance

Taking the momentum equation of the Navier-Stokes equations in their compressible form, and following Lessani and Papalexandris [7] the low Mach momentum equations are

$$\frac{\partial \rho u_j}{\partial t} + \frac{\partial}{\partial x_j}(\rho u_i u_j) = \frac{\partial \sigma_{i,j}}{\partial x_j} + \rho \sum_{k=1}^{N_s} Y_k f_{k,j} \tag{1.23}$$

where viscous and pressure tensors are combined into the $\sigma_{i,j}$ tensor and $f_{k,j}$ the volume force acting on species k. The former is composed of a pressure isotropic part and viscous part, which can be further expanded as

$$\sigma_{i,j} = -P\delta_{i,j} + \tau_{i,j} = -P\delta_{i,j} + \mu\Big(\frac{\partial u_i}{\partial x_j} + \frac{\partial u_j}{\partial x_i} - \frac{2}{3}\frac{\partial u_k}{\partial x_k}\delta_{i,j}\Big) \tag{1.24}$$

where $\delta_{i,j}$ is the Kronecker delta. Dynamic viscosity μ and fluid density ρ are changed due to the strong variations in temperature through the flame front. Consequently, the local Reynolds number varies significantly.

1.4.3 Energy balance

Energy conservation can be expressed in multiple forms, i.e. expressed as a function of enthalpy or temperature. In the present study, a temperature equation is

added into the set of equations to be solved.

$$\rho c_p \frac{DT}{Dt} = \dot{\omega}'_T + \frac{Dp}{Dt} + \frac{\partial}{\partial x_i}\Big(\lambda \frac{\partial T}{\partial x_i}\Big) - \underbrace{\Big(\rho \sum_{k=1}^{N_s} c_{p,k} Y_k V_{k,i}\Big)\frac{\partial T}{\partial x_i}}_{\text{part of diffusion term}} + \underbrace{\tau_{i,j}\frac{\partial u_i}{\partial x_j}}_{\text{viscous heating}} + \dot{Q} + \underbrace{\rho \sum_{k=1}^{N_s} Y_k f_{k,i} V_{k,i}}_{\text{volume force}} \tag{1.25}$$

where $\dot{\omega}'_T = -\sum_{k=1}^{N_s} h_k \dot{\omega}_k$ is the heat release, $\dot{Q}$ is a heat source term (due to electric, radiative, laser spark, etc.).

1.4.4 Species balance

The transport equation for the k^{kh} species is

$$\frac{\partial \rho Y_k}{\partial t} + \frac{\partial}{\partial x_j}(\rho u_j Y_k) = -\frac{\partial}{\partial x_j}(\rho V_{k,j} Y_k) + \dot{\omega}_k \quad ; \quad k = 1, 2, ..., N_s \tag{1.26}$$

where $V_{k,j}$ is the diffusion velocity of the k^{th} species in j^{th} direction, $\dot{\omega}_k$ is the chemical reaction rate of k^{th} species. Since the summation of Eq. (1.26) for the N_s species must yield the continuity equation, the following identities must be satisfied to ensure mass conservation [8]

$$\sum_{k=1}^{N_s} V_{k,j} Y_k = 0 \quad \text{and} \quad \sum_{k=1}^{N_s} \dot{\omega}_k = 0. \tag{1.27}$$

According to Williams [9], the diffusion velocity V_k can be obtained by solving the Maxwell's equations without considering body forces and Soret effect.

$$\nabla X_p = \sum_{k=1}^{N_s} \frac{X_p X_k}{D_{p,k}}(V_k - V_p) + (Y_p - X_p)\frac{\nabla P}{P} \quad ; \quad p = 1, 2, ..., N_s \tag{1.28}$$

where $D_{p,k}$ is the diffusion coefficient of species p toward species k. Solution of this equation is complex and a highly expensive task. Hirschfelder and Curtiss [10] proposed a model for the diffusion velocities, which is the best first-order approximation to the exact solution of the system of Eqs. (1.28) [11, 12].

$$V_k X_k = -D_k \nabla X_k \quad \text{with} \quad D_k = \frac{1 - Y_k}{\sum_{p \neq k} \frac{X_j}{D_{p,k}}} \tag{1.29}$$

where D_k is called the equivalent species diffusion coefficient into the mixture. However, this approximation does not satisfy mass conservation, as expressed by the left expression in Eq. (1.27).

$$\sum_{k=1}^{N_s} V_k Y_k = -\sum_{k=1}^{N_s} D_k \frac{W_k}{W} \frac{\partial X_k}{\partial x_j} = -\sum_{k=1}^{N_s} \frac{D_k}{W} \frac{\partial}{\partial x_j}(W Y_k) \neq 0 \tag{1.30}$$

Thus, it is important to add a correction to ensure the conservation. The approach reported by Coffee and Heimerl [13] is here adopted to enforce mass conservation, where a correction diffusion velocity V_j^c is introduced and computed as

$$V_j^c = \sum_{k=1}^{N_s} \frac{D_k}{W} \frac{\partial}{\partial x_j}(W Y_k) \tag{1.31}$$

and leading to

$$V_{k,j} Y_k = -D_k \frac{W_k}{W} \frac{\partial X_k}{\partial x_j} + V_j^c Y_k. \tag{1.32}$$

Using Eq. (1.32), Eq. (1.26) is rewritten as

$$\frac{\partial \rho Y_k}{\partial t} + \frac{\partial}{\partial x_j}(\rho(u_j + V_j^c) Y_k) = \frac{\partial}{\partial x_j}\Big(\frac{\rho D_k}{W} \frac{\partial (W Y_k)}{\partial x_j}\Big) + \dot{\omega}_k \quad ; \quad k = 1, 2, ..., N_s. \tag{1.33}$$

The latter equation is sometimes simplified by assuming $D_k = D$ and neglecting molar mass gradients thus, becoming

$$\frac{\partial \rho Y_k}{\partial t} + \frac{\partial}{\partial x_j}(\rho u_j Y_k) = \frac{\partial}{\partial x_j}\Big(\rho D \frac{\partial Y_k}{\partial x_j}\Big) + \dot{\omega}_k \tag{1.34}$$

which is usually referred as Fick's approximation [14].

It should be borne in mind that in the mass transport equation, the Soret effect has been neglected. The Soret effect is the diffusion of mass due to temperature gradients. This term has been found to be significant for the mixture of liquids [8]. Hence, in the present study it is neglected.

1.4.5 Non-dimensional number

One of the most common dimensionless number used throughout the thesis is the Lewis number. The D_k diffusion coefficients of species are often characterized in terms of Lewis number defined by

$$Le_k = \frac{\frac{\lambda}{\rho c_p}}{D_k} = \frac{\text{Heat Diffusion}}{\text{Species Diffusion}}$$

Lewis numbers of individual species are usually vary by small amounts in flame fronts. Therefore, by fixing a constant Lewis number for each species (and setting a suitable expression for the thermal conductivity) may be adequate for simplified analysis.

References

[1] W. C. Reynolds and H. C. Perkins. *Engineering thermodynamics*. McGraw-Hill, 1977.

[2] S. Arrhenius. On the rate of reaction of the inversion of sucrose by acids. *Journal of Physical Chemistry*, 4:226–48, 1883.

[3] I. Glassman and R. A Yetter. *Combustion*. Elsevier, 2008.

[4] C. T. Bowman, M. Frenklach, G. Smith, W. C. Gardiner, and et al. http://www.me.berkeley.edu/gri-mech/releases.html.

[5] M. A. Mueller, T. J. Kim, R. A. Yetter, and F. L. Dryer. Flow reactor studies and kinetic modeling of the H2/O2 reactions. *International Journal of Chemical Kinetics*, 31:113–125, 1999.

[6] M. D. Smooke, I. K. Puri, and K. Seshadri. A comparison between numerical calculations and experimental measurements of the structure of a counter-flow diffusion flame burning diluted methane in diluted air. *Proceedings of the Combustion Institute*, 21(1):1783–1792, 1988.

[7] B. Lessani and M. V. Papalexandris. Time-accurate calculation of variable density flows with strong temperature gradients and combustion. *Journal of Computational Physics*, 212:218–46, 2006.

[8] T. Poinsot and D. Veynante. *Theoretical and Numerical Combustion*. R.T. Edwards Inc., 2005.

[9] F. A. Williams. *Combustion Theory*. Addison-Wesley Publishing Company, Redwood City, 1985.

[10] J. O. Hirschfelder, C. F. Curtiss, and et al. *Proceedings of the Combustion Institute*, 19:190, 1953.

[11] A. Ern and V. Giovangigli. *Multicomponent Transport Algorithms*. Springer Verlag, Heidelberg, 1994.

[12] V. Giovangigli. *Multicomponent Flow Modeling*. Birkhauser, Boston, 1999.

[13] T. P. Coffee and J. M. Heimerl. Transport algorithms for premixed laminar steady-state flames. *Combustion and Flame*, 43:273–89, 1981.

[14] K. K. Kuo. *Principles of Combustion*. John Wiley, New York, 1986.

[15] N. Peters. *Turbulent Combustion*. Cambridge University Press, 2000.

[16] J. O. Hirschfelder and et al. *Molecular theory of gases and liquids*. John Wiley and Sons, 1954.

[17] S. Chapman and T. G. Cowling. *The Mathematical Theory of Non-Uniform Gases*. Chambridge University Press, London, New York, 1970.

[18] A. G Gaydon and H. G. Wolfhard. *Flames, Their Structure, Radiation and Temperature*. 4th ed. Chapman and Halls, London, 1979.

[19] J. Jarosinski and B. Veyssiere. *Combustion Phenomena,Selected Mechanisms of Flame Formation,Propagation, and Extinction*. CRC Press, Taylor and Francis Group, London, New York, 2013.

[20] G. L. Borman and K. W Ragland. *Combustion Engineering*. McGraw-Hill, 1998.

2

Laminar premixed flame, combustion modeling and numerical simulations

Abstract. In the present chapter, a fundamental background of laminar premixed flames is given and an appropriate flamelet model is described to model these flames. The development of a C++ code for numerical simulation of 1-D laminar premixed flame is detailed. The transport equation of mass, energy and species for reacting flows using non-uniform meshes are presented. A finite difference scheme is employed to discretise the flamelet equations. A special Gaussian function is explored for efficient mesh generation to capture the steep variation of temperature and species mass fractions. Because the resulting system of equations is stiff, specific numerical methods are used. The damped Newton method is implemented to solve the system of highly non-linear and stiff equations. Due to the large variation in magnitude of the solutions temperature and species mass fraction, equations are changed into reduced forms, in order to avoid scaling and numerical issues. The code takes into account multiple solver parameters, to control and ensure the convergence of the solution. Numerical simulation of 1D premixed flames is carried out successfully for methane/air, hydrogen/air and blended mixtures. Very good agreement is found between experimental and other numerical simulation codes. The results demonstrate that the proposed methodology is a robust and accurate tool for the numerical simulation of premixed flames.

2.1 Introduction

The investigation of laminar flames is a fundamental problem and of major interest in combustion science. It allows for detailed comparisons between theory, experiments, and numerical modelling. Many practical combustors, such as internal combustion engines rely on premixed flame propagation. Through detailed study of these flames, fundamental insight can be gained of the combustion process. Fig. 2.1 illustrates a typical premixed flat flame structure. In 1883, Mallard et al. [1] defined the temperature distribution into two zones. The first zone is known as the preheating zone, or pre-flame zone, where the unburned gas is heated up to ignition. The Second zone is the reaction zone, where combustion takes place. In this region, heat release as well as composition changes occur very quickly. This process does not stop until combustion reaches equilibrium. At this stage the system achieves the adiabatic temperature and henceforth remains constant.

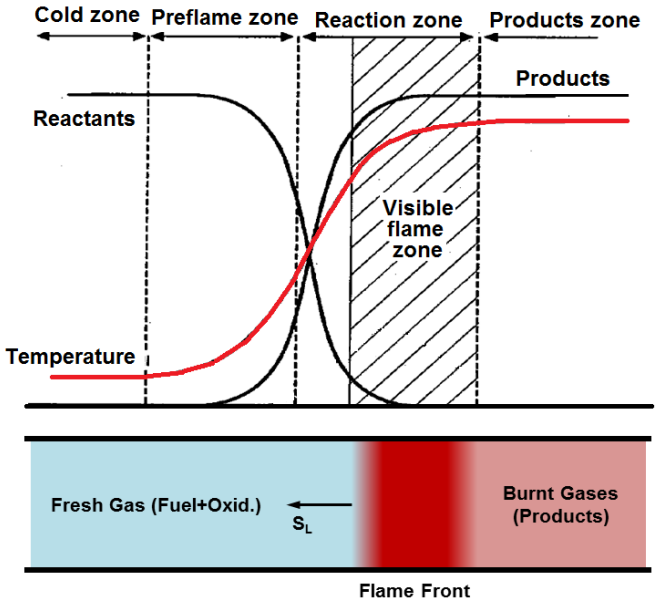

Figure 2.1: Schematic diagram of one-dimensional premixed flame.

Numerical modelling is becoming an important, powerful and effective tool for the design and analysis combustion systems. The modelling and analysis tools enhance the design and analysis capabilities to integrate and upgrade these systems. The numerical models can be used to characterize a combustion process, not only in terms

of temperature and flow field, also in terms of formation of pollutant species, such as nitrogen oxides (NOx), polycyclic aromatic hydrocarbons (PAHs), soot, etc.. These emission of pollutants are required to help in the design of gas turbines, industrial furnaces, internal combustion engines, industrial and domestic burners, etc.

The elementary case of a 1-D laminar propagating flame into a premixed gas is a basic problem in combustion, both from a theoretical and a numerical point of view. Numerical solution of laminar premixed flames is of interest because it is one of the few configuration where a detailed comparison between experiments, theory, and computation can be performed. It may be used to validate chemical models as well. Laminar flames are viewed in many turbulent combustion models as the elementary building blocks of turbulent flames. It is the first step toward more complex configurations to establish the tools for design and analysis.

One of the fundamental parameters for the analysis of premixed combustion is the laminar burning velocity, S_L [2]. It is a key parameter in characterizing a combustible mixture. It can be regarded as the rate with which the combustible mixture is being consumed by a propagating laminar flame. Besides, the S_L is used for the study of the structure and stability of premixed flames, validation of reaction mechanism, and the analysis of turbulent premixed combustion. Then, considering a 1D domain, if the inlet velocity equals the laminar burning velocity of flame, the system achieves a steady state. It can readily be seen that the laminar burning velocity is an eigenvalue of the system. Thus, the problem is an eigenvalue problem.

There are many ways to solve for the laminar flame speed and flame structure. However, it depends on the complexity of the chemistry model and transport description. Typically, chemical schemes involve from a few to hundreds of species with one to thousands of reactions. Due to the complexity of this calculation, which involves fluid dynamics, heat transfer and chemical reactions there is not an analytical solution.

The earliest efforts to develop numerical tools for premixed combustion problems was the shooting technique introduced by Hirschfelder [3]. However, this technique was limited by the choice of chemical kinetics. Spalding [4] introduced the use of implicit finite difference technique to obtain steady state solution of flames as the asymptotic limit of a transient problem. Early works in premixed flame modelling are summarized in the proceedings of a workshop by Peters and Warnatz [5]. Other examples are the works of Wilde [6] and Kendall and Kelly [7] where they adopted the steady state idea to approach the solution of premixed flame by finite difference methods.

Nowadays, in the combustion field, a few codes can be found, e.g. PREMIX [8], FlameMaster [9] and OpenSmoke [10], etc. that solve the basic characteristics of 1-D flame. In this present work, a C++ code for numerical simulation of 1-D premixed laminar flames is developed in order to gain deep insight in the target phenomenon.

It is fully capable of predicting all basic flame characteristics such as temperature and species mass fraction profiles as well as flame burning velocity and flame thickness. The transport equation of mass, energy and species for reacting flows are solved on non-uniform meshes. Second order finite difference schemes are used to discretise the flamelet equations. The equations involved in combustion systems are usually highly stiff and coupled through a highly non-linear reaction rate term. A damped Newton method is used to solve such kind of non-linear systems. To capture the steep variation of species mass fractions as well as temperature, a concentrated mesh is generated through Gaussian function. In this chapter, freely propagating adiabatic flames with no heat losses are considered. Laminar premixed flames are solved using different chemistry kinetic mechanisms. Finally, the validation and verification of the C++ code is presented.

To this end, the current chapter is divided as follows. Next section presents the conservation equations and associated boundary conditions. The third section describes in complete detail the numerical method. Furthermore, the scaling and change of variable of the flamelet equations, the discretization technique, transformation and mesh generation are also addressed in the same section. Fourth section is focused on the results and discussions. The last section is related with conclusions.

2.2 Governing equations

A one-dimensional laminar adiabatic flame is considered. It is assumed that the flame is propagating into a premixed mixture of fuel and oxidizer. Recalling the non-steady state conservation equations, Eq. (1.22), Eq. (1.25) and Eq. (1.26) and rewriting them in 1D (x-component).

- Mass Conservation
$$\frac{\partial \rho}{\partial t} + \frac{\partial \rho u}{\partial x} = 0 \tag{2.1a}$$
- Species Conservation
$$\frac{\partial \rho Y_k}{\partial t} + \frac{\partial (\rho(u+V_k)Y_k)}{\partial x} = \dot{\omega}_k \tag{2.1b}$$
- Energy Conservation
$$\rho c_p\big(\frac{\partial T}{\partial t} + u\frac{\partial T}{\partial x}\big) = \dot{\omega}'_T + \frac{\partial}{\partial x}\big(\lambda \frac{\partial T}{\partial x}\big) - \rho\big(\sum_{k=1}^{N_s} c_{p,k} Y_k V_k\big)\frac{\partial T}{\partial x} \tag{2.1c}$$

where $\dot{\omega}'_T = -\sum_{k=1}^{M} h_k \dot{\omega}_k$ is the heat release. $h_k, \dot{\omega}_k, V_k, Y_k$ denote species enthalpy, chemical reaction rate, diffusion velocity and mass fraction, respectively. Furthermore, T and u represent temperature, velocity and ρ, λ, c_p denote the density, thermal conductivity, and specific heat respectively. Regarding the momentum equation, it can be shown [11] that for 1D case it collapses to

- Momentum Equation
$$\frac{\partial p}{\partial x} = -\rho u \frac{\partial u}{\partial x} = -\rho_u S_L \frac{\partial u}{\partial x}$$

The momentum equation may be solved neglecting viscous stresses to obtain the dynamic pressure jump $p(x)$ across the flame front. If the changes in the molecular mass are neglected, then $\frac{\rho_u}{\rho} = \frac{T}{T_u}$. One may estimate the pressure difference across a propagating laminar premixed flame $p_b - p_u \approx \rho_u S_L^2(1 - \frac{T_b}{T_u})$, where subscript b and u stand for burnt and unburnt respectively. It is remarkable here, that the momentum equation is not needed any more. Due to small flame speed, there is small pressure jump that can be calculated through the above defined expression.

Eqs. (2.1) describe a wave propagation from the burnt to fresh (unburnt) gases. When the flame is settled, it propagates into the quiescent unburnt gases at a constant speed S_L. Hence, it is more advantageous to consider the conservation equation written in an inertial frame of reference attached to the flame front. Thus, Eqs. (2.1) may be rewritten in the flame frame of reference and expressed in its steady state form

$$\dot{m} = const = \rho_u S_L \tag{2.2a}$$

$$\dot{m}\frac{\partial Y_k}{\partial x} + \frac{\partial(\rho V_k Y_k)}{\partial x} = \dot{\omega}_k \tag{2.2b}$$

$$\dot{m}\frac{\partial T}{\partial x} = \frac{\dot{\omega}'_T}{c_p} + \frac{1}{c_p}\frac{\partial}{\partial x}\left(\lambda\frac{\partial T}{\partial x}\right) - \frac{\rho}{c_p}\left(\sum_{k=1}^{N_s} c_{p,k} Y_k V_k\right)\frac{\partial T}{\partial x} \tag{2.2c}$$

In the above equations $\dot{m}$ represents the mass flow rate, which is independent of x. Eqs. (2.2) are complemented with the equation of state $\rho = \frac{p_0}{RT}$. The set of Eq. (2.2) is also known as flamelet equations. Their solution is a function of the unburned temperature, the considered species and pressure $(T_u, Y_1, ..., Y_{N_s}, p_0)$ where N_s denotes the number of species.

The evaluation procedure to calculate the net chemical production rate $\dot{\omega}_k$ of each species is important, Also, it is a computationally expensive task. Recalling Eq. (1.20), the Arrhenius law to calculate the $\dot{\omega}_k$, the values of the pre-exponent, temperature exponent and activation energy are required. Secondly, the species diffusion model is also a key element which is composed as $V_k = \mathbb{V}_k + V^c$. The ordinary diffusion velocity $\mathbb{V}_k$ is here modelled by the Hirschfelder-Curtiss approximation Eq. (1.29) [11]. V^c is the correction velocity as given in Eq. (1.32) of introduction. Hence, the species Eq. (2.2b) can be replaced with Eq. (1.33) as

$$\dot{m}\frac{\partial Y_k}{\partial x} + \frac{\partial}{\partial x}(\rho V^c Y_k) = \frac{\partial}{\partial x}\left(\frac{\rho D_k}{W}\frac{\partial(W Y_k)}{\partial x}\right) + \dot{\omega}_k. \tag{2.3}$$

Still, because of expensive computational cost of the Hirschfelder and Curtiss approximation, sometime the selection of Fick's model Eq. (1.34) is worth considering. In this chapter and the following, further insight is provided on the model effect.

2.2.1 Boundary conditions

The conservation Eqs. (2.2) are associated with boundary value problems. For the complete description of premixed flames, appropriate boundary conditions for species and energy conservation equations are required. Specifically, the unknowns $T(x)$ and $Y_k(x)$ have to be set at the upstream and downstream boundaries. The energy conservation equation is second order differential equation (DE) in T and requires two boundary conditions. Upstream the value is known. Thus, a Dirichlet condition is set. On the other hand, downstream the boundary is placed for away from the region of interest. Thus, no significant changes occur near it.

$$T(x \to -\infty) = T_u \tag{2.4a}$$

$$\frac{dT}{dx}(x \to +\infty) = 0 \tag{2.4b}$$

In general, the domain lies $-\infty < x < \infty$ which is truncated by only few centimeters for numerical solutions. Particularly, for premixed cases the length of domain size is between 2 to 4 centimeters. In addition, comparative long domain (4 centimeters) is required for rich cases.

The species conservation equation, Eq. (2.2b), is a first order ordinary differential equation (ODE), in both Y_k and u or S_L. However, by substituting the constitutive relation defined in Eq. (1.29), the species equation. Eq. (2.2b) becomes second order in Y_k. Thus, Y_k's have to be set at both upstream and downstream locations. The boundary condition are analogous to those of the energy equation. Hence, the boundary conditions are

$$Y_k(x \to -\infty) = Y_{k,u} \tag{2.5a}$$

$$\frac{dY_k}{dx}(x \to +\infty) = 0 \tag{2.5b}$$

2.3 Numerical methodology

An important step in the numerical solution starts from handling the partial differential equation (PDE). First, the development of stable, consistent and accurate algebraic replacement of PDE's (or boundary value problems) is needed. This algebraic procedure must retain most of the global information of the original problem and inherit its structure. Several methods can be used, such as finite volume method (FVM), finite element method (FEM) and finite difference method (FDM). These discretization schemes provide a means of replacing the PDE's system with an algebraic one. In the present study, FDM is adopted because of its easiness in handling one-dimensional problems and implementation.

In combustion problems, detailed kinetic mechanisms involve hundreds of species and thousands of reaction. Thus, the number of coupled equations can become very

large. Furthermore, the transport equations of species and energy are highly non-linear because of the chemical reaction rate. The second difficulty is the characteristic time scales of the chemical reactions. These time scales are associated with a kinetic scheme and may differ by several orders of magnitude. In consequence, the system of equations can be categorized as a stiff system.

In this situation, to solve the system of non-linear equations a well known modified Newton method is employed. Before solving the system of non-linear equations, we will have to rewrite the equations. First, the system is scaled by a change of variable. Second, a transformation from the physical domain to a logical domain is performed. These modifications are intended to handle the arising computational difficulties from stiff systems of equations.

2.3.1 Scaling and change of variable

In combustion problems, the magnitude of the unknowns can be significantly different from one to the other. While the mass fraction of a species or sum of the mass fraction of all species can never be greater than unity, the adiabatic temperature (depends on fuel) is in order of 10^3. Furthermore, some species may lie in the range of tenths while others are found in concentrations of part-per-million (ppm). Besides, their variation across the flame front may be significantly different.

In general, a numerical solution of PDE's evolves the discrete form of a system. The solution of the discrete system is also based on scalar coefficients of discrete equations (or matrix coefficients). The magnitude of coefficients depend on different parameters (physical parameter, etc.) and spatial length (δx). While the computational domain is in order of 10^{-3} in premixed flames and close to the flame front the mesh-size is further reduced to achieve better accuracy. In consequence, the solution of a system becomes more complicated as compared to another non-reacting flow problems. There are two causes: large variation in the magnitude of coefficients and variation of the magnitude of expected solution (species and temperature). As a result, the occurrence of numerical instabilities is very common in such systems. Sometimes it becomes quite a big issue, and in consequence, a solution of the system is not often found.

Scaling sometimes becomes an important issue in mathematical computations. Computer stores floating-point numbers with limited precision. When performing calculations, problems can arise because of this. Especially, if small and large values are added, subtracted or divided from each other. In that case, the precision of the small number is lost. As a result, it can affect the calculated values, that aren't correct any more. The numerical solution is typically an iterative process, where thousands of floating calculations are done to find a solution. The chance of numerical instabilities is consequently also quite big. However, scaling does not only improve numerical stability, it also increases the performance as well [12]. Besides, scaling preserves the structure of the system but modifies the coefficients. In other words, it improves the

numerical characteristics of the system without altering the structure at all. Mathematically, solver convergence depends on the condition number of the matrix (or system). Therefore, scaling the variables often reduces the condition number, thus improving the convergence [13].

To tackle the explained issues mass fractions and temperature are scaled. Furthermore, they are recast in rescaled domain z. New variables are introduced such as

$$
\begin{aligned}
y_k &= \frac{Y_k}{Y_r} \quad ; \quad Y_r \geq \max(Y_1,Y_2,...,Y_{N_s}) \quad \Rightarrow \quad 0 \leq y_k \leq 1 \\
\theta &= \frac{T}{T_r} \quad ; \quad T_r \geq T_{adia} \quad \Rightarrow \quad 0 \leq \theta \leq 1 \\
z &= \alpha x \quad ; \quad \alpha \geq 1
\end{aligned}
$$

where Y_r, T_r are the scaling reference values for species and temperature respectively. Applying these changes, Eqs. (2.2) become

$$\dot{m} = const = \rho_u S_L \tag{2.6a}$$

$$\dot{m}(\alpha Y_r)\frac{\partial y_k}{\partial z} + (\alpha Y_r)\frac{\partial(\rho V_k y_k)}{\partial z} = \dot{\omega}_k \tag{2.6b}$$

$$\dot{m}(\alpha T_r)\frac{\partial \theta}{\partial z} = \frac{\dot{\omega}'_T}{c_p} + \left(\frac{\alpha^2 T_r}{c_p}\right)\frac{\partial}{\partial z}\left(\lambda\frac{\partial \theta}{\partial z}\right) - \left(\frac{\rho\alpha Y_r}{c_p}\right)\left(\sum_{k=1}^{N_s} c_{p,k} y_k V_k\right)\frac{\partial \theta}{\partial z} \tag{2.6c}$$

It is important to note: both $\dot{\omega}_k$ and $\dot{\omega}'_T$ are function of unscaled variables that is Y_k and T. Hence $\dot{\omega}_k(Y_k, T)$ and $\dot{\omega}'_T(Y_k, T)$.

2.3.2 Transformation: physical to logical domain

In most combustion applications, non-uniform grids allow refining in regions of interest, for example where strong gradients are expected. Specifically, when dealing with stiff PDE's, grid generation becomes important. In combustion problems, second order discretization schemes for derivatives, are commonly used. However, the order of accuracy of the discretization scheme degrades when non-uniform grids are employed. This degradation also depends on grid expansion ratio. This effect can be easily evidenced using Taylor series approximation for central difference formulation.

To preserve the order of accuracy of the scheme, we transform the non-uniform physical space grid to a uniform logical space grid as shown in Fig. 2.2. The procedure uses a non-uniform grid in physical-space which is related to a uniform grid in logical-space. Then, the flamelet Eqs. (2.6) are rewritten in logical space and solved using FDM. Finally, solution variables are converted from logical-space to physical-space.

To convert the uniform mesh in logical-space to the non-uniform mesh in physical-space two steps are required. First, a transformation procedure from physical to

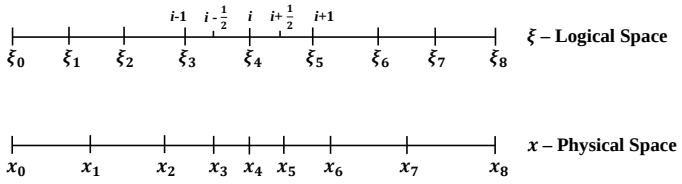

Figure 2.2: A one dimensional grid.

logical space. Second, a function to concentrate the mesh in physical space. Regarding the first step, consider a mesh with M number of grid points, the transformation from logical space to physical space $[a\,,b]$ is given by

$$x(\xi) = a + c\int_0^{\xi} \phi(y)dy \quad ; \quad \xi \in [0\,,1] \tag{2.7}$$

where $\triangle\xi = \frac{i}{M}$, $\xi_i = i\triangle\xi$, $x(0) = a$ and $x(1) = b$ which implies $\frac{1}{c} = \frac{1}{b-a}\int_0^1 \phi(y)dy$. The function $\phi(\xi)$ which depends on a logical space variable $\xi \in [0\,,1]$, controls the mesh spacing in physical-space and it must be continuous and differentiable function. The actual function is defined in the next section. The transformation Jacobian is calculated as $J = \frac{dx(\xi)}{d\xi} = c\phi(\xi) = x_\xi$. Then, 1^{st} and 2^{nd} derivatives of function $f(x)$ are defined as

$$f_x = \frac{df}{dx} = \frac{df}{d\xi}\frac{d\xi}{dx} = \frac{f_\xi}{x_\xi} = \frac{f_\xi}{J}$$
$$f_{xx} = \left(\frac{f_\xi}{J}\right)_\xi \frac{1}{J}.$$

Rewriting the flamelet equations, Eqs. (2.6) into logical ξ space, they become

$$\dot{m} = const = \rho_u S_L \tag{2.8a}$$
$$\dot{m}(\alpha Y_r)\frac{\partial y_k}{\partial \xi} + (\alpha Y_r)\frac{\partial(\rho V_k y_k)}{\partial \xi} = J\dot{\omega}_k \tag{2.8b}$$
$$\dot{m}(\alpha T_r)\frac{\partial \theta}{\partial \xi} = \frac{J\dot{\omega}'_T}{c_p} + \left(\frac{\alpha^2 T_r}{c_p}\right)\frac{\partial}{\partial \xi}\left(\frac{\lambda}{J}\frac{\partial \theta}{\partial \xi}\right) - \left(\frac{\rho\alpha Y_r}{c_p}\right)\left(\sum_{k=1}^{N_s} c_{p,k} y_k V_k\right)\frac{\partial \theta}{\partial \xi} \tag{2.8c}$$

Final version of species Eq. (2.8b) can be recast using Hirschfelder and Curtiss approximation as according Eq. (2.3)

$$\dot{m}(\alpha Y_r)\frac{\partial y_k}{\partial \xi} + (\alpha Y_r)\frac{\partial}{\partial \xi}(\rho V^c y_k) = (\alpha Y_r)\frac{\partial}{\partial \xi}\left(\left(\frac{\rho D_k}{JW}\right)\frac{\partial(W y_k)}{\partial \xi}\right) + J\dot{\omega}_k. \tag{2.9}$$

2.3.3 Grid generation

The mesh is a discrete representation of the geometry or domain of the problem. Computationally, the solution rate of convergence or accuracy and computational cost depend on the mesh used to calculate the solution. In Sec. 2.3.2, the transformation was established using a mesh function to generate a non-uniform grid in physical space. The Gaussian function $\phi(\xi)$ is

$$\phi(\xi) = a - b\, exp(-c|\xi - d|^e) \qquad ; \qquad \xi \in [0\,, 1]$$

The $\phi(\xi)$ function is continuous and differentiable in the domain $[0, 1]$. The controlling parameters a, b, c, d and e

a : maximum grid size $\triangle x$ in physical domain (typical value 1.0)

b : weight parameter (typical value 0.99)

c : number of points to be stretch around reference point (typical value 10)

d : reference point, around which mesh points are stretched (typical value 0.5)

e : stretching parameter (typical value 4.0 and can varies in between 0 and 8)

Of all parameters, d and e are the most important ones to handle mesh quality. In some solvers, mesh adaptive strategies are used to refine the mesh in specific region of interest. In the present work, we are taking a computationally advantageous approach by using a special mesh generating function, which is simple and easy to implement. In present simulations, we are solving for premixed flames in a fix reference frame and attached to the flame. Then mesh resolution is controlled through the above function by predefining a fix reference location according to fixed reference position.

2.3.4 Finite difference method

The final task before solving the problem is the discretization of the governing Eqs. (2.8). The finite difference scheme is used to discretise the flamelet equations in uniform ($\xi - space$) grid. A second order central [1] difference formulation is adopted for convective as well as diffusive terms in both species and energy equations. By

[1] The central difference scheme requires a suitably fine grid for convergence. However, in case of coarse meshes, this can be controlled using the mesh function $\phi(\xi)$ (see grid generation section).

discretising the ξ space into M uniform points, all mesh related terms are defined as

$$\begin{aligned}
&\triangle\xi = \frac{i}{M}, \quad \xi_i = i\triangle\xi && ; \quad 0 \leq i \leq M_x \quad \text{and} \quad M_x = M-1 \\
&\xi_{i+\frac{1}{2}} = (i+\frac{1}{2})\triangle\xi && ; \quad 0 \leq i \leq M_x - 1 \\
&x_i = x(\xi_i) && ; \quad 0 \leq i \leq M_x \\
&J_i = (x_\xi)_i = \frac{x_{i+1} - x_{i-1}}{2\triangle\xi} && ; \quad 1 \leq i \leq M_x - 1 \\
&J_{i+\frac{1}{2}} = (x_\xi)_{i+\frac{1}{2}} = \frac{x_{i+1} - x_i}{\triangle\xi} && ; \quad 0 \leq i \leq M_x - 1.
\end{aligned}$$

The first derivative namely, the convection term, of the flamelet equations is approximated as

$$\begin{aligned}
f_x = \frac{f_\xi}{J} \implies \Big[\frac{1}{J}\frac{dy}{d\xi}\Big]_i &\cong \frac{1}{J_i}\frac{y(\xi_{i+\frac{1}{2}}) - y(\xi_{i-\frac{1}{2}})}{\triangle\xi} \\
&= \frac{1}{J_i}\frac{y(\xi_{i+1}) - y(\xi_{i-1})}{2\triangle\xi}
\end{aligned}$$

where

$$y(\xi_{i+\frac{1}{2}}) = \frac{y(\xi_{i+1}) + y(\xi_i)}{2}.$$

Similarly, the second derivative, namely the diffusion term, is

$$f_{xx} = \left(\frac{f_\xi}{J}\right)_\xi \frac{1}{J}$$

resulting in,

$$\begin{aligned}
f_{xx} = \Big[\frac{1}{J}\frac{d}{d\xi}\Big(\Big(\frac{\Gamma}{J}\Big)\frac{dy}{d\xi}\Big)\Big]_i &= \Big[\frac{1}{J}\frac{d}{d\xi}\Big(\eta\frac{dy}{d\xi}\Big)\Big]_i \\
&\cong \frac{1}{J_i}\frac{\big(\eta y_\xi\big)_{i+\frac{1}{2}} - \big(\eta y_\xi\big)_{i-\frac{1}{2}}}{\triangle\xi}
\end{aligned}$$

where Γ represents the diffusion coefficient. By setting $\frac{\Gamma}{J} = \eta$ and $\big(\eta y_\xi\big)_{i+\frac{1}{2}} \cong \eta_{i+\frac{1}{2}}\frac{y_{i+1}-y_i}{\triangle\xi}$, the second derivative can be expressed as

$$\begin{aligned}
\Big[\frac{1}{J}\frac{d}{d\xi}\Big(\eta\frac{dy}{d\xi}\Big)\Big]_i &\cong \frac{1}{J_i}\frac{\eta_{i+\frac{1}{2}}\Big(\frac{y_{i+1}-y_i}{\triangle\xi}\Big) - \eta_{i-\frac{1}{2}}\Big(\frac{y_i-y_{i-1}}{\triangle\xi}\Big)}{\triangle\xi} \\
&= \frac{1}{J_i}\Big[\Big(\frac{\eta_{i+\frac{1}{2}}}{\triangle\xi^2}\Big)y_{i+1} - \Big(\frac{\eta_{i+\frac{1}{2}} + \eta_{i-\frac{1}{2}}}{\triangle\xi^2}\Big)y_i + \Big(\frac{\eta_{i-\frac{1}{2}}}{\triangle\xi^2}\Big)y_{i-1}\Big].
\end{aligned}$$

Comparatively, boundary conditions are easier to transform. Dirichlet conditions are imposed as $T_0 = T_u$ and $Y_k = Y_{k,0}$ on the cold side (x $\rightarrow -\infty$) of the flame. Neumann conditions are set on the hot boundary (x $\rightarrow \infty$), which are recast into ξ-space as

$$\Big[\frac{dY_k}{dx}\Big]_{N-\frac{1}{2}} \quad \Rightarrow \quad \Big[\Big(\frac{\alpha Y_r}{J}\Big)\frac{dy_k}{d\xi}\Big]_{N-\frac{1}{2}} \cong \Big[\frac{\alpha Y_r}{J}\Big]_{N-\frac{1}{2}} \frac{y_{k,N} - y_{k,N-1}}{\triangle\xi} = 0$$
$$\Big[\frac{d\theta}{dx}\Big]_{N-\frac{1}{2}} \quad \Rightarrow \quad \Big[\Big(\frac{\alpha T_r}{J}\Big)\frac{d\theta}{d\xi}\Big]_{N-\frac{1}{2}} \cong \Big[\frac{\alpha T_r}{J}\Big]_{N-\frac{1}{2}} \frac{\theta_N - \theta_{N-1}}{\triangle\xi} = 0.$$

The transformation yields a second order approximation. It is important to note that the above discrete set of boundary conditions are associated with the scaled equations. The coefficients $\frac{\alpha Y_r}{J}$ and $\frac{\alpha T_r}{J}$ in above equations are derived through scaling and transformation procedures. Thus, it is important to take into account these coefficients as then appear in the discrete equation and can't be simplified. For example, considering the some algebraic operations, the above equation can be simplified as

$$y_{k,N} - y_{k,N-1} = 0$$

and coefficients become 1 and -1. Mathematically, there is absolutely no difference. However, numerically it has big scaling effect on computations and as a result solution may suffer numerical instabilities.

2.3.5 Laminar burning velocity

To find the solution of Eqs. (2.8), two configurations can be considered: burner stabilized flames and adiabatic freely propagating flames. Focusing on the case of freely propagating flames $\dot{m}$ (indirectly flame velocity) is an unknown and an eigenvalue of the system, which must be determined as part of solution [7]. Furthermore, the mass flow rate is independent of the spatial coordinate, $\dot{m}$ is a constant scalar for any given flame mixture. Thus, this can be expressed as

$$\frac{d\dot{m}}{dx} = 0. \tag{2.10}$$

Therefore, the addition of Eq. (2.10) to the flamelet equations Eqs. (2.2) would require setting an extra boundary condition. However, the problem can also be solved if one degree of freedom is removed from the system.

In premixed flames, the flame front moves towards the fresh gases with a speed given by the S_L. A problem that may arise, during the solution process is that the flame may move too close to the boundaries of the computational domain and be affected by the boundary condition. Furthermore, if the flame can traverse the computational domain, mesh resolution must be fine enough throughout the domain,

which is computationally expensive. To handle this situation, a reference frame attached to the flame front is used. This is achieved by fixing the temperature at one point. Therefore, the selection of this point must ensure that temperature and species gradients nearly vanish at the cold boundary. Now, the only thing remaining, the unknown $\dot{m}$. The energy equation is used at a fix location, to calculate the mass flow rate. Using the energy equation Eq. (2.8c), $\dot{m}$ can be found in the following way

$$\dot{m} = \frac{\frac{J\dot{\omega}'_T}{c_p} + \left(\frac{\alpha^2 T_r}{c_p}\right)\frac{\partial}{\partial\xi}\left(\frac{\lambda}{J}\frac{\partial\theta}{\partial\xi}\right) - \left(\frac{\rho\alpha Y_r}{c_p}\right)\left(\sum_{k=1}^{N_s} c_{p,k} y_k V_k\right)\frac{\partial\theta}{\partial\xi}}{(\alpha T_r)\frac{\partial\theta}{\partial\xi}}. \tag{2.11}$$

The discrete form of Eq. (2.11) used is of second order and deduced from the energy equation, Eq. (2.8c). Being consistent with rest of the system formulation is important. Otherwise, it can pose some numerical discrepancies. Then, the laminar burning velocity or flow velocity can easily be calculated as

$$S_L = \frac{\dot{m}}{\rho_u} \tag{2.12a}$$

$$u(x) = \frac{\dot{m}}{\rho(x)}. \tag{2.12b}$$

2.3.6 Initial estimation

Initial temperature in premixed flame cases is usually low and most reaction terms at this temperature are almost zero. If this flow is started to compute from $x = 0$ (cold boundary) and updating all variables for increasing x, the mass fractions remain constant. In general reaction rates of species rise very slowly so that the ignition point is rejected to infinity. This is known as the cold boundary problem [14]. On other hand, numerically this limitation can easily solved by introducing that an additional condition must be imposed in the initial conditions: the flame must have been ignited.

To start numerical solution, the C++ code is equipped with an initial profile function that generates an initial guess to solve a premixed case. The general trend of this initial guess is shown in Fig. 2.3. For this estimation, the reaction zone is presumed, in which the reactants change from unburned to burnt gases. To sketch the initial guess, the initial mass fractions of fuel and oxidizer must be provided. Optionally, the user can also sketch other important species profiles by providing their mass fractions. The latter is important for some fuels specially in case of hydrogen. The temperature profile can be initialized by providing the initial temperature and estimated adiabatic temperature. It is remarkable here, that the temperature profile should be ignited to start reactions the adiabatic temperature. Within the reaction zone the initial profile function uses a linear interpolation between initial and final values for both reactants and product. On cold and hot sides profiles are flat.

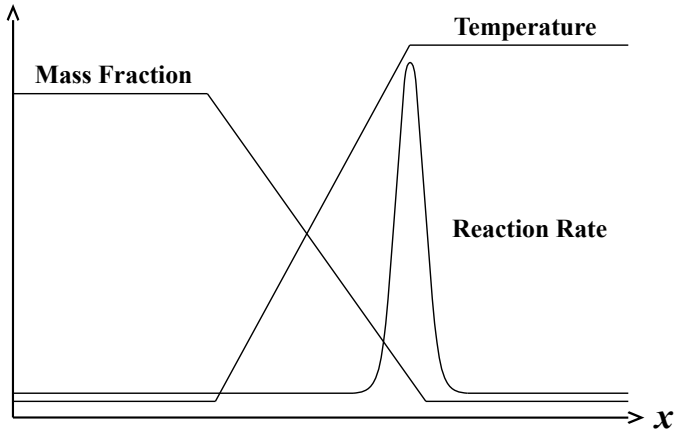

Figure 2.3: Schematic behaviour of the solution of premixed flame.

2.3.7 Computational frame work

To solve the set of governing equations Eqs. (2.8), it is needed to replace the system of differential equations with an algebraic one using FDM as defined in Sec. 2.3.4. After this, the equation set Eqs. (2.8) can be recast into the following functional form

$$\mathbf{F}(\boldsymbol{\phi}) = \begin{pmatrix} \dot{m}(\alpha T_r)\frac{\partial\theta}{\partial\xi} - (\frac{\alpha^2 T_r}{c_p})\frac{\partial}{\partial\xi}(\frac{\lambda}{J}\frac{\partial\theta}{\partial\xi}) + (\frac{\rho\alpha Y_r}{c_p})(\sum_{k=1}^{N_s} c_{pk} y_k V_k)\frac{\partial\theta}{\partial\xi} - \frac{J\dot{\omega}'_T}{c_p} \\ \dot{m}(\alpha Y_r)\frac{\partial y_1}{\partial\xi} + (\alpha Y_r)\frac{\partial}{\partial\xi}(\rho V^c y_1) - (\alpha^2 Y_r)\frac{\partial}{\partial\xi}(\frac{\rho D_k}{JW}\frac{\partial(W y_1)}{\partial\xi}) - J\dot{\omega}_1 \\ \vdots \\ \dot{m}(\alpha Y_r)\frac{\partial y_{N_s}}{\partial\xi} + (\alpha Y_r)\frac{\partial}{\partial\xi}(\rho V^c y_{N_s}) - (\alpha^2 Y_r)\frac{\partial}{\partial\xi}(\frac{\rho D_k}{JW}\frac{\partial(W y_{N_s})}{\partial\xi}) - J\dot{\omega}_{N_s} \end{pmatrix}$$

or equivalently by

$$\mathbf{F}(\boldsymbol{\phi}) = \begin{pmatrix} \Big[f(\theta)\Big]^T \\ \Big[f(y_1)\Big]^T \\ \vdots \\ \Big[f(y_{N_s})\Big]^T \end{pmatrix}$$

θ and y are discretised by M points. Thus, vector $\boldsymbol{\phi}$ can be written as $\boldsymbol{\phi} = (\underline{\theta_1, \theta_2, ...\theta_M}, \underline{y_{(1,1)}, ..., y_{(1,M)}}, ..., \underline{y_{(N_s,1)}, ..., y_{(N_s,M)}})^T$ and superscripts T stands

for transpose of vector. Rewriting $\boldsymbol{\phi}$ for simple notation such that $\boldsymbol{\phi} = (\phi_1, \phi_2, ..., \phi_{\mathcal{M}})^T$ where $\mathcal{M} = (N_s + 1)M$. The corresponding $\mathbf{F}$ vector is composed of residuals of the energy and species equations. $\mathbf{F}$ is a non-linear function of $\boldsymbol{\phi}$. The goal is to find a suitable $\boldsymbol{\phi}$ that satisfies the residual equation $\mathbf{F}(\boldsymbol{\phi}) = \mathbf{0}$.

The system of equations here discussed is stiff. These systems are usually very sensitive to the initial guess. Furthermore, iterative methods for the solution of non-linear system have a narrow region of convergence. For instance, the Newton-Raphson method has quadratic rate of convergence, but the convergence to the desired solution is not guaranteed unless the initial guess is sufficiently close to the solution. The method may diverge, or converge to an unwanted (non-feasible) solution.

To get more flexibility for convergence, a Damped Newton Method (DNM) is implemented. With this method, a damping parameter can be toggled to ensure convergence. Damped Newton technique to solve residual equations for $\boldsymbol{\phi}$ is adopted in the following way, similar to the one described by Smooke et al. [15]:

$$\boldsymbol{\phi}^{(n+1)} = \boldsymbol{\phi}^{(n)} - \lambda_d \left(\frac{d\mathbf{F}}{d\boldsymbol{\phi}} \right)^{-1}_{\boldsymbol{\phi}^{(n)}} \mathbf{F}(\boldsymbol{\phi}^{(n)}) = \boldsymbol{\phi}^{(n)} - \lambda_d \mathcal{J}^{-1} \mathbf{F}(\boldsymbol{\phi}^{(n)}) \quad ; \quad 0 \leq \lambda_d \leq 1$$

where λ_d is a damping parameter and $\left(\frac{d\mathbf{F}}{d\boldsymbol{\phi}}\right)_{\boldsymbol{\phi}^{(n)}} = \mathcal{J}$ is the Jacobian of $\mathbf{F}(\boldsymbol{\phi})$. Equivalently this can be rewritten as

$$\boldsymbol{\phi}^{(n+1)} = \boldsymbol{\phi}^{(n)} - \lambda_d \triangle \boldsymbol{\phi}^{(n)} \tag{2.13}$$

where

$$\triangle \boldsymbol{\phi}^{(n)} = \mathcal{J}^{-1} \mathbf{F}(\boldsymbol{\phi}^{(n)})$$

or expressed as a linear system

$$\mathcal{J} \triangle \boldsymbol{\phi}^{(n)} = \mathbf{F}(\boldsymbol{\phi}^{(n)}) \tag{2.14}$$

Newton's method evolves Eq. (2.13) and the solution of the $(n+1)^{th}$ iteration is the solution of the system of Eqs. (2.8) which satisfies $\mathbf{F}(\boldsymbol{\phi}) = \mathbf{0}$. To solve Eqs. (2.13) for $\boldsymbol{\phi}$, Jacobian matrix and linear solver are required.

Jacobian computation The structure of the Jacobian matrix is completely determined by the discretization, which leads to a block tri-diagonal structure of the matrix.

$$\left[\mathcal{J}\right] = \begin{pmatrix} \frac{\partial \mathbf{F}(\phi_1)}{\partial \phi_1} & \frac{\partial \mathbf{F}(\phi_1)}{\partial \phi_2} \cdots & \frac{\partial \mathbf{F}(\phi_1)}{\partial y^{\mathcal{M}}} \\ \frac{\partial \mathbf{F}(\phi_2)}{\partial \phi_1} & \frac{\partial \mathbf{F}(\phi_2)}{\partial \phi_2} \cdots & \frac{\partial \mathbf{F}(\phi_2)}{\partial y^{\mathcal{M}}} \\ \vdots & \cdots & \vdots \\ \frac{\partial \mathbf{F}(\phi_{\mathcal{M}})}{\partial \phi_1} & \frac{\partial \mathbf{F}(\phi_{\mathcal{M}})}{\partial \phi_2} \cdots & \frac{\partial \mathbf{F}(\phi_{\mathcal{M}})}{\partial y^{\mathcal{M}}} \end{pmatrix}$$

The size of $\mathcal{J}$ is $((N_s+1)M \times (N_s+1)M)$, and if we suppose, for example, a single step combustion problem ($F + O \rightarrow P$), then only two species and one energy equation are involved. In this case, the size of Jacobian is $(3M \times 3M)$.

For the construction of the Jacobian, there are two options: one is a symbolic (analytical) computation, and the other one is numerical. The symbolic computation of Jacobian is more accurate and computation-wise less expensive. However, it is effort-full and complex because of the complex structure of the chemical reaction terms. Furthermore, inclusion of further equations is not automatic. Instead a numerical Jacobian evaluation is adopted. The numerical Jacobian is calculated by a finite perturbation, as suggested by Curtiss [16]. Many researchers have proposed several finite difference approximations of the Jacobian [17]. First order finite difference approximation of the Jacobian is written as

$$\left[\boldsymbol{\psi}, \boldsymbol{\phi}; \mathbf{F}\right]_{i,j} = \frac{F_i(\psi_1, \cdots, \psi_j, \cdots, \phi_{\mathcal{M}}) - F_i(\psi_1, \cdots, \phi_j, \cdots, \phi_{\mathcal{M}})}{\psi_j - \phi_j},$$

or equivalently expressed in compact notation

$$\mathcal{J}_{i,j} = [\boldsymbol{\phi} + \boldsymbol{\delta}, \boldsymbol{\phi}; \mathbf{F}]_{i,j} = \frac{F_i(\boldsymbol{\phi} + \boldsymbol{\delta}_j) - F_i(\boldsymbol{\phi})}{\delta} \tag{2.15}$$

where $\boldsymbol{\phi} + \boldsymbol{\delta}_j = [\phi_1, \phi_2, \cdots, \phi_{j-1}, \phi_j + \delta, \phi_{j+1}, \cdots, \phi_{\mathcal{M}}]$ and δ is the numerical perturbation. Similarly, the second order finite difference approximation of the Jacobian [17] can be expressed as

$$\mathcal{J}_{i,j} = \frac{F_i(\boldsymbol{\phi} + \boldsymbol{\delta}_j) - F_i(\boldsymbol{\phi} - \boldsymbol{\delta}_j)}{2\delta}. \tag{2.16}$$

The computational cost of Eq. (2.16) is higher compared to Eq. (2.15). Detailed discussion about the order of approximation can be found in Appendix A.

In general, the Jacobian evaluation is a machine-intensive task. Therefore, it is not a good idea to re-evaluate the Jacobian at each iteration. We employ a remedy to improve the computations. The Damped Newton methodology is implemented along with a frozen Jacobian approach namely, multi-step methods [18–21]. These methods are computationally less expensive and the best candidate to use as the iterative solver for the solution of the system of Eqs. (2.8). A multi-step damped Newton iterative method with frozen Jacobian is shown in Algorithm 1.

Regarding the accuracy of the method, when $\lambda_d = 1$ and $\boldsymbol{\delta} = \beta\, \mathbf{F}(\boldsymbol{\phi}_0)$ for any given non-zero scalar β, the order of convergence of multi-step method becomes $p + 1$. Furthermore, if the values of all used damping parameters $\lambda_d^{(n)} \neq 1$ or $\boldsymbol{\delta} \neq \beta\, \mathbf{F}(\boldsymbol{\phi}_0)$ then the multi-step method has linear convergence.

Algorithm 1 Multi-step damped Newton method with frozen Jacobian

1: **while** $\frac{\left\|\boldsymbol{\phi}^{new}-\boldsymbol{\phi}^{old}\right\|_2}{\left\|\boldsymbol{\phi}^{old}\right\|_2} \geq \epsilon$ **do**
2: $\quad\boldsymbol{\phi}^{(n)} =$ initial guess;
3: $\quad\mathcal{J}^{(n)} = \left[\boldsymbol{\phi}^{(n)} + \boldsymbol{\delta}, \boldsymbol{\phi}; \mathbf{F}\right]$
4: $\quad\mathcal{J}^{(n)} \triangle\boldsymbol{\phi}^{(n)} = \mathbf{F}(\boldsymbol{\phi}^{(n)})$ ▷ Solved using iterative/direct methods
5: $\quad\boldsymbol{\phi}^{(n+1)} = \boldsymbol{\phi}^{(n)} - \lambda_d^{(n)} \triangle\boldsymbol{\phi}^{(n)}$
6: $\quad f = n$; freezing the index.
7: $\quad$**for** i=2:p **do** ▷ Frozen Jocobian loop for p iterations
8: $\quad\quad\mathcal{J}^{(f)} \triangle\boldsymbol{\phi}^{(i)} = \mathbf{F}(\boldsymbol{\phi}^{(i)})$ ▷ Solved using iterative/direct methods
9: $\quad\quad\boldsymbol{\phi}^{(i+1)} = \boldsymbol{\phi}^{(i)} - \lambda_d^{(n)} \triangle\boldsymbol{\phi}^{(i)}$
10: $\quad\quad n++$; iterations
11: $\quad$**end for**
12: **end while**

Linear solver In the linear solver part, there are also two options: use an iterative or a direct solver to solve Eq. (2.14). For the moderately large system of linear equations, a LU factorization of Jacobian $\mathcal{J}$ may be viable option. This factorization can be utilized in the multi-step part repeatedly; that makes the solver efficient computationally. On the other hand, the use of iterative solvers (for instance GMRES, SOR) could provide a reasonable approximation of the system of linear equations. Since a damped Newton frozen Jacobian multi-step iterative method is used, and which has linear order of convergence, the exact solution of the system of linear equation Eq. (2.14) is not strictly required. Hence a reasonable approximation of the solution of the system of linear equations also serves as a remedy for the treatment of the stiff system of nonlinear equations. In other words, solutions not being exact at each intermediate step represents a certain level of damping.

In the case of combustion a good initial guess is very important. It is observed from our numerical experimentation, that the blend of direct and iterative methods is a good method for the solution of the system of Eqs. (2.8). It is advisable to start the multi-step method with iterative solver to approximate the solution for some initial iterations without freezing the Jacobian. After the solution becomes stable, the use of direct solvers such as LU factorization is recommendable for fast convergence.

2.4 Results and discussions

In the following, numerical simulations of one-dimensional laminar adiabatic freely propagation flames are carried out with C++ code using several chemical mechanisms GRI3.0, Smooke and Mueller mechanisms. The GRI3.0 mechanism [22] is a detailed

mechanism and consists of 53 species and 325 chemical reactions. The Smooke mechanism [23] is a reduced mechanism for CH_4 and contains 14 species and 46 chemical reactions. The Mueller mechanism [24] is also a reduced mechanism for H_2 and consists of 9 species and 21 chemical reactions. The GRI3.0 has bean validated by experimental data for methane, ethane, carbon monoxide and hydrogen fuels. The GRI mechanisms have been used in different studies and shown to accurately represent chemical kinetics [25–28]. On the other hand, Smooke and Mueller's mechanisms are specifically designed for methane/air and hydrogen/air mixture, respectively. These reduced mechanisms have been studied for methane/air and hydrogen/air flames [24, 29, 30].

In the present calculations the computational domain is 2 cm long and kept the same for all fuel mixtures cases. Typically total number of grid points is 101. The mesh is generated using the mesh function, as described in Sec. 2.3.3, and it is concentrated at the middle of the domain. All calculations of CH_4 and H_2 are performed with regular air (21% O_2 and 79% N_2) at atmospheric pressure. Initial temperature varies from case to case.

2.4.1 Methane/air

CH_4/air flame simulations are performed with an initial temperature of 300 K. For this mixture many experimental measurements are available. Therefore, comparison is made with a few of them. Additionally, the current results are compared with reported simulation results of others authors. Fig. 2.4 shows the comparison between numerically calculated and experimentally evaluated laminar burning velocities. The data is represented as a function of CH_4/air mixture equivalence ratios. The presented results are compared with literature data [11, 26, 30–38], where measurements were carried out using different experimental methods.

Additionally, in Table 2.1 the laminar burning velocities S_L presented in Fig. 2.4 for stoichiometric mixture in chronological order are shown. The experimental data shows a small degree of scatter, corresponding to different measurement methods. The simulation results of present work are presented in Fig. 2.4 using Hirschfelder and Curtiss diffusion model [11]. For a stoichiometric mixture, the calculated laminar burning velocity is 37.7 cm/s, which is within a bound of the measure of disperse about the mean of the experimental data, that is 37.14 ± 1.45 cm/s. The relative error of the calculated burning velocity to the mean experimental value is 1.5 %. For further verification of the present results comparison with existing simulation codes namely, PREMIX [11] and Cosilab [38] is also performed. Fig. 2.4 shows excellent agreement with the experimental results. Furthermore, good agreement with other computational software is found as shown in Fig. 2.4 and Fig. 2.5. The latter figure presents the adiabatic temperature as a function of equivalence ratio. A very good match with Cosilab simulation results [38] is found. The maximum temperature is around the stoichiometric mixture, as is expected.

The typical flame structure is presented in Fig. 2.6, Fig. 2.7. These figures depict

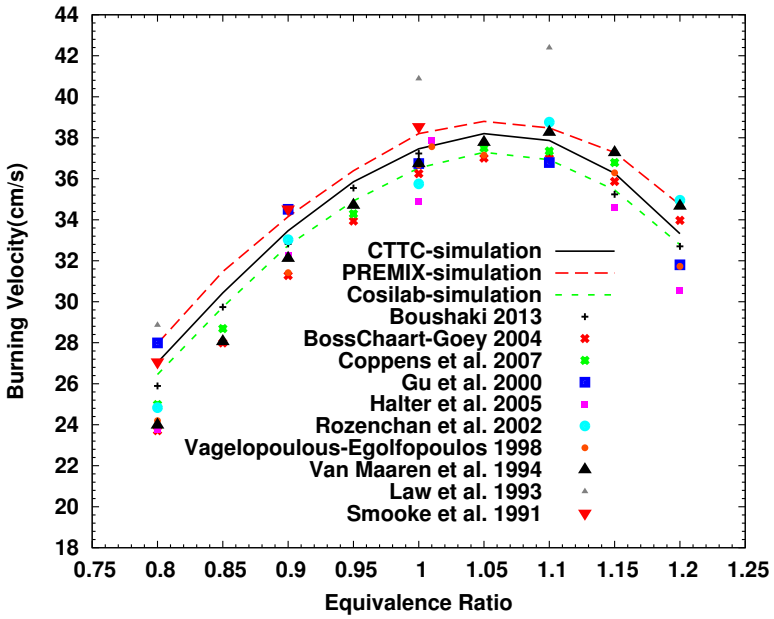

Figure 2.4: Calculated laminar burning velocity of CH_4/air mixtures. Comparison with experimental data from literature. Symbols represent experimental data; lines represent simulation results (using GRI3.0 chemical mechanism). PREMIX simulation results are taken from [11] and Cosilab-simulation from [38]

the species mass fractions and temperature distribution along the computational domain. It can be seen from Fig. 2.6 and Fig. 2.7, that in the preheat zone the unburned gas is heated up to the ignition temperature. After this, the main combustion process takes place and the heat release occurs. This zone is marked by the rapid increase in temperature and concentration of the main radicals H, O, OH as shown in Fig. 2.7. Additionally, these minor species play an important role in highly diffusive mixtures for instance hydrogen/air flame. Still, as Fig. 2.7 shows, these species appear in the reaction zone and are consumed shortly after. These radicals recombine after the active oxidation process is completed, and contribute to the temperature increase until they reach their equilibrium [39]. Further on, because of the assumption of an adiabatic system, the temperature of the burnt gases remains constant to the end of the domain.

Table 2.1: CH_4/air laminar flame speed (cm/s). Experimental results for $\phi = 1.0$ from literature, in chronological order.

Year	Author	Reference	Technique	$S_L(cm/s)$
1991	Smooke et al.	[31]	Plug burner	38.5
1993	Law et al.	[32]	Counterflow	40.5
1994	Van Maaren et al.	[33]	Flat flame	37.0
1998	Vagelopoulous et al.	[34]	Counterflow	36.7
2000	Gu et al.	[35]	Closed vessel	36.8
2002	Rozenchan et al.	[36]	Closed vessel	36.6
2004	Bosschaart et al.	[30]	Flat flame	35.7
2005	Halter et al.	[26]	Closed vessel	34.9
2007	Coppens et al.	[37]	Flat flame	37.5
2013	Boushaki et al.	[38]	Burner	37.2

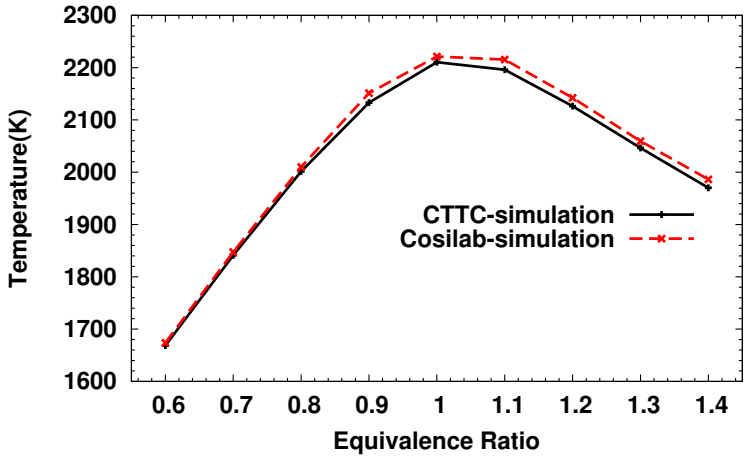

Figure 2.5: Calculated adiabatic temperature of CH_4/air mixtures, comparison with simulation results of Cosilab [38].

2.4.2 Hydrogen/air

H_2/air flame simulations are carried out at an initial temperature of 298 K. This temperature initialization is taken in order to validate the available data from the literature. Table 2.2 presents the available data, together with the experimental technique used, for the stoichiometric mixture fraction in chronological order. Laminar

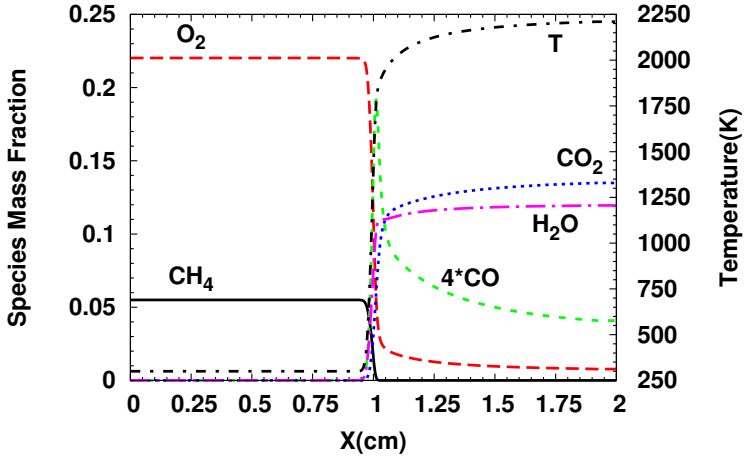

Figure 2.6: Calculated mass fractions of major species of CH_4/air flame for stoichiometric mixtures. Legend multiplier represents the increase of the concerned entity for better presentation.

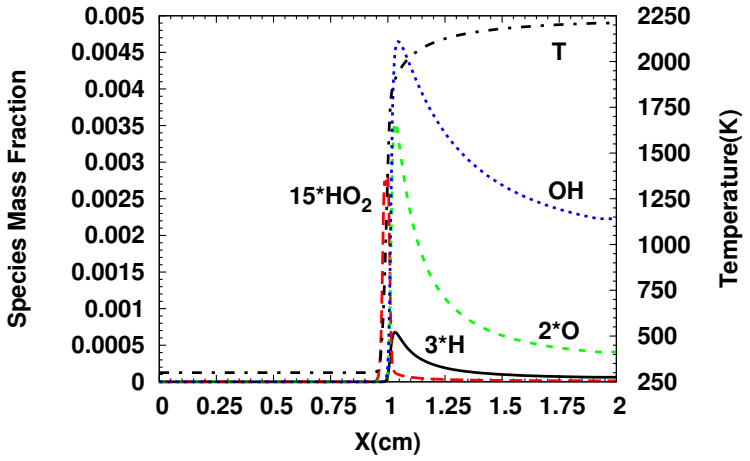

Figure 2.7: Calculated mass fractions of minor species of CH_4/air flame for stoichiometric mixtures. Legend multiplier represents the increase of the concerned entity for better presentation.

burning velocities for different equivalence ratios are shown in Fig. 2.8. Present results are compared against literature data [40–48]. The experimental measurements are associated with different measurement methods e.g. burner, bomb, and particle tracking velocimetry (PTV) methods. Simulation results are obtained using Mueller and GRI3.0 chemical mechanisms. Comparison is also made against results from the PREMIX code [8].

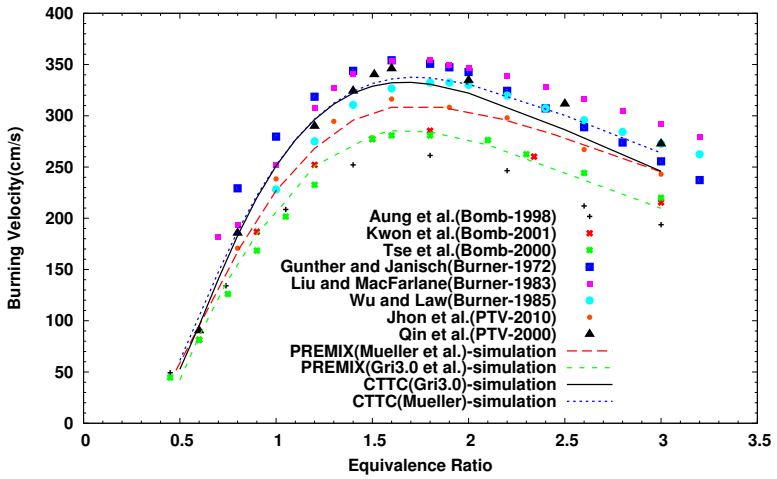

Figure 2.8: Calculated laminar burning velocity of H_2/air mixtures, comparison with experimental data from literature using different configurations. Symbols represent experimental data lines represent simulation results (using GRI3.0 and Mueller chemical mechanisms). PREMIX-simulation results taken from [38]

Current results show very good agreements with experimental data with either chemical mechanism. The calculated adiabatic temperature, 2369 K, is excellently matched with Erjiang work [49], which was found to be 2364 K for a stoichiometric mixture. The calculated laminar burning velocity for the stoichiometric mixture is 251.0 and 251.8 cm/s using GRI3.0 and Mueller mechanisms, respectively. These results are within a bound of the measure of disperse about the mean of the experimental data that is 256.5±22.2 cm/s and relative percentage error with respect to the experimental mean value is 1.8%. In other words, this variation is within experimental uncertainty because of the different experimental techniques reported. Fig. 2.8 shows that the overall behaviour of numerical results are well matched with experimental data. Specially, those from burner and PTV techniques, which have less stretch effects than other techniques. In the case of the bomb technique, the flame is 3D. In this technique stretch effects are more significant. Thus, results are more deviated from

Table 2.2: H_2/air laminar flame speed (cm/s). Experimental results for $\phi = 1.0$ in literature, in chronological order. PTV stands for particle tracking velocimetry.

Year	Author	Reference	Technique	$S_L(cm/s)$
1972	Gunther et al.	[40]	Burner	279.5
1983	Liu et al.	[41]	Burner	252.1
1985	Wu et al.	[42]	Burner	228.1
2003	IIbas et al.	[43]	Bomb	284.5
2010	Jhon et al.	[44]	PTV	238.4

the rest. In the current numerical calculations, it is assumed the flame has no stretch effect (1D case). Additionally, the deviation of numerical results between Muller and GRI3.0 is due to detailed and reduced mechanisms, which is commonly mentioned in literature [50].

A detailed flame structure is presented in Fig. 2.9 and Fig. 2.10. In these figures, the species mass fractions are shown along the computational domain for a stoichiometric mixture. It can be seen that minor species exist only in a small fraction of domain. Additionally, their dynamics is much faster than the major species, thus accounting for the stiffness of the system. The laminar burning velocities and distribution of mass fractions can be observed to be significantly different than the CH_4/air flame because of the high mass and thermal diffusivity of the hydrogen. The maximum laminar burning velocity is found in between equivalence ratios of 1.7 to 1.8.

2.4.3 Blended mixture

In this section flames burning blended fuel mixtures are analysed. Blended fuel mixtures are mixtures of CH_4 and H_2. Five different cases are studied by increasingly adding hydrogen fuel into methane/air mixture. The volumetric percentage of hydrogen in fuel blends X_{H_2} is defined as

$$X_{H_2} = \frac{V_{H_2}}{V_{CH_4} + V_{H_2}}$$

where V_{CH_4} and V_{H_2} are the volume fraction of methane and hydrogen in the fuel mixture respectively. The chemical reaction for the stoichiometric CH_4/air and H_2/air is

$$CH_4 + 2(O_2 + 3.762N_2) \rightarrow CO_2 + 2H_2O + 2 \times 3.762N_2$$
$$H_2 + 0.5(O_2 + 3.762N_2) \rightarrow H_2O + 0.5 \times 3.762N_2.$$

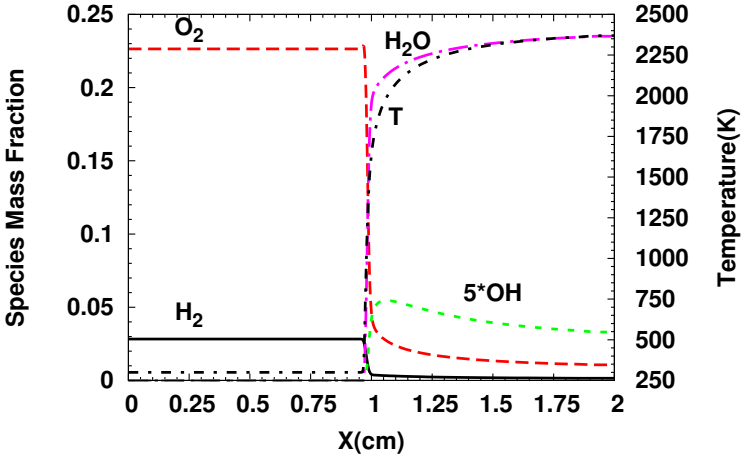

Figure 2.9: Calculated mass fractions of major species of H_2/air flame for stoichiometric mixtures. Legend multiplier represents the increase of the concerned entity for better presentation.

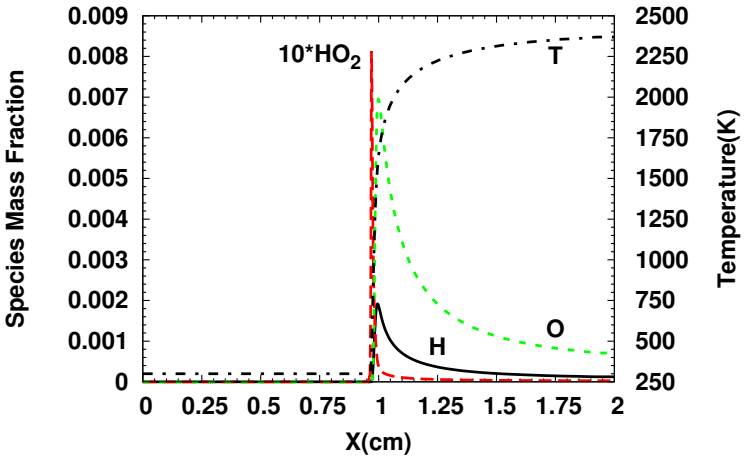

Figure 2.10: Calculated mass fractions of minor species of CH_4/air flame for stoichiometric mixtures. Legend multiplier represents the increase of the concerned entity for better presentation.

Combining both reactions, the chemical reaction for a blended mixture is

$$(1 - X_{H_2})CH_4 + X_{H_2}H_2 + \left(\frac{2}{\phi}(1 - X_{H_2}) + \frac{X_{H_2}}{2\phi}\right)(O_2 + 3.762N_2)$$
$$\rightarrow (1 - X_{H_2})CO_2 + (2 - X_{H_2})H_2O + \left(\frac{3.76}{2\phi}(4 - 3X_{H_2})\right)N_2$$

where ϕ is fuel/oxidizer equivalence ratio as defined in Chapter 1.

The effect of hydrogen addition on laminar velocity is studied at 300 K and atmospheric pressure. The chemical kinetic mechanism GRI3.0 [22] is used. The hydrogen content in the fuel, represented by α, is varied from 0% to 30%. The comparison of experimental and calculated results are shown in Fig. 2.11 and Fig. 2.12. Results show that the laminar burning velocity increases linearly with increasing hydrogen content. Present results are in very good agreement and consistent with experimental results from the literature. Furthermore, the linearity of S_L with hydrogen fraction is found for all equivalence ratios which is not presented here. The same behavior is reported by several authors [27, 38, 51].

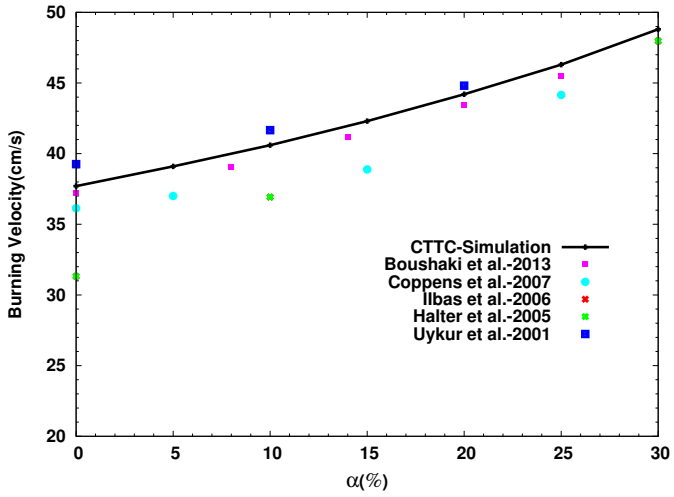

Figure 2.11: Laminar burning velocity versus the percentage of H_2 in the fuel for $\phi = 1.0$ mixture using GRI3.0 chemical mechanism. Comparison with experimental results from the literature.

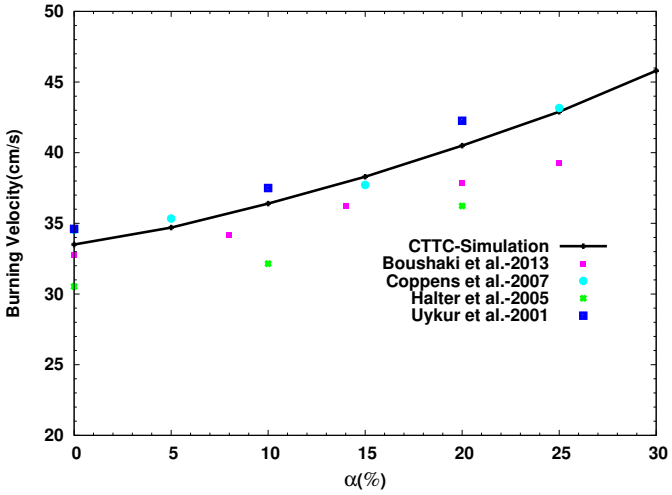

Figure 2.12: Laminar burning velocity versus the percentage of H_2 in the fuel for $\phi = 1.2$ mixture using GRI3.0 chemical mechanism. Comparison with experimental results from the literature.

2.4.4 Effect of Lewis number in transport models

In the previous sections, a non-fix and non-unity Lewis number, Le_k, is used together with a complex transport model in Eq. (2.9), namely the Hirschfelder and Curtiss diffusion model [11]. The use of $Le_k \neq 1$ is a more realistic assumption. However, the assumption $Le_k = 1$ is commonly used for theoretical treatments because it leads to an easier treatment of the equations. This simplification poses that mixture mass and thermal diffusivity behaved in the same way during a combustion process. Mostly, this $Le_k = 1$ assumption is made to simplify the calculations.

To evidence the effect of the $Le_k = 1$ assumption, results for a CH_4/air and H_2/air flames are presented. For the CH_4/air flame, the unity Lewis assumption does not have a notable effect on the species structure. Species mass fractions and temperature distributions are almost indistinguishable. However, as Fig. 2.13 shows, the flame propagation speed is prominently different when $Le_k \neq 1$ are considered. Consequently, these differences affect the flame topology in terms of flame position and extinction limit.

For H_2/air flame, the case is studied for a lean mixture, $\phi = 0.8$. Minor species are presented in Fig. 2.14, showing a notable different behaviour between $Le_k = 1$ and $Le_k \neq 1$. H_2O_2 and HO_2 species play an important role in the preheat zone, especially for hydrogen flames. Thus, flame dynamics are significantly affected. For instance,

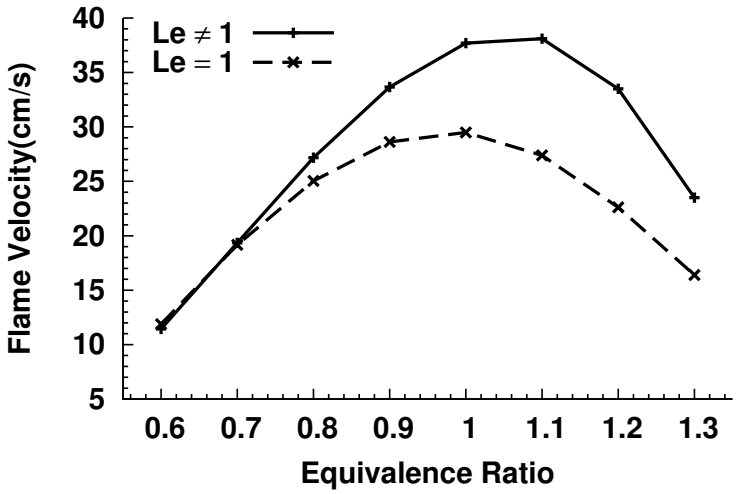

Figure 2.13: CH_4/air premixed flame laminar burning velocity for $\phi = 1.0$ mixture using GRI3.0 chemical mechanism. Both cases are solved considering Hirschfelder and Curtiss diffusion model.

the flame burning velocity is also affected with transport coefficients assumption: with non-unity Lewis it is 185 cm/s and with unity Lewis it is 138 cm/s. Present results are consistent and within less than 1% error compared to results of Gicquel et al. [52].

2.4.5 Conclusions

In this chapter, we have described the development of a C++ code and established a numerical platform for the simulation of laminar premixed flames under steady state condition. The code has been applied to simulate several flames using various chemical schemes. Excellent agreement with published numerical and experimental data has been found. The developed platform has been shown to be robust and accurate for laminar premixed flames. The main features of code are summarized as follows:

i- The platform was based on structured mesh and explored a new mesh function to meet the mesh requirement for the flame solution in a simple and efficient way.

ii- The algorithm solves the flame in logical space on a uniform mesh, and results showed the accuracy of code which proved the choice of transformation technique.

iii- Scaling and change of variable techniques increased the robustness of the code to achieve convergence.

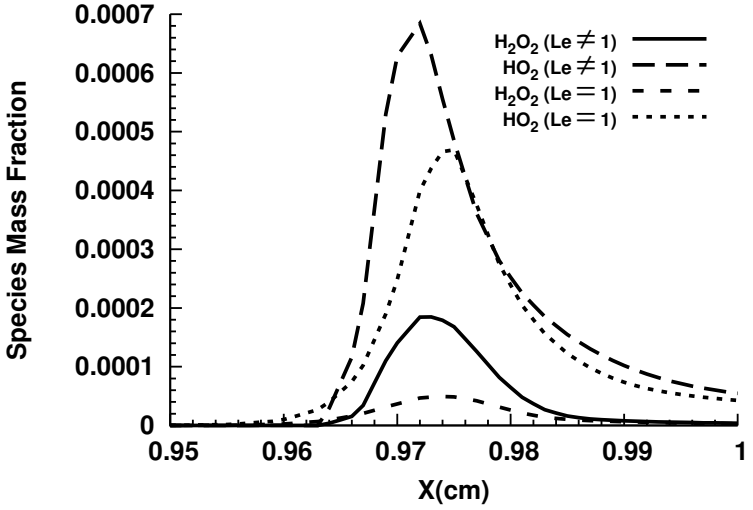

Figure 2.14: Minor species mass fraction of H_2/air flame for $\phi = 0.8$ mixtures using GRI3.0 chemical mechanism. Both cases are solved considering detailed/complex transport equations. The simulation domain range between 0 to 2 cm. Shown is subset of domain.

iv- A multi-step damped Newton method is used to efficiently solve the linear system of equations.

Appendix A

This appendix is devoted to mathematically prove the order of accuracy of the Jacobian formulation, which is defined using divided difference. Assume that $\mathbf{F}(\cdot)$ has, at least, four continuous derivatives on $D(\subset \mathcal{R}^m)$. The divided difference operator of $\mathbf{F}(\cdot)$ on $\mathcal{R}^m$ is a mapping

$$[\cdot, \cdot; \mathbf{F}] : D \times D \subset \mathcal{R}^m \times \mathcal{R}^m \to \mathcal{L}(\mathcal{R}^m)\,,$$

where $\mathcal{L}(\mathcal{R}^m)$ is the space of linear operators defined over $\mathcal{R}^m$ and it is defined as

$$[\boldsymbol{\phi} + \boldsymbol{\delta}, \boldsymbol{\phi}; \mathbf{F}] = \int_0^1 \mathbf{F}'(\boldsymbol{\phi} + t\,\boldsymbol{\delta}) dt\,, \qquad \forall (\boldsymbol{\phi}, \boldsymbol{\delta}) \in \mathcal{R}^m \times \mathcal{R}^m\,. \tag{2.17}$$

The Taylor series expansion of $\mathbf{F}'(\cdot)$ around $\boldsymbol{\phi}$ gives

$$[\boldsymbol{\phi} + \boldsymbol{\delta}, \boldsymbol{\phi}; \mathbf{F}] = \mathbf{F}'(\boldsymbol{\phi}) + 1/2\,\mathbf{F}''(\boldsymbol{\phi})\boldsymbol{\delta} + 1/6\,\mathbf{F}'''(\boldsymbol{\phi})\boldsymbol{\delta}^2 + O\left(\boldsymbol{\delta}^3\right)\,. \tag{2.18}$$

We have two finite difference approximation of (2.17)

$$\begin{aligned}
[\boldsymbol{\psi}, \boldsymbol{\phi}; \mathbf{F}]^{(1)}_{i,j} &= \frac{F_i(\psi_1 \cdots, \psi_j, \cdots, \phi_n) - F_i(\psi_1, \cdots, \phi_j, \cdots, \phi_n)}{\psi_j - \phi_j}, \\
[\boldsymbol{\psi}, \boldsymbol{\phi}; \mathbf{F}]^{(2)}_{i,j} &= \Big(F_i(\psi_1, \cdots, \psi_j, \cdots, \phi_n) - F_i(\psi_1, \cdots, \phi_j, \cdots, \phi_n) \\
&\quad + F_i(\phi_1, \cdots, \phi_j, \cdots, \psi_n) - F_i(\phi_1, \cdots, \psi_j, \cdots, \psi_n) \Big) \Big/ (2(\psi_j - \phi_j)).
\end{aligned} \tag{2.19}$$

The application of Taylor series gives

$$\begin{aligned}
\int_0^1 D_j F_i(\boldsymbol{\phi} + t\,\boldsymbol{\delta}) dt =& D_j F_i(\boldsymbol{\phi}) + 1/2 \sum_{k=1}^{m} D_{kj} F_i(\boldsymbol{\phi}) \delta_k \\
&+ 1/6 \sum_{k,l=1}^{m} D_{klj} F_i(\boldsymbol{\phi}) \delta_k \delta_l + O\left(\boldsymbol{\delta}^3\right)\,,
\end{aligned} \tag{2.20}$$

where D_j is the partial derivative with respect to jth coordinate. By using (2.19) and (2.20), we obtain

$$
\begin{aligned}
[\boldsymbol{\psi},\boldsymbol{\phi};\mathbf{F}]^{(1)}_{i,j} &= D_j F_i(\boldsymbol{\phi}) + \sum_{k=1}^{j-1} D_{kj} F_i(\boldsymbol{\phi})\delta_k + 1/2\, D_{jj} F_i(\boldsymbol{\phi})\delta_j + O\left(\boldsymbol{\delta}^2\right) \\
[\boldsymbol{\psi},\boldsymbol{\phi};\mathbf{F}]^{(2)}_{i,j} &= D_j F_i(\boldsymbol{\phi}) + 1/2 \sum_{k=1}^{m} D_{kj} F_i(\boldsymbol{\phi})\delta_k + 1/4 \sum_{\substack{k,\,l=1 \\ k+l<2j}}^{j} D_{klj} F_i(\boldsymbol{\phi})\delta_k\delta_l \\
&\quad + 1/6\, D_{jjj} F_i(\boldsymbol{\phi})\delta_j^2 + 1/4 \sum_{\substack{k,\,l=j \\ k+l>2j}}^{m} D_{klj} F_i(\boldsymbol{\phi})\delta_k\delta_l + O\left(\boldsymbol{\delta}^3\right) . \qquad (2.21)
\end{aligned}
$$

By using (Eq. (2.20)) and (Eq. (2.21)), we have

$$
\begin{aligned}
\int_0^1 D_j F_i(\boldsymbol{\phi} + t\,\boldsymbol{\delta})dt - [\boldsymbol{\psi},\boldsymbol{\phi};\mathbf{F}]^{(1)}_{i,j} &= O\left(\boldsymbol{\delta}\right) \\
\int_0^1 D_j F_i(\boldsymbol{\phi} + t\,\boldsymbol{\delta})dt - [\boldsymbol{\psi},\boldsymbol{\phi};\mathbf{F}]^{(2)}_{i,j} &= O\left(\boldsymbol{\delta}^2\right) .
\end{aligned} \qquad (2.22)
$$

References

[1] E. Mallard and H. L. Le Chatelier. Sur la vitesse de propagation de la flamme. *Ann. Mines*, 4(8):379–568, 1883.

[2] R. Sankaran, K. Law, and et al. Direct numerical simulations of turbulent lean premixed combustion. *Journal of Physics*, 46:38–42, 2006.

[3] J. O. Hirschfelder, C. F. Curtiss, and et al. *Proceedings of the Combustion Institute*, 19:190, 1953.

[4] B. Spalding. In *Philosophical Transactions of the Royal Society, London 249A: 1*, 1967.

[5] N. Peters and J. Warnatz. Numerical methods in laminar flame propagation. In *Notes on Numerical Fluid Mechanics*, 1982.

[6] K. A Wilde. Boundary-value solutions of the one-dimensional laminar flame propagation equations. *Combustion and Flame*, 18(1):43–52, 1972.

[7] R. M. Kendall and J. T. Kelly. Premixed one-dimensional flame (PROF) code user's manual. In *EPA Report EPA-600/7-78-172a*, 1978.

[8] R. J Kee, J. F. Grcar, and et al. Premix: A Fortran program for modeling a steady laminar one-dimensional premixed flame. In *Technical Report SAND85-8240, Sandia National Laboratory*, 1985.

[9] H. Pitsch and et al. Flamemaster: A C++ computer 1D laminar flame calculations. In *http://web.stanford.edu/group/pitsch/FlameMaster.htm*, 2007.

[10] A. Cuoci, Frassoldati, T. Faravelli, and E. Ranzi. laminarsmoke: numerical modeling of laminar reacting flows. In *http://www.opensmoke.polimi.it/*, 2013.

[11] T. Poinsot and D. Veynante. *Theoretical and Numerical Combustion.* R.T. Edwards Inc., 2005.

[12] A. C. N. Van Duin, P. C. Hansen, Tz. Ostromsky, H. Wijshoff, and Z. Zlatev. Improving the numerical stability and the performance of a parallel sparse solver. *Computers and Mathematics with Applications*, 30(12):81–86, 1995.

[13] N. J. Higham. *Accuracy and Stability of Numerical Algorithms.* Society for Industrial and Applied Mathematics, second edition, 2002.

[14] F. A. Williams. *Combustion Theory.* Addison-Wesley Publishing Company, Redwood City, 1985.

[15] M. D. Smooke, J. A Miller, and R. J. Kee. Determination of adiabatic flame speeds by boundary value methods. *Combustion Science and Technology*, 34(1-6):79–90, 1983.

[16] A. R. Curtis, M. J. Powell, and J. K Reid. *Institute of Mathematics and its Applications*, 13:117–119, 1974.

[17] M. Grau-Sanchez, M. Noguera, and S. Amat. On the approximation of derivatives using divided difference operators preserving the local convergence order of iterative methods. *Journal of Computational and Applied Mathematics*, 237:363–72, 2013.

[18] F. Ahmad, E. Tohidi, M. Z. Ullah, and J. A. Carrasco. Higher order multi-step Jarratt-like method for solving systems of nonlinear equations: Application to PDEs and ODEs. *Computers and Mathematics with Applications*, 70(4):624–636, 2015.

[19] F. Ahmad, E. Tohidi, and J. A. Carrasco. A parameterized multi-step Newton method for solving systems of nonlinear equations. *Numerical Algorithms*, 71(3):631–653, 2016.

[20] M. Z. Ullah, S. S-Capizzano, and F. Ahmad. An efficient multi-step iterative method for computing the numerical solution of systems of nonlinear equations associated with ODEs. *Applied Mathematics and Computation*, 250:249–259, 2015.

[21] S. Qasim, Z. Ali, F. Ahmad, S. S-Capizzano, M. Z. Ullah, and A. Mahmood. Solving systems of nonlinear equations when the nonlinearity is expensive. *Computers and Mathematics with Applications*, 71(7):1464–478, 2016.

[22] C. T. Bowman, M. Frenklach, G. Smith, W. C. Gardiner, and et al. http://www.me.berkeley.edu/gri-mech/releases.html.

[23] M. D. Smooke, I. K. Puri, and K. Seshadri. A comparison between numerical calculations and experimental measurements of the structure of a counter-flow diffusion flame burning diluted methane in diluted air. *Proceedings of the Combustion Institute*, 21(1):1783–1792, 1988.

[24] M. A. Mueller, T. J. Kim, R. A. Yetter, and F. L. Dryer. Flow reactor studies and kinetic modeling of the H2/O2 reactions. *International Journal of Chemical Kinetics*, 31:113–125, 1999.

[25] J. Wang, Z. Huang, H. Miao, X. Wang, and D. Jiang. Characteristics of direct injection combustion fuelled by natural gas-hydrogen mixtures using a constant volume vessel. *International Journal of Hydrogen Energy*, 33(7):1947–56, 2008.

[26] F. Halter, C. Chauveau, N. Djebaili-Chaumeix, and I. Gokalp. Characterization of the effects of pressure and hydrogen concentration on laminar burning velocities of methane-hydrogen-air mixtures. *Proceedings of the Combustion Institute*, 30(1):201–208, 2005.

[27] D. V. Sarli and D. A. Benedetto. Laminar burning velocity of hydrogen-methane/air premixed flames. *International Journal of Hydrogen Energy*, 32(5):637–647, 2007.

[28] N. Lamoureux, N. Djebaili-Chaumeix, and C. E. Paillard. Laminar flame velocity determination for H2-air-He-CO2 mixtures using the spherical bomb method. *Experimental Thermal and Fluid Science*, 27:385–393, 2003.

[29] J. F. Grcar, R. J Kee, M. D. Smooke, and J. A. Miller. A hybrid Newton/time-integration procedure for the solution of steady, laminar, one-dimensional, premixed flames. *Proceedings of the Combustion Institute*, 21(1):1773–1782, 1986.

[30] K. J. Bosschaart and L. P. H. de Goey. The laminar burning velocity of flames propagating in mixtures of hydrocarbons and air measured with the heat flux method. *Combustion and Flame*, 136:261–269, 2004.

[31] M. D. Smooke. *Reduced Kinetic Mechanisms and Asymptotic Approximations for Methane-Air Flames, Lecture Notes in Physics*. Springer-Verlag, Berlin Heidelberg, 1991.

[32] C. K Law. *Reduced Kinetic Mechanisms for Applications in Combustion Systems, Lecture Notes in Physic*. Springer-Verlag, Berlin Heidelberg, 1993.

[33] V. A. Maaren, D. S. Thung, and L. P. H. De Goey. Measurement of flame temperature and adiabatic burning velocity of methane/air mixtures. *Combustion Science and Technology*, 96(4-6):327–344, 1994.

[34] C. M. Vagelopoulos and F. N. Egolfopoulos. Direct experimental determination of laminar flame speeds. *Proceedings of the Combustion Institute*, 27(1):513–519, 1998.

[35] X. J. Gu, M. Z. Haq, M. Lawes, and R. Woolley. Laminar burning velocity and markstein lengths of methane-air mixtures. *Combustion and Flame*, 121(1-2):41–58, 2000.

[36] G. Rozenchan, D. L. Zhu, C. K. Tse Law, and S. D. Outward propagation, burning velocities, and chemical effects of methane flames up to 60 ATM. *Proceedings of the Combustion Institute*, 29(2):1461–70, 2002.

[37] F. H. V. Coppens, D. J. Ruyck, and A. A. Konnov. Effects of hydrogen enrichment on adiabatic burning velocity and no formation in methane+air flames. *Experimental Thermal Fluid Science*, 31(5):437–444, 2007.

[38] T. Boushaki, Y. Dhué, L. Selle, B. Ferret, and T. Poinsot. Effects of hydrogen and steam addition on laminar burning velocity of methane–air premixed flame: Experimental and numerical analysis. *International Journal of Hydrogen Energy*, 37(11):9412–22, 2012.

[39] O. Kruger. *On the Influence of Steam in Premixed Hydrogen Flames for Future Gas Turbine Applications*. PhD thesis, Technische Universität Berlin, Berlin, 2015.

[40] R. Gunther and G. Janisch. Measurements of burning velocity in a flat flame front. *Combustion and Flame*, 19(1):49–53, 1972.

[41] D. D. S. Liu and R. MacFarlane. Laminar burning velocities of hydrogen-air and hydrogen air-steam flames. *Combustion and Flame*, 49(1-3):59–71, 1983.

[42] C. K. Wu and C. K. Law. On the determination of laminar flame speeds from stretched flames. *Proceedings of the Combustion Institute*, 20(1):1941–49, 1985.

[43] M. IIbas, A. P Crayford, I. Yilmaz, P. J. Bowen, and N. Syred. Laminar-burning velocities of hydrogen–air and hydrogen–methane–air mixtures: An experimental study. *International Journal of Hydrogen Energy*, 31:1768–1779, 2006.

[44] J. Pareja, J. B. Hugo, and Y. Ogami. Measurements of the laminar burning velocity of hydrogen-air premixed flames. *International Journal of Hydrogen Energy*, 35:1812–1818, 2010.

[45] K. T. Aung, M. I. Hassan, and G. M. Faeth. Effects of pressure and nitrogen dilution on flame/stretch interactions of laminar premixed H2/O2/N2 flames. *Combustion and Flame*, 112(1-2):1–15, 1998.

[46] S. D. Tse, D. L. Zhu, and Law C. K. Morphology and burning rates of expanding spherical flames in H2/O2/inert mixtures up to 60 atmospheres. *Proceedings of the Combustion Institute*, 28(2):1793–1800, 2000.

[47] X. Qin, H. Kobayashi, and T. Niioka. Laminar burning velocity of hydrogen–air premixed flames at elevated pressure. *Experimental Thermal Fluid Science*, 21(1-3):58–63, 2000.

[48] O. C. Kwon and G. M. Faeth. Flame/stretch interactions of premixed hydrogen-fueled flames: measurements and predictions. *Combustion and Flame*, 124(4):590–610, 2001.

[49] H. Erjiang, H. Zuahua, H. Jiajia, J. Chun, and Z. Jianjun. Experimental and numerical study on laminar burning characteristics of premixed methane-hydrogen-air flames. *International Journal of Hydrogen Energy*, 34:4876–888, 2009.

[50] B. Somers. *The simulation of flat flames with detailed and reduced chemical models*. PhD thesis, Eindhoven University of Technology, Eindhoven, Netherlands, 1994.

[51] G. Yu, C. K. Law, and C. K. Wu. Laminar flame speeds of hydrocarbon+air mixtures with hydrogen addition. *Combustion and Flame*, 63(3):339–47, 1986.

[52] O. Gicquel, N. Darabiha, and D. Thevenin. Laminar premixed hydrogen/air counter-flow flame simulations using flame prolongation of ILDM with differential diffusion. *Proceedings of the Combustion Institute*, 28:1901–1908, 2000.

3

Correction technique and inclusion of differential diffusion

Abstract. The present work is concerned with developing a tabulated chemistry method to capture differential diffusion effects for practical combustion systems. To take into account differential diffusion effects several approaches use at least 2 or 3-dimensional manifolds. In the present work, a new approach is proposed where a correction to the source term of the progress-variable equation is introduced. The method is developed in the context of the flamelet prolongation of ILDM (FPI) framework. The main feature of this new approach is the use of only one progress-variable equation (1D manifold). This correction technique enables incorporating the complex transport model to the flamelet database. The correction to the source term of the flamelet progress-variable model is made by evaluating the difference between the species equation with unity and non-unity Lewis number. To analyse the performance of the model, one-dimensional freely propagating adiabatic laminar premixed flames, and a two-dimensional adiabatic burner stabilized flame cases are considered. The one-dimensional cases use two different mixtures: CH_4/air and H_2/air. The burner stabilized simulations are performed for a CH_4/air mixture. Additionally, the correction technique is tested for both lean and rich mixture cases. Solutions using the flamelet database are presented with and without correction of the flamelet progress-variable model. Excellent agreement is found between the database with the proposed source term correction and the detailed chemistry solutions.

3.1 Introduction

Reactive flow simulations of practical combustion systems, e.g. engines, furnaces, gas turbines, etc., require the accurate prediction of chemical features like heat release, ignition delay time, flame structure and pollutant formation, etc. Chemical mechanisms are usually designed to accurately model all flame characteristics. A detailed chemical mechanism for hydrocarbon fuels may consists of thousands of species and hundreds or thousands of chemical reactions. To characterise any thermochemical multi-component system, mixture composition and two state variables are needed. Hence, the system has $N_s + 2$ degrees of freedom, being N_s the number of species. For instance, if pressure and temperature are chosen as state variables, then the state vector is an ensemble of state spaces $(P, T, Y_1, Y_2, ..., Y_{N_s})$. However, it is not feasible nowadays to directly simulate the aforementioned system using detailed chemical schemes. Hence, techniques to reduce the computational requirements enable the simulation of these combustion systems with reasonable computational costs.

One approach to reduce the computational cost of chemical reactions has been the reduction of chemical schemes [1, 2], while trying to retain the main features of the complete mechanism. These schemes are mostly based on partial equilibrium and steady state assumptions for specific reactions and or species. In general, these kind of mechanisms give good results. However, their application domain is quite limited, as several suppositions are required to simplify the mechanism and thus, limiting them to given ranges of equivalence ratio, temperature or pressure.

In 1992, Mass and Pope [3] introduced the Intrinsic Low-Dimensional Manifold (ILDM), a new approach to address these difficulties to reduce chemical kinetic schemes. ILDM is based on a mathematical analysis of the chemical process, and therefore, independent of the topology of the flame. By using this method, it is possible to tabulate chemistry and consequently perform numerical computation with reduced computational costs [4–6].

The classical ILDM provides very good results at the high temperature limit close to equilibrium. However, in cold zones, for low temperatures, it is not able to produce correct results when the manifold is described by a small number of coordinates [7]. Besides, the tabulated manifold mostly corresponds to constant atomic mass fractions of the elements present in the chemical system. However, in actual flames the element mass fractions locally vary along the flame front, which is associated with differential diffusion. In general, differential diffusion drives the local equivalence ratio along the flame front. Particularly, this effect is more strong for hydrogen flames. This effect can be taken into account by using an additional coordinate in composition space. However, the result is a higher-dimensional manifold, which in turn increases the computational storage requirements.

To solve this deficiency, a new version of the classical ILDM method was proposed by Gicquel et al. [7]. It enables the solution of combustion phenomena associated

with fast time-scales. The method is known as Flamelet Prolongation of ILDM (FPI). It carries the basic tabulation idea of ILDM, but takes into account differential diffusion modelling. The FPI method deals with differential diffusion by using at least a two-dimensional manifold. This technique consists of an ILDM method in the high temperature range and one-dimensional flame calculations for the low temperature zone instead of the single linear prolongation, as originally proposed in the ILDM. One coordinate is used in state space to describe the mass fractions and a second one for the element mass fractions, thus taking into account differential diffusion. This implementation of the detailed transport progress-variable model for tabulation is complex and computationally expensive. The reason is that this two-dimensional manifold involves storing in and retrieving from the chemical database the transport coefficients of all species. A similar approach was introduced by Oijen and de Goey [8], denoted as Flamelet Generated Manifolds (FGM), but using a different manifold. This approach also gives a good approximation for the major flame characteristics. However, in terms of flame speed and minor species, the flame calculation might still be far from the detailed chemistry and transport model results [7]. For instance, this is the case of large differential diffusivities such as in hydrogen flames. Besides, in that work the enthalpy was introduced as an extra coordinate in order to account for heat losses. Later, Oijen and de Goey [9] also presented a similar method and suggested of using a 1D manifold for the case of unity Lewis number and 2D manifold for non-unity Lewis number cases.

Both FPI and FGM methods provide a basis to replace the detailed chemistry calculation by a chemistry database. Later, to accommodate differential diffusion phenomena, many researchers proposed several extensions. Regele et al. [10] proposed a progress-variable model along with a level-set approach and resolved the local changes of the flame front. Mercier et al. [11] explore these effects through the tabulation of complex transport models and detailed chemistry. Doost et al. [12] captures local composition changes due to differential diffusion by using a 3D manifold and introduces all three transport models, controlling variable equations, in the form of Schmidt numbers. Swart et al. [13] and Donini et al. [14] use similar approaches with the exception of the manifold dimension. Both used a fixed non-unity Lewis number and a progress-variable approach. In the progress-variable model the diffusion term is split into two parts (for constant D and variable D_k). A new diffusion coefficient is introduced and calculated in a preprocessing stage and then stored in the look-up table. Donini et al. [14] extended the work of Swart et al. [13] by including the enthalpy in the manifold coordinate. Therefore, in this case, the one-dimensional manifold is not sufficient to capture differential diffusion effects. Furthermore, in order to improve numerical predictions, one additional control variable has to be included in order to compute the local composition of element mass fraction.

In this paper, and in the context of FPI framework, a new approach to include

differential diffusion effects is presented. The main objective of the present work is the development of a simple and efficient progress-variable model to handle non-unity Lewis number effects by using a 1D manifold. The method is based on correcting the source term of the reaction progress-variable equation. This correction is calculated during the construction of look-up table. The present technique enables the inclusion of differential diffusion in a straightforward way in the flame calculation, without increasing the manifold dimension. In the present work, this technique is studied using one-dimensional laminar adiabatic premixed freely propagating flames, as well as a 2D adiabatic burner stabilized flame.

The outline of this paper is as follows. In the second section, the flamelet model for detailed chemistry is presented. Additionally, the flamelet/progress-variable model for tabulated chemistry is briefly detailed. Following, the FPI database technique and the selection of progress-variable is briefly discussed. It is explained how the manifold can be constructed using the solution of flamelet equations. The development of a relation to correct the source term of the unity Lewis Fickian progress-variable transport equation by taking into account complex transport model is presented. Results of 1D numerical computations are presented in section three. This section is divided in two parts, detailing the results of a methane/air and a hydrogen/air flames, respectively. The fourth section is focused on the coupling of the flamelet model with a corrected source term in the context of a two-dimensional flame. Simulation results of a 2D adiabatic burner stabilized methane/air flame are presented. Conclusions are drawn in the final section.

3.2 Flamelet model

Combustion is a multi-disciplinary phenomena, encompassing fluid dynamics, heat transfer, and chemical kinetics. Thus, the set of equations involved are the Navier-Stokes equations and the energy and species transport equations:

$$\frac{\partial \rho}{\partial t} + \frac{\partial}{\partial x_j}\left(\rho u_j\right) = 0 \tag{3.1a}$$

$$\frac{\partial \rho u_i}{\partial t} + \frac{\partial}{\partial x_j}(\rho u_i u_j) = -\frac{\partial p}{\partial x_i} + \frac{\partial \tau_{ij}}{\partial x_j} + \rho g_i \tag{3.1b}$$

$$\frac{\partial \rho Y_k}{\partial t} + \frac{\partial}{\partial x_j}\left(\rho(u_j + V_j^c)Y_k\right) = \frac{\partial}{\partial x_j}\left(\frac{\rho D_k}{W}\frac{\partial (WY_k)}{\partial x_j}\right) + \dot{\omega}_k \tag{3.1c}$$

$$\rho c_p\left(\frac{\partial T}{\partial t} + u_j\frac{\partial T}{\partial x_j}\right) = \dot{\omega}_T' + \frac{\partial}{\partial x_j}\left(\lambda\frac{\partial T}{\partial x_j}\right) + \rho\left(\sum_{k=1}^{N_s}\frac{c_{p,k}D_k}{W}\frac{\partial (WY_k)}{\partial x_j}\right)\frac{\partial T}{\partial x_j}. \tag{3.1d}$$

where density, viscosity, thermal conductivity and specific heat of mixture are denoted by ρ, μ, λ, c_p, respectively. Sub-index k denotes a species' property. In the momentum

Eq. (3.1b), u_j is the fluid velocity component, $\tau_{ij} = \mu\left(\frac{\partial u_i}{\partial x_j} + \frac{\partial u_j}{\partial x_i} - \frac{2}{3}\frac{\partial u_k}{\partial x_k}\delta_{ij}\right)$ the viscous stress and p the pressure. Additionally, terms $\dot{\omega}_k$ and $\dot{\omega}'_T = \sum_k \dot{\omega}_k h_k$ denote the chemical reaction rate of species and heat release respectively. Enthalpy is denoted by h. In the above equations, species diffusion is described through the Hirschfelder and Curtiss diffusion model, with D_k being the species' diffusivity into the mixture; V_j^c represents the correction velocity to ensure mass conservation [15], and W the mean molecular mass of the mixture.

The primary focus of the present analysis are laminar premixed flames, specifically deflagration ones, where pressure is constant. For a one-dimensional adiabatic steady laminar freely propagating premixed flame, the above equations, can be restated in the flame reference frame, which yields:

$$\dot{m} = const = \rho_u S_L \tag{3.2a}$$

$$\dot{m}\frac{\partial Y_k}{\partial x} + \frac{\partial(\rho V^c Y_k)}{\partial x} = \frac{\partial}{\partial x}\left(\frac{\rho D_k}{W}\frac{\partial(W Y_k)}{\partial x}\right) + \dot{\omega}_k \tag{3.2b}$$

$$\dot{m}\frac{\partial T}{\partial x} = \frac{\dot{\omega}'_T}{c_p} + \frac{1}{c_p}\frac{\partial}{\partial x}\left(\lambda\frac{\partial T}{\partial x}\right) + \frac{\rho}{c_p}\left(\sum_{k=1}^{N_s}\frac{c_{p,k}D_k}{W}\frac{\partial(W Y_k)}{\partial x}\right)\frac{\partial T}{\partial x} \tag{3.2c}$$

where ρ_u represents the fresh gases density and S_L is the laminar flame velocity, which depends on ambient conditions. The system of equations can be solved, along with appropriate boundary conditions for the mass flow rate $\dot{m}$, mass fractions Y_k of all species and temperature T. However, in freely propagating flames $\dot{m}$ is an eigenvalue and must be calculated as part of the flame solution [16]. Therefore, one degree of freedom has to be removed from the system. This is achieved by fixing the reference frame position with respect to the flame. The mass flow $\dot{m}$ can then be found by specifying the temperature at one point and consequently Eq. (3.2c) can be rewritten as follows:

$$\dot{m} = \frac{\frac{\dot{\omega}'_T}{c_p} + \frac{1}{c_p}\frac{\partial}{\partial x}\left(\lambda\frac{\partial T}{\partial x}\right) - \frac{\rho}{c_p}\left(\sum_{k=1}^{N_s} c_{p,k}Y_k V_k\right)\frac{\partial T}{\partial x}}{\frac{\partial T}{\partial x}}. \tag{2d}$$

3.2.1 Flamelet database approach

Tabulation techniques consist of building a database where the flame structure is stored. For premixed cases, a common approach is to use one-dimensional flame solutions to represent the thermochemical data as a function of one coordinate, namely a progress-variable Y_c. This database can be extended to handle different equivalence ratios by adding a further coordinate, the mixture fraction Z. The coordinates or controlling parameters Y_c and Z represent the progress of reaction and fuel/oxidizer ratio, or equivalence ratio, respectively. Such a database, associated with (Y_c, Z), has

been commonly denoted as FPI database [17]. The purpose of defining Z for the premixed case is just to handle different equivalence ratios within a single database, which is associated with different flamelets. In present study, the mixture fraction Z for purely premixed flames is a fixed number.

Laminar flamelets evaluated at a given ambient pressure P_0, and fresh gases temperature, T_0. The FPI database parameters are: (i) Y_c expressed as a linear combination of the species mass fractions discretised by l points; (ii) Z, the equivalence ratio or mixture fraction in case of diffusion flame, discretised by m points. Thus, the look-up table consists of $\mathcal{N}$ discretised info such that $\mathcal{N} = l \times m$ and all number corresponding species or reaction rates or thermodynamic properties are stored N_s. According to all information the size of look-up table must be $N_s \times \mathcal{N}$.

In the construction of the look-up table, the selection of Y_c needs careful attention. Y_c is usually defined as a linear combination of species mass fraction of major species [17, 18]

$$Y_c = \sum_{k=1}^{N} a_k Y_k \tag{3.3}$$

where $a_k \in \mathbb{R}$ denotes a coefficient for the kth species and N number of species used in the progress-variable definition. The a_k values must ensure a unique representation of all flamelet solutions.

It is observed that from lean mixture up to stoichiometric mixtures, specifically CO_2 and H_2O species, for CH_4/air and H_2/air respectively, provide a unique representation of thermochemical data. However, on the rich side, it can not retained uniqueness for all thermochemical data. Therefore, a linear combination of more than one species can be used. For example, the sum of carbon dioxide Y_{CO_2} and carbon monoxide Y_{CO} mass fractions are found to be well adapted for CH_4/air. To track all thermochemical data, it is mandatory to define a one-to-one correspondence between Y_c and all relevant entities of the database. If the progress-variable violates this condition, then Y_c cannot represent the flame solution. Figure 3.1 shows a unique representation of laminar premixed flame projection on (Y_c, T) plane for the different range of CH_4/air mixture. conditions at the unburnt side, and Neumann at burnt side.

Progress-variable model

Having defined a database containing the flame structure as described in Sec. 3.2.1, premixed flames can be computed by solving the Navier-Stokes equations, Eq. (3.1a) and Eq. (3.1b) together with a transport equation for Y_c:

$$\frac{\partial \rho Y_c}{\partial t} + \frac{\partial}{\partial x_j}\left(\rho u_j Y_c\right) = \frac{\partial}{\partial x_j}\left(\rho D \frac{\partial Y_c}{\partial x_j}\right) + \dot{\omega}_c \tag{3.4}$$

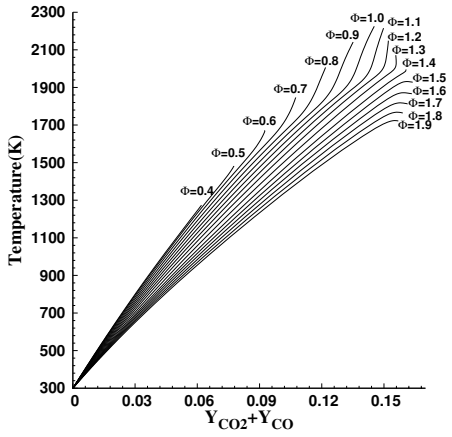

Figure 3.1: Projection of a 2-dimensional FPI onto $(CO_2 + CO, T)$ plane for methane/air stoichiometric mixture using unity Lewis number. GRI3.0 chemical mechanism is used at $T_0 = 300K$ and atmospheric pressure.

where $D = \frac{\lambda}{\rho c_p}$ and $\dot{\omega}_c$ are the progress-variable diffusivity and reaction rate, respectively. The former equation implies the assumption of a unity Lewis number ($Le_k = 1$), as it is detailed afterwards in Sec. 3.2.2. The progress-variable Y_c is a reactive scalar. When normalised, a zero value represents the fresh gasses and a unity value the burnt gasses. Its solution can be regarded as a tracker of progress of the chemical reactions through the database, namely the flamelet solutions. Therefore, its definition depends on the considered fuel. For one-dimensional adiabatic steady laminar freely propagating premixed flames, Eq. (3.4) becomes

$$\dot{m}\frac{\partial Y_c}{\partial x} = \frac{\partial}{\partial x}\left(\rho D \frac{\partial Y_c}{\partial x}\right) + \dot{\omega}_c \tag{3.5}$$

However, to fully capture the flame structure, the combustion model should also be able to represent all flame dynamics. Therefore, it is important to capture the Lewis number variation of the flame. For example, Fig. 3.2 shows that the Lewis number plays a dominant role in the flame propagation speed for the case of CH_4/air adiabatic propagating flame.
Furthermore, the unity Lewis assumption also affects the structure of the flame in general. Additionally, this hypothesis ensures that element mass fractions along the flame are kept constant. For non-unity cases, the atomic mass fraction of elements may locally change, meaning that the local equivalence ratio changes along the flame front due to differential diffusion. Thus, the consideration of differential diffusion

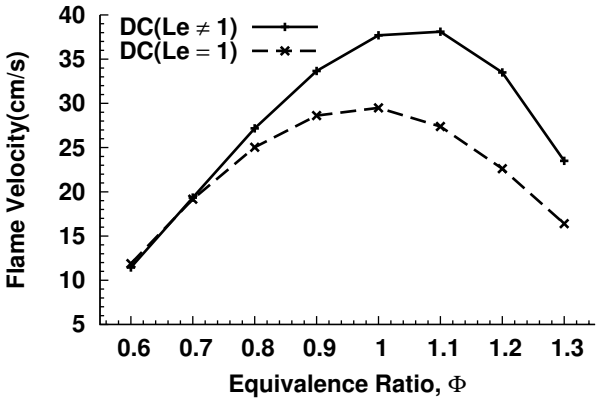

Figure 3.2: CH_4/air premixed flame laminar burning velocity using GRI3.0. DC denotes detailed chemistry solution. In brackets the unity or non-unity Lewis number assumption.

effects is very important for practical combustion systems [19].

3.2.2 Source term correction

Many researchers have proposed different techniques to include differential diffusion effects in a tabulated chemistry framework [12–14]. In general, by adding an additional parameter, that is, by using 2 or 3-dimensional manifolds. In this work, a one-dimensional manifold with a correction to the source term of a flamelet progress-variable model is proposed. With this approach, prediction of the differential diffusion effects only requires one progress-variable parameter. In general, the progress-variable equation, Eq. (3.5), can be directly obtained from Eq. (3.2b) when the assumption of the unity Lewis number ($D = D_k$ for all species) is made. However, it is not able to express the solution for non-unity Lewis number, the complex transport case, as further evidenced by the results shown in Sec. 3.3.

To proceed with the analysis, first it is shown how the flamelet equations and the progress-variable transport equation are related and how complex transport fits in. Recalling the species flamelet Eq. (3.2b) and rewriting them considering unity and non-unity Lewis number,

$$\dot{m}\frac{\partial Y_k}{\partial x} = \frac{\partial}{\partial x}\left(\rho D \frac{\partial Y_k}{\partial x}\right) + \dot{\omega}_k \tag{3.6a}$$

$$\dot{m}\frac{\partial Y_k}{\partial x} = \frac{\partial}{\partial x}\left(\rho D_k \frac{\partial Y_k}{\partial x} + \frac{\rho D_k Y_k}{W}\frac{\partial W}{\partial x}\right) + \dot{\omega}_k \tag{3.6b}$$

In these equations the velocity correction has not been considered for the sake of simplicity. Beginning with the Fickian diffusion case with unity Lewis number, Eq. (3.5) can be derived from flamelet Eq. (3.6a) as $\frac{\partial}{\partial x}$ is a linear operator and, by definition, the reaction progress-variable can be expressed as $\frac{\partial}{\partial x}\left(\sum_{k=1}^{N} a_k Y_k\right) = \sum_{k=1}^{N}\left(\frac{\partial}{\partial x} a_k Y_k\right)$. Therefore, addition of the N flamelet Eqs. (3.6a) results in the unity Lewis Y_c transport equation, in which it has been taken $a_k = 1$ for the sake of simplicity and without loss of generality,

$$\begin{aligned} &\dot{m}\frac{\partial}{\partial x}\left(\sum_{k=1}^{N} Y_k\right) = \frac{\partial}{\partial x}\left(\rho D \frac{\partial\left(\sum_{k=1}^{N} Y_k\right)}{\partial x}\right) + \sum_{k=1}^{N}\dot{\omega}_k \\ &\implies \dot{m}\frac{\partial Y_c}{\partial x} = \frac{\partial}{\partial x}\left(\rho D \frac{\partial Y_c}{\partial x}\right) + \dot{\omega}_c \end{aligned}$$

since $Y_c = \sum_{k=1}^{N} Y_k$ and $\dot{\omega}_c = \sum_{k=1}^{N}\dot{\omega}_k$. Hence, for the unity Lewis assumption, the progress-variable equation, when solved along with mass and momentum equations, correctly represents the flamelet solutions. In case of non-unity Lewis number, the above equation does not satisfy the flamelet complex transport equation. Proceeding as previously, but now considering Eq. (3.6b), the resulting equation is

$$\dot{m}\frac{\partial}{\partial x}\underbrace{\left(\sum_{k=1}^{N} Y_k\right)}_{Y_c} = \underbrace{\sum_{k=1}^{N}\frac{\partial}{\partial x}\left(\rho D_k \frac{\partial Y_k}{\partial x} + \frac{\rho D_k Y_k}{W}\frac{\partial W}{\partial x}\right)}_{\neq \frac{\partial}{\partial x}\left(\rho D \frac{\partial Y_c}{\partial x}\right)} + \underbrace{\sum_{k=1}^{N}\dot{\omega}_k}_{\dot{\omega}_c} \tag{3.8}$$

where $D \neq D_k$. Then, the aim is to modify Eq. (3.5) to represent the dynamics described by Eq. (3.8), which include complex transport coefficients. In other words, it is intended to use a database based on flamelet solutions evaluated with complex transport, but using Eq. (3.5) for Y_c with a modified source term S' (defined below) instead of $\dot{\omega}_c$. The modified source term is evaluated by relating (3.5) and (3.8). For convenience, tags are introduced for the terms of both equations to ease the algebraic operations. Defining

$$\begin{aligned} A &= \dot{m}\frac{\partial Y_c}{\partial x} \\ B &= \sum_{k=1}^{N}\left(\frac{\partial}{\partial x}\left(\rho D_k \frac{\partial Y_k}{\partial x} + \frac{\rho D_k Y_k}{W}\frac{\partial W}{\partial x}\right)\right) \\ S &= \dot{\omega}_c \end{aligned}$$

Eq. (3.8), can then be rewritten as follows

$$A = B + S \tag{3.9}$$

where S represents its source term. Therefore, the modified source term S' can be found writing the progress-variable transport equation including differential diffusion as

$$A = B' + B + S - B' \quad \Longrightarrow \quad S' = B + S - B' \implies A = B' + S'$$

where B' represents the diffusion term when $Le_k = 1$, i.e. $B' = \frac{\partial}{\partial x}\left(\rho D \frac{\partial Y_c}{\partial x}\right)$. The S' the source term can then be evaluated from the above expression as

$$S' = \dot{\omega}_c + \sum_{k=1}^{N}\left(\frac{\partial}{\partial x}\left(\rho D_k \frac{\partial Y_k}{\partial x} + \frac{\rho D_k Y_k}{W}\frac{\partial W}{\partial x}\right)\right) - \frac{\partial}{\partial x}\left(\rho D \frac{\partial Y_c}{\partial x}\right) \tag{3.10a}$$

or equivalently by

$$S' = \dot{m}\frac{\partial Y_c}{\partial x} - \frac{\partial}{\partial x}\left(\rho D \frac{\partial Y_c}{\partial x}\right). \tag{3.10b}$$

This correction is performed after having solved the flamelet equations with differential diffusion Eq. (3.2). Hence, once the solution of a flamelet has been computed, the corrected source term S' is evaluated and stored into the look-up table instead of $\dot{\omega}_c$. Therefore, this source term includes both chemical reaction rates and differential diffusion effects. With this approach differential diffusion effects are accounted for by Y_c while only using a one parameter tabulation and retaining the unity Lewis number assumption for the definition of the progress-variable diffusivity.

3.3 Numerical results : 1D cases

In this section, numerical results for 1D steady adiabatic laminar premixed flames are presented. Specifically, two freely adiabatic propagating flames are considered: CH_4/air and H_2/air. All 1D computations are performed for equivalence ratios $\phi = 0.7, 1.0, 2.0$ at $T_0 = 300K$ and atmospheric pressure. Furthermore in both cases, the GRI3.0 chemical mechanism is used [20], which involves $N_s = 53$ species and 325 reactions. In all cases, solutions using detailed chemistry are obtained, namely solving Eq. (3.2). The set of flamelet Eqs. (3.2) are solved using an in-house one-dimensional C++ code. It is a dedicated 1D numerical simulation code to solve laminar premixed flame using detailed chemical schemes. The C++ code is based on finite difference formulation. Discretization used is of second order. The 1D flamelet equations are solved by using a modified Newton damped method.

Flamelet look-up tables are built by taking the detailed chemistry solutions and using Y_c as coordinate. Two look-up tables are generated for comparison: one taking

into account the source correction term, Eq. (3.10b), to the progress-variable Eq. (3.5), and without correcting the source term. Then, using the databases, 1D laminar flames are computed by solving Eq. (3.5). In the case of tabulated/database chemistry solution, the unknowns of the system are $\dot{m}$ and Y_c. Eq. (3.2a) and Eq. (3.5) are solved together and $\dot{m}$ can be found by reducing one degree of freedom from the system.

$$\dot{m} = \frac{\frac{\partial}{\partial x}(\rho D \frac{\partial Y_c}{\partial x}) + \dot{\omega}_c}{\frac{\partial Y_c}{\partial x}} \tag{3.11}$$

The $\dot{m}$ equation is solved at the specific node where the flame reference is fixed.

In the following, two abbreviations are introduced to ease the discussion: wSC and $woSC$ denote a flamelet model with and without source correction, respectively. Furthermore, DC stands for detailed chemistry, that is, solving Eq. (3.2). Four different cases are studied for the two considered flames and described as

(a) Detailed chemistry with unity Le_k: DC(Le_k= 1)
(b) Detailed chemistry with non-unity Le_k: DC($Le_k \neq$1)
(c) Non-unity Le tabulated/database chemistry with source correction: TC(wSC)
(d) Non-unity Le tabulated/database chemistry without source correction: TC($woSC$)

All cases are solved using the same mesh. The length of the domain is 4cm. However, for better presentation of the results, plots are presented using a shorter domain. It is important to note here the difference between cases (c) and (d): the progress-variable model is the same, i.e, they are build using DC solutions with non-unity Le_k. However, the databases differ only by the source term of the Eq. (3.5): $\dot{\omega}_c$ or S'.

3.3.1 Methane/air

Three different equivalence ratios of CH_4/air are studied. Results are presented in Fig. 3.3, Fig. 3.4 and Fig. 3.5. For this fuel, differences between detailed chemistry solutions with unity and non-unity Lewis number are marginal, specifically concerning the flame structure. However, the flame propagation speed is prominently different as shown in Figure 3.2 as well as in the Table 3.1 for particular cases.
Furthermore, because of differential diffusion effects, the differences are most noticeable for rich mixtures. Specifically, for an equivalence ratio of $\phi = 2.0$, results of both $Le = 1$ and also database $woSC$ show the limits of the model. This indicates that the unity Lewis number assumption in both DC and database case $woSC$ do not describe the flame characteristics correctly, particularly on the rich side.
However, there is an excellent agreement between the DC case with $Le_k \neq 1$ and the database case wSC. Major species such as CO_2 and H_2O are adequately reproduced. Additionally, minor species, such as HCO and OH, are also well represented, which are not shown here for the sake of brevity. It follows that the database wSC correctly captures the structure of the flame as well as the flame propagation speed.

Table 3.1: CH_4/air laminar flame speed (cm/s). Experimental results for ϕ =0.7 and 1.0 correspond to Park et al. [21] and for ϕ =2.0 to Erjiang et al. [22], which are retrieved by curve fitting.

ϕ	S_L DC($Le = 1$)	S_L DC($Le_k \neq 1$)	S_L TC(wSC)	S_L TC($woSC$)	S_L Exp.
0.7	19.16	19.35	19.36	22.63	19.48
1.0	29.49	37.70	37.76	44.01	37.40
2.0	3.22	3.65	3.66	4.36	4.02

3.3.2 Hydrogen/air

An H_2/air flame is also studied for the same equivalence ratios. In this case, results for a minor species HO_2 are also shown. This species is important because it plays a significant role in the preheating zone of hydrogen flames [7].

Table 3.2: H_2/air flame speed(m/s). The experimental results are retrieved by curve fitting from Liu and MacFarlane [23].

ϕ	S_L DC($Le = 1$)	S_L DC($Le_k \neq 1$)	S_L TC(wSC)	S_L TC($woSC$)	S_L Exp.
0.7	1.19	1.42	1.43	1.46	1.41
1.0	1.66	2.53	2.57	40.80	2.52
2.0	1.85	3.25	3.29	54.24	3.46

Flame propagating speeds for all cases are presented in the Table 3.2. For this case, the unity Lewis number assumption results in laminar flame speeds markedly different from reported experimental values. Inclusion of differential diffusion effects results in flames with correct values. Regarding the flamelet computations, the database $woSC$ produces incorrect flame speeds, specially for rich mixture cases. Besides, for the detailed chemistry case with unity Lewis number, the propagation speed is found to be lower compared to the non-unity DC and database wSC cases.

Additionally, as Fig. 3.6, Fig. 3.7 and Fig. 3.8 show, inclusion of differential diffusion effects result in significant changes in the flame structure. For instance, in flames as the one here considered, HO_2 is a radical with stiff kinetics. Correct computation of its kinetics is very important at low temperatures, because this species is formed and destroyed in the preheating zone [7], as can be seen in Fig. 3.6, Fig. 3.7 and Fig. 3.8. For this species, the maximum relative differences between $Le_k = 1$ and $Le_k \neq 1$

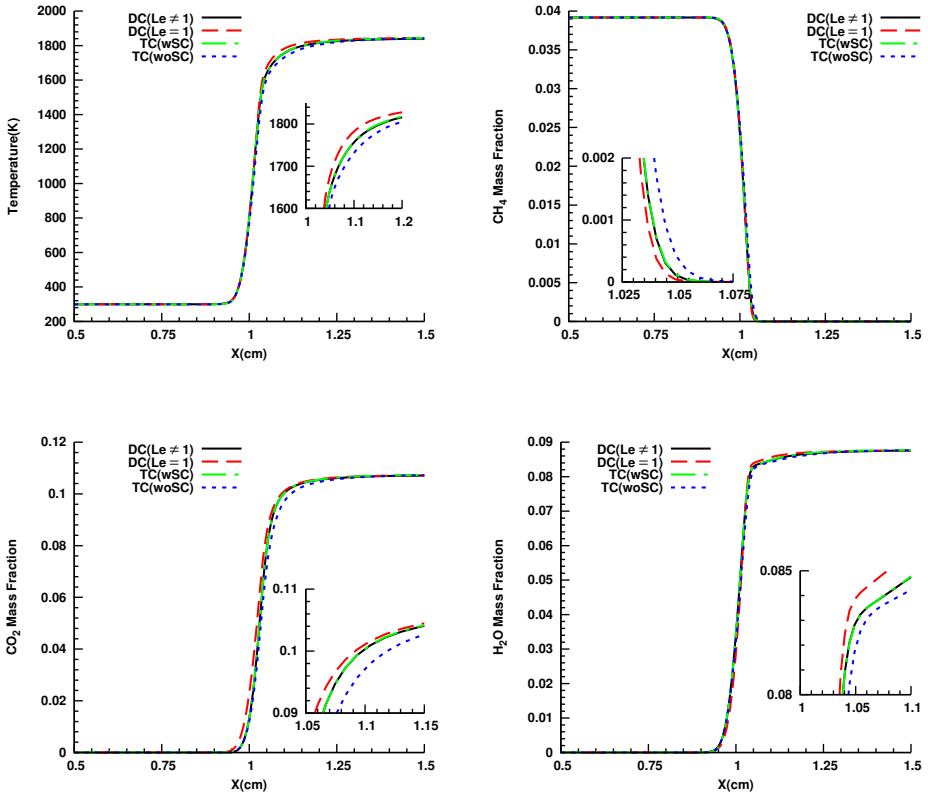

Figure 3.3: 1D flame solutions of CH_4/air mixture $\phi = 0.7$. Simulation domain ranges between 0 and 4 cm. Shown is a subset.

cases, found at the peak value of the curve, are 33%, 37% and 33% corresponding to ϕ=0.7, 1.0 and 2.0, respectively.

Regarding the results obtained using the database approach, the flamelet database *woSC* is unable to predict the propagation speed as well as the structure of the flame, specially for rich mixtures. On the other hand, as it can be seen in the figures, there is a very good agreement between the DC($Le_k \neq 1$) and database *wSC* solutions. This agreement is found not only for the temperature and major species, but also for radicals such as OH and H_2O_2, here not presented. Consequently, the database *wSC* calculations correctly captures the flame structure as well as the flame propagation

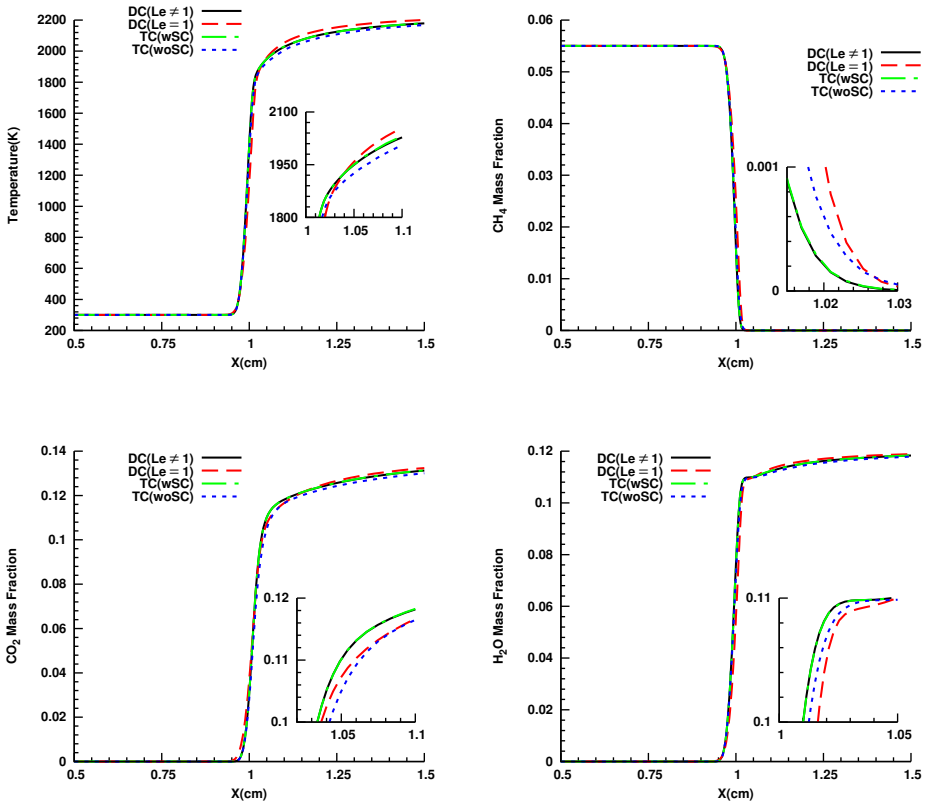

Figure 3.4: 1D flame solutions of CH_4/air mixture $\phi = 1.0$. Simulation domain ranges between 0 and 4 cm. Shown is a subset.

speed. This comparison between detailed chemistry $Le_k \neq 1$ and database with correction shows that the 1D manifold can accurately capture all features of one-dimensional flames.

3.4 2D case: Slot-burner

3.4.1 Case definition

In order to further analyse the behaviour of the flamelet correction technique, numerical simulations of a 2-dimensional slot-burner is performed. Its geometry is

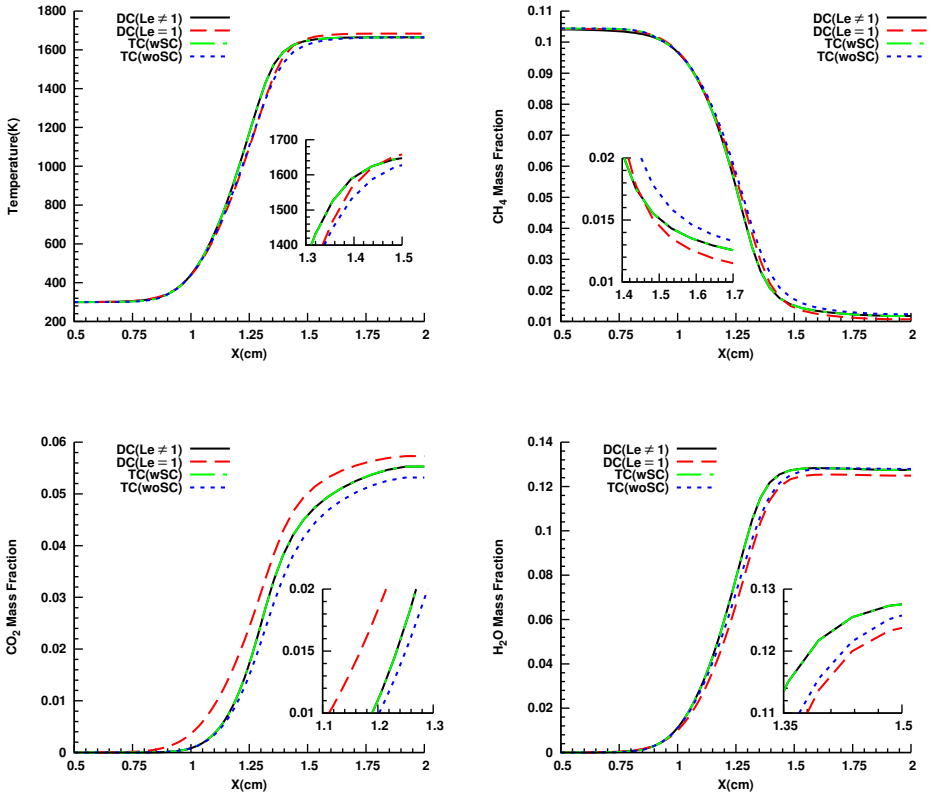

Figure 3.5: 1D flame solutions of CH_4/air mixture $\phi = 2.0$. Simulation domain ranges between 0 and 4 cm. Shown is a subset.

shown in Fig. 3.9. The case geometry corresponds to the one studied by Somers and de Goey [24]. The slot-burner is 4 mm wide, while the chamber is 12 mm wide. In the present study, all chamber walls are considered adiabatic. Furthermore, radiation heat losses are neglected. Inflow velocity profile is parabolic with a peak value of 1.1 m/s. In this section, all computations are performed for half-domain, because of the symmetry of the domain.

Inflow gases are a mixture of CH_4 and air. Fresh gases mixture is at $T_0 = 300K$ and atmospheric pressure. Chemical kinetics are modelled using the Smooke mechanism [25], which consists of 15 species and 46 reactions. This chemical mechanism is used

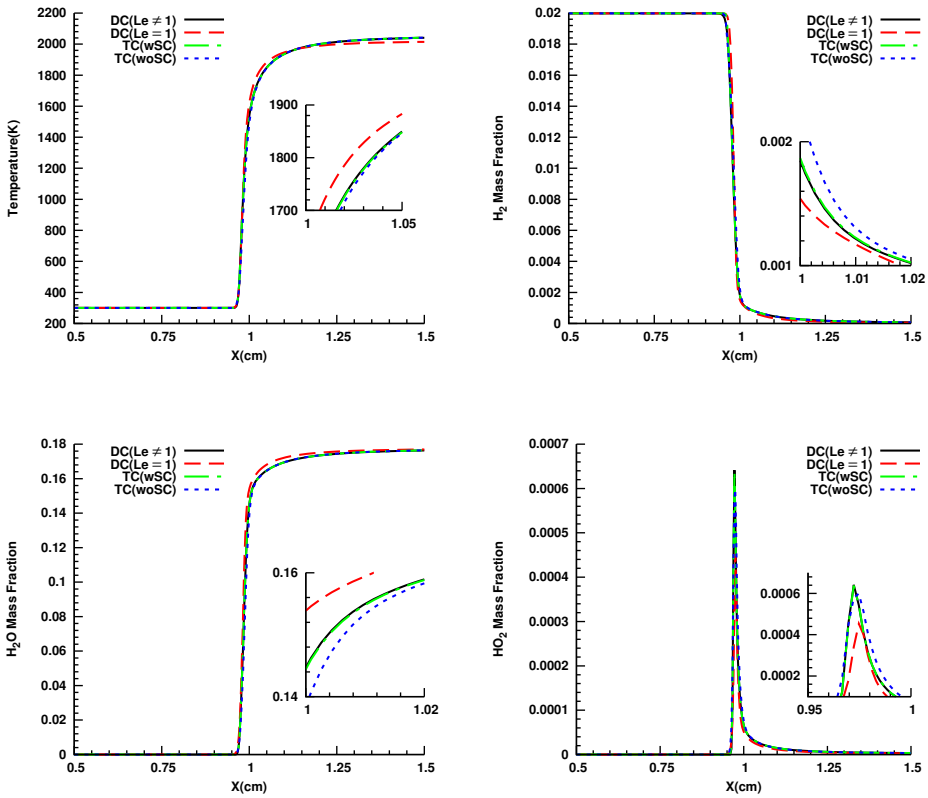

Figure 3.6: 1D flame solutions of H_2/air mixture $\phi = 0.7$. Simulation domain ranges between 0 and 4 cm. Shown is a subset.

for both detailed chemistry and tabulated chemistry simulations.

Numerical computations are carried out using the general purpose unstructured and parallel object-oriented Computational Fluid Dynamics (CFD) code TermoFluids [26]. A finite-volume approach is used to solve the different transport equations. Temporal integration is performed using a 2nd order predictor-corrector scheme [27]. A symmetry-preserving scheme [28] is used to discretise the convective terms in the momentum equations. For the scalar equations, a QUICK scheme is used [27]. A second order central difference scheme is used to construct the discrete diffusive term for all transported quantities.

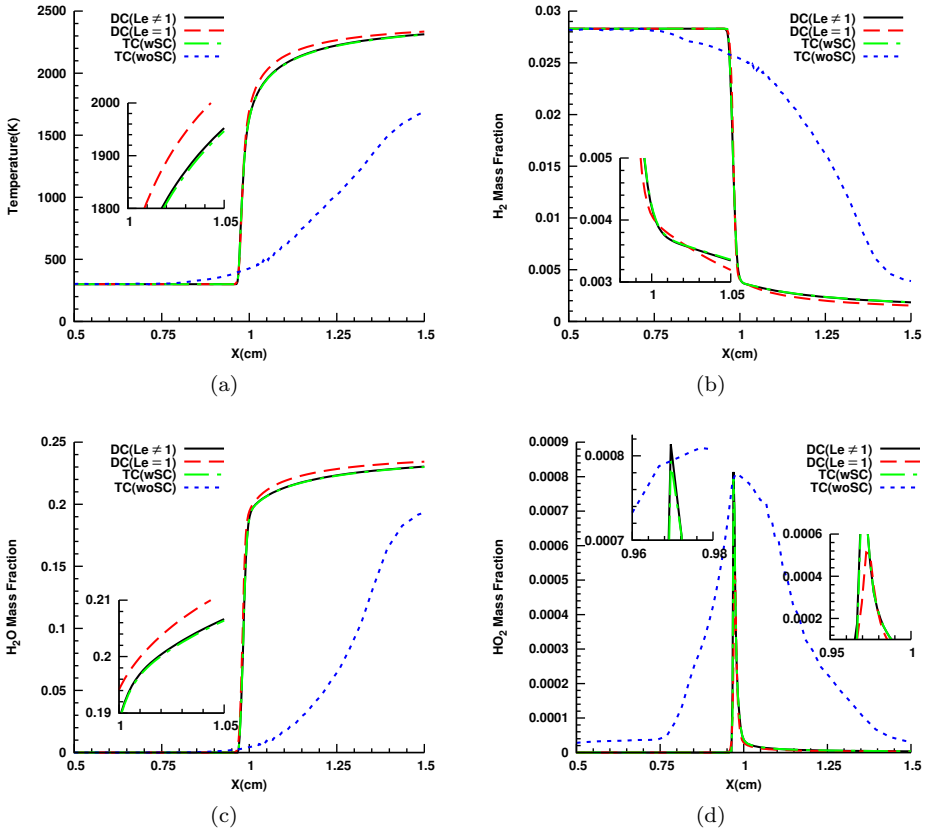

Figure 3.7: 1D flame solutions of H_2/air mixture $\phi = 1.0$. Simulation domain ranges between 0 and 4 cm. Shown is a subset.

The equations are solved on a body-fitted mesh, with a minimum size of $\Delta x = 0.05$ mm and maximum size $\Delta x = 0.28$ mm. Simulations were run on different meshes to achieve mesh independent solutions. Reported results correspond to the finest mesh, which consists of approximately 14700 cells. A high mesh resolution is used in the area near the flame front to correctly capture the flame front structure. With this mesh, the flame front was represented by five control volumes. Comparatively, the rest of the domain features a lower mesh density.

In this section, the slot-burner is studied using detailed chemistry (DC) and tabulated chemistry (TC). For the latter case, both corrected and uncorrected databases

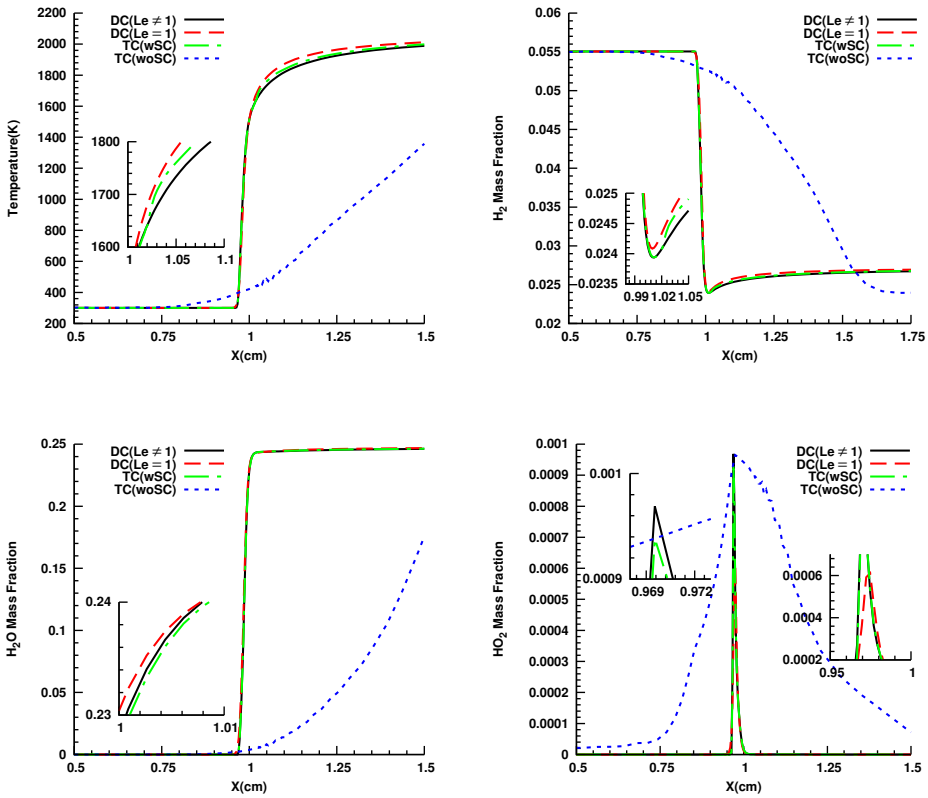

Figure 3.8: 1D flame solutions of H_2/air mixture $\phi = 2.0$. Simulation domain ranges between 0 and 4 cm. Shown is a subset.

are considered. Additionally, Lewis number effects are discussed. All cases are run on the same mesh and initial conditions for both detailed and tabulated chemistry. The flamelet database for this test simulation is generated by computing unstretched 1D adiabatic freely propagating flames, with differential diffusion effects included. However, it is important to note that the 2D slot-burner configuration affects the flame topology due to stretch and curvature effects [8]. Nonetheless, under appropriate conditions, the influence of these two effects can be minimised.

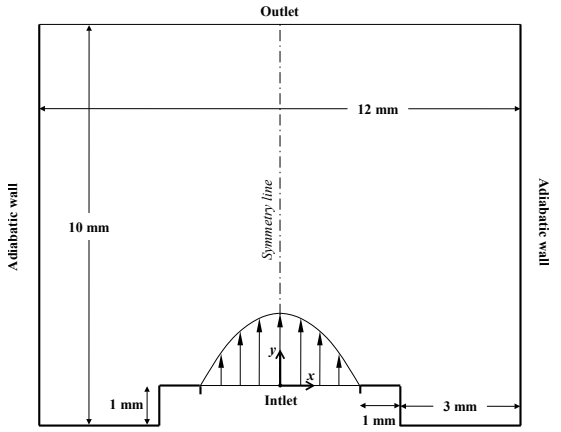

Figure 3.9: Slot-burner configuration for CH_4/air premixed flame.

3.4.2 Numerical results for stoichiometric mixture

Considering a stoichiometric mixture, results using DC($Le_k \neq 1$) and TC(wSC) are presented in Fig. 3.10. In the former, the temperature distribution as well as relevant mass fractions, specifically H_2O, CO and HCO are shown. As can be observed, the flame height is represented rather well by the TC(wSC) approach comparative to DC($Le_k \neq 1$). Still, two main differences can be observed between them. First, the flame peak position, defined by the position of the maximum temperature gradient in the axial direction, is slightly under-predicted by the TC computations. The relative difference in flame height between TC(wSC) and DC($Le_k \neq 1$) is approximately 1.3 %, being the former shorter. Nonetheless, without the source correction, differences between DC($Le_k \neq 1$) and TC($woSC$) are much more pronounced, as depicted in Fig. 3.12, where results for the database without correction case are shown.

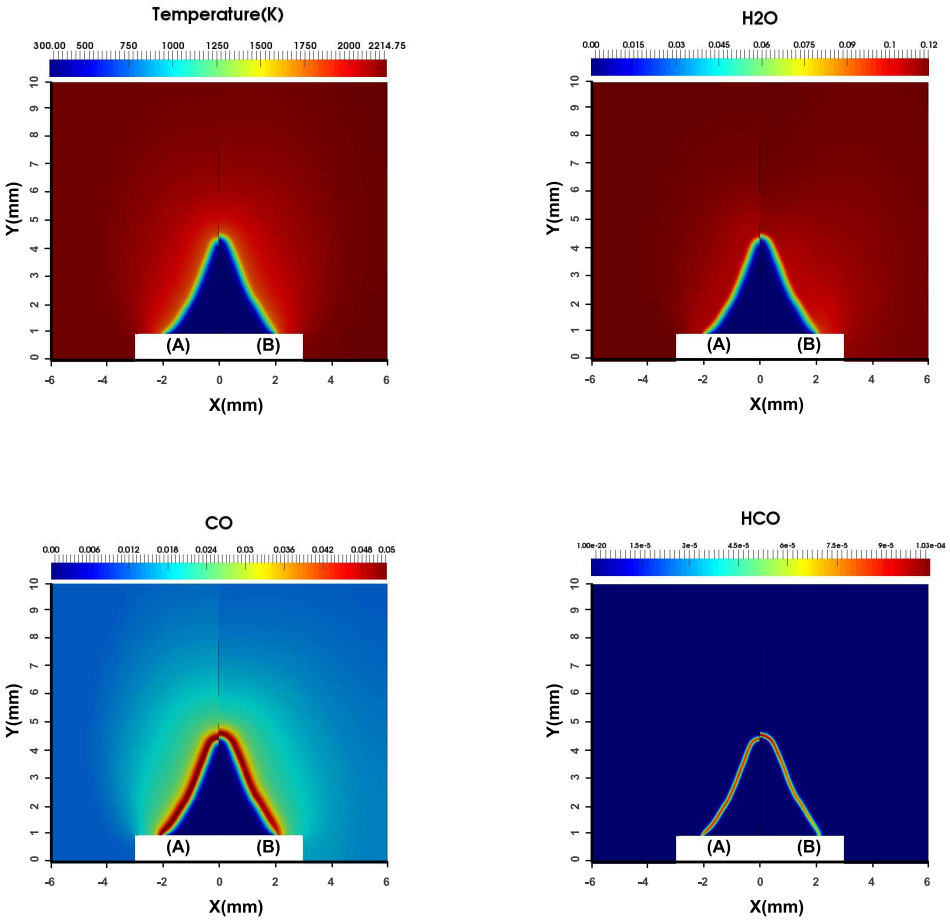

Figure 3.10: Colour-level representation of temperature and mass fractions of H_2O, CO and HCO for ϕ=1.0. In each figure, results on the left side (indicated with letter A) correspond to TC(wSC) and on the right side (letter B) to DC($Le_k \neq 1$).

Sectional profiles of temperature and mass fractions are shown in Fig. 3.11. As can be observed in Fig. 3.11b, CO_2 presents a deviation at the tip of the flame due to the different heights of the flame fronts, which is mainly caused by stretch, which presents its maximum value at the tip. The calculated deviations between DC($Le_k \neq 1$) and TC(wSC) are approximately 1 %, 11 %, 9 % and 9 % for temperature, CO, CO_2

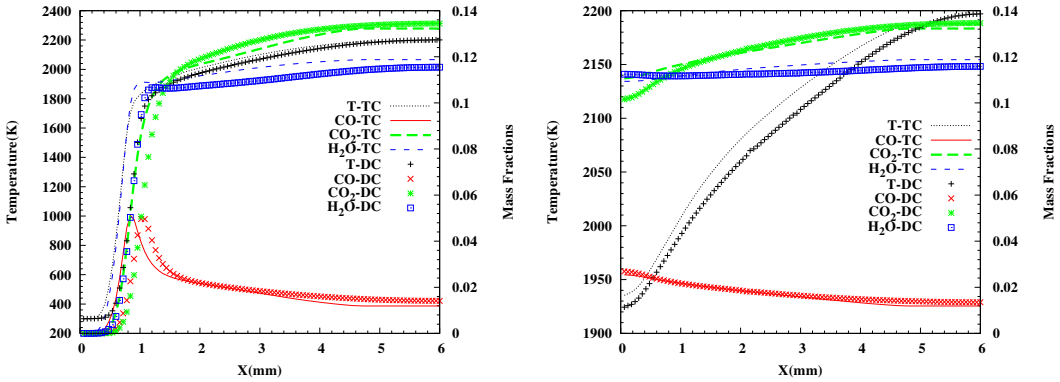

(a) y = 3 mm (b) y = 5 mm

Figure 3.11: Section profiles of temperature and mass fractions of CO, CO_2 and H_2O along x-axis at two different axial positions (y = 3 mm and y = 5 mm); for mixture ϕ=1.0. TC computations are performed with wSC.

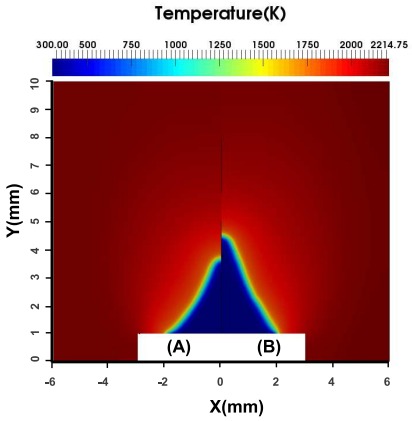

Figure 3.12: Comparison of temperature between TC($woSC$) and DC($Le_k \neq 1$) for mixture ϕ=1.0 (see caption of Fig. 3.10 for further detail).

and H_2O, respectively. Furthermore, it is observed that the temperature for the TC case reaches a maximum, namely the adiabatic flame temperature, different than the one predicted by the DC case. This difference is attributed to flame stretch, which is not accounted for in the construction of the flamelet database. Thus, adiabatic flame

temperatures of TC and DC are different. Further discussion in relation to this point is given afterwards.

Second, the shape of the flame front is slightly different. Furthermore, as evidenced by the HCO mass fraction, the flame structure obtained using the database approach is not exactly the same as with the detailed chemistry computations. Considering the TC case, chemical reactions are uniformly distributed along the flame front, from the flame base up to the flame peak. However, for the DC, chemical reactions are located close to the flame peak, whereas close to the flame base chemical reactions are not as significant, as depicted by the value lower HCO mass fraction in that region.

The differences observed between DC($Le_k \neq 1$) and TC(wSC) are mainly attributed to stretch effects. Hence, simulations considering $Le_k = 1$ for stoichiometric mixture and $Le_k \neq 1$ for lean mixture are presented in the next section in order to evidence this.

3.4.3 Flame stretch and Lewis number

In this section, the cause of slightly different flame height and flame front shape in the former case is investigated. For this, same stoichiometric mixture case is studied. However, a unity Lewis number assumption is made to compute the solution.

It is well known that deviations from 1D flow in premixed flames, such as flame curvature and non-uniform flow along the flame, might lead to local variations in flame temperature and mass burning rate. Stretching changes the burning rate and hydrodynamics of the flame. Still, the flame front dependence on stretching is not the only cause. Buckmaster [29] presents a critical assessment of flame stretch. There, it is concluded that the burning velocity does not only depend on the flame stretch but also on the Lewis number of the flame. Further, this statement is also confirmed by Law et al. [30], who states that flame stretch can only influence the flame response in combination with preferential diffusion effects.

To assess the later statement, DC and TC simulations using unity Lewis number have been computed. Results are presented in Fig. 3.13. In this case temperature and three different species are shown (H_2O, CO, HCO). This comparison shows that the main characteristics of the flame between TC and DC match very well. For example flame front position, the magnitude of species and temperature are reproduced excellently.

To show further details, two sectional profiles of temperature, CO_2, H_2O and CO are presented in Figure 3.14. These profiles are taken at 4 mm and 6 mm along the flame direction (y-axis). The profiles show an excellent agreement between detailed chemistry and tabulated chemistry solutions. At the 6 mm sectional profile, only the temperature slightly deviates (less than 1%), which may be due to numerical errors that are related to the database interpolations. These results show that the database created with a Fickian diffusion model with unity Lewis number assumption correctly captures all major flame characteristics of a flame with unity Lewis number. This

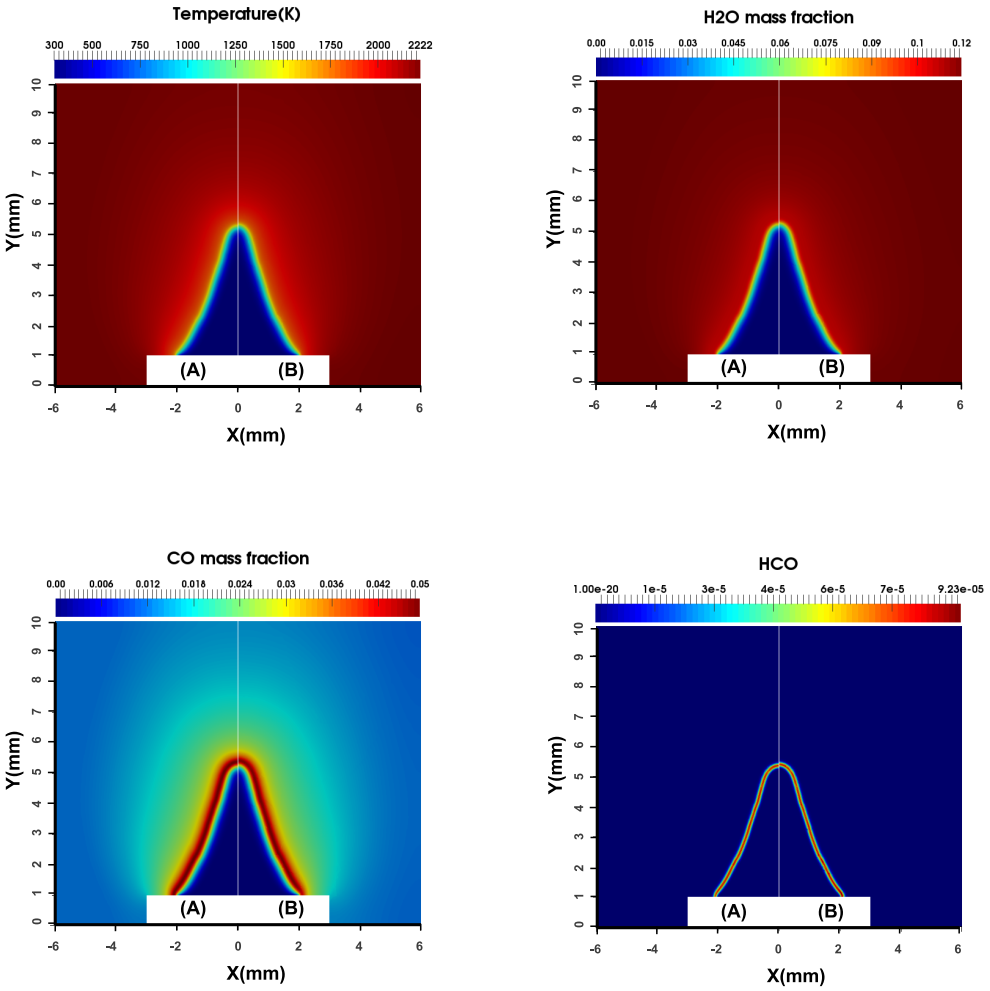

Figure 3.13: Colour-level representation of temperature and mass fractions of H_2O, CO and HCO with unity Lewis assumption (see caption of Fig. 3.10 for further detail).

solution is in accordance with the findings of Law et al. [30, 31], that is, the unity

Lewis number flame is unaffected by stretch. In the same vein, Oijen and de Goey [9] presented 1D manifold solutions computed with unity *Le* number for the case of counter-flow flames, and showed good agreement between detailed chemistry computations and simulations using a flamelet database. Therefore, in present results, this is a somewhat validation of Oijen and de Goey work, however with a new configuration (adiabatic slot-burner flame).

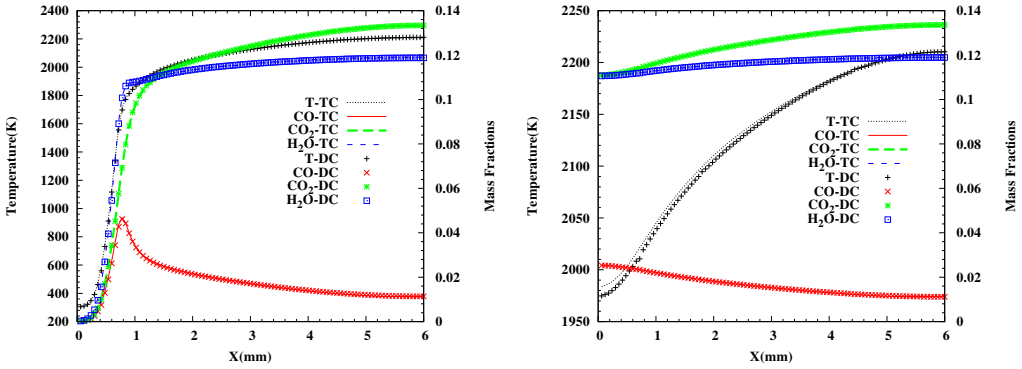

(a) y = 4 mm (b) y = 6 mm

Figure 3.14: Section profiles of temperature and mass fractions of CO, CO_2 and H_2O along x-axis at two different axial positions (y = 4 mm and y = 6 mm); for mixture ϕ=1.0.

Overall, considering the above presented and 1D simulation results, shown in Sec. 3.3, it can be concluded that the differences observed in the results of Sec. 3.4.2 are caused by stretch. Furthermore, the results using DC($Le_k \neq 1$) in Fig. 3.10 show that the flame front is slightly uplifted with respect to the TC(wSC) cases. This implies that the burning velocity in the DC is lower than in the TC cases, which in turn translates into lower temperatures for the former one, as also detailed by Law et al. [30, 31].

3.4.4 Numerical results for lean mixture

In order to minimise the effect of flame stretch on the flame, and thus not having to increase the size of the manifold, inflow velocities are reduced for the following case of study. Furthermore, in the following a leaner flame ($\phi = 0.7$) is considered.

The maximum flow velocity of the fresh gases is set to $0.2m/s$, instead of the calculated 1D propagating speed of an unstretched adiabatic laminar premixed flame. A slightly higher velocity is used in the simulations in order to avoid flame flashback because of the multi-dimensional geometry, which affects the flame dynamics.

Regarding the latter, the equivalence ratio is also reduced to further decrease the stretch effects. In this sense, Bechtold and Matalon [32] presented a correlation of Markstein number, namely flame stretch, versus equivalence ratios of several fuels, among them CH_4/air, which is in accordance to the experimental findings of Dowdy et. al. [33] and Aung et. al. [34]. Based on these findings, it can be stated that since a stoichiometric flame results in higher temperatures, it leads to a higher flow expansion. Consequently, through this higher flow expansion a higher stretch effect will be present. Therefore, in the following the equivalence ratio is decreased in order to decrease the flow expansion and consequently, the stretch. Besides, if the equivalence ratio were increased, since the adiabatic temperature would decrease, the same effect would be achieved. For the sake of brevity, only results for a lean case are presented.

In this case, numerical simulation results are also obtained by using both databases, wSC and $woSC$. Comparing the results between DC($Le_k \neq 1$) and TC(wSC) are shown in Fig. 3.15. Shown are temperature, H_2O, CO and HCO mass fractions. As it can be seen, there is excellent agreement between both results, indicating the suitability of the proposed technique.
A detail view of the calculations is shown in Fig. 3.16. It can be observed a good match between TC(wSC) and the DC($Le_k \neq 1$) solutions. The maximum difference found, among all variables of this case, is 3.5% for the CO mass fraction.

For the case of DC($Le_k \neq 1$) versus TC($woSC$), only the temperature colour-plot is shown in Fig. 3.17. Again, the database without the correction, and built using flamelets with differential diffusion, shows a deviation from the detailed chemistry calculations, indicating its inability to reproduce the complex transport phenomena. However, simulation results that are based on the proposed correction technique correctly reproduce both major and minor species. Hence, with a 1D manifold, differential diffusion effects are correctly accounted for.

3.5 Conclusions

A novel approach to include differential diffusion effects into flamelet models using chemistry stored in a database has been proposed. Specifically, the work has been carried out in the context of the Flame Prolongation of ILDM (FPI).

The proposed model has been first validated for 1D laminar adiabatic premixed propagating flames. Comparison of detailed chemistry solutions DC($Le_k \neq 1$) and corrected database solutions TC(wSC), shows an excellent agreement. On the basis of the presented results for the CH_4/air and H_2/air flames, it can be concluded that consistency between flamelet solutions included into the flamelet database and the transport equation used for Y_c is an important issue. It has been shown that flamelet database created using flamelet solutions including differential diffusion is not cor-

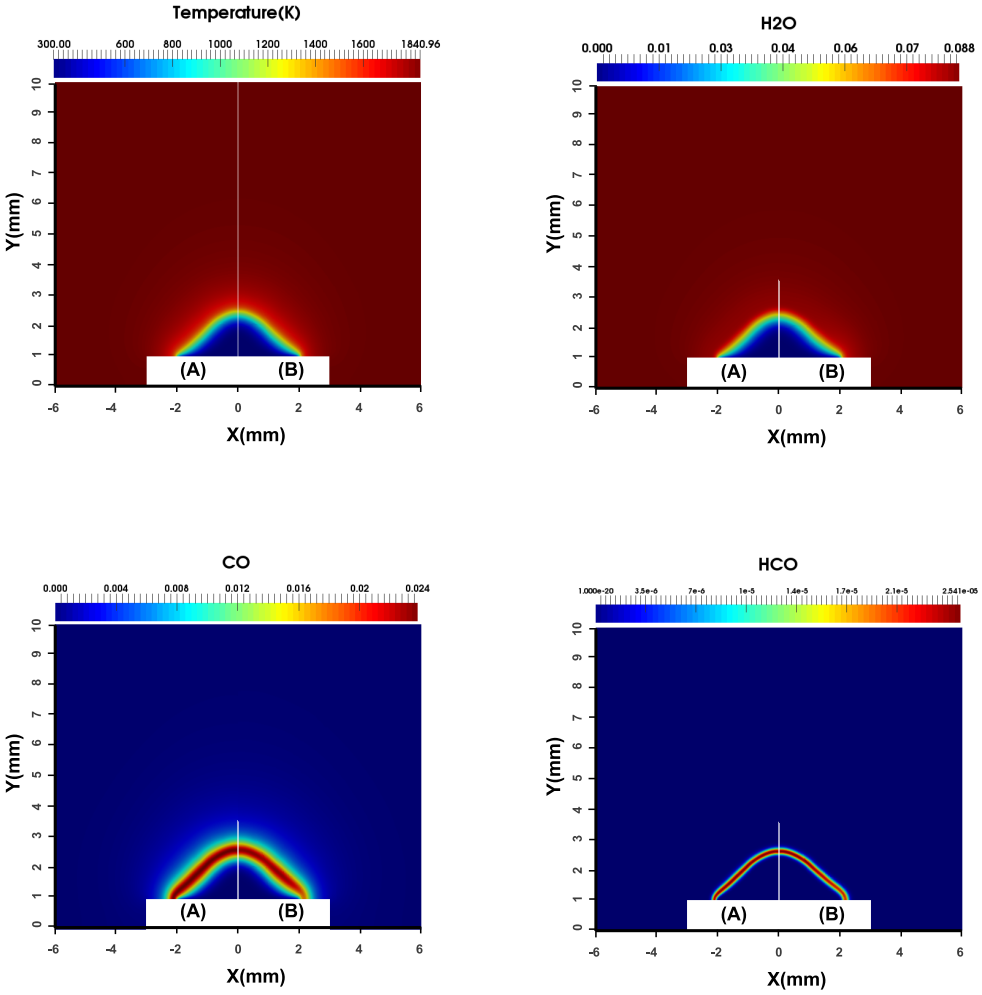

Figure 3.15: Colour-level representation of temperature and mass fractions of H_2O, CO and HCO for mixture ϕ=0.7 (see caption of Fig. 3.10 for further detail).

rectly represented by a Y_c transport equation with a unity Lewis number, namely the database without source correction ($woSC$). Results show a deviation compared to

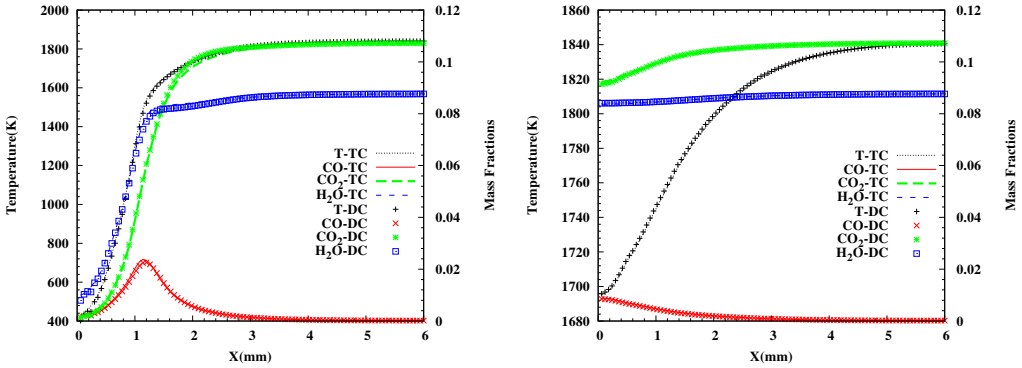

(a) y = 2 mm (b) y = 3 mm

Figure 3.16: Section profiles of temperature and mass fractions of CO, CO_2 and H_2O along x-axis at two different axial positions (y = 2 mm and y = 3 mm); for mixture ϕ=0.7. TC computations are performed with wSC.

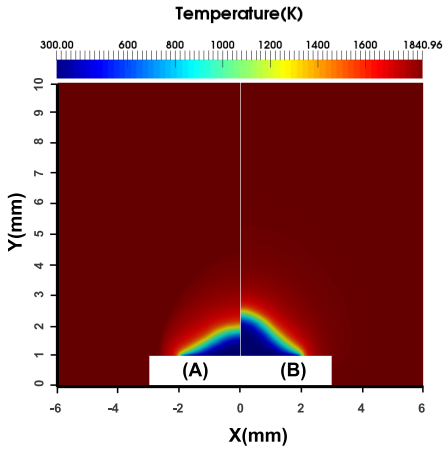

Figure 3.17: Comparison of temperature between TC($woSC$) and DC($Le_k \neq 1$) for mixture ϕ=0.7 (see caption of Fig. 3.10 for further detail).

the reference solutions, namely the detailed chemistry DC, and the evaluated ones from the database. Hence, the database TC($woSC$) is not able to correctly capture the flame front structure as well as its position. However, in the case of a complex

transport model and database with source correction TC(wSC), the results are excellently matched. Thus, the proposed method is able to account for differential diffusion effects without increasing the size of the flamelet manifold.

Following, a 2D premixed adiabatic burner stabilized flame is studied. Flamelet databases for this case were built using 1D unstretched flames. The primary goal is to present the effectiveness of the correction technique to integrate differential diffusion effects in a multidimensional case in a flamelet modelling context, specifically in the context of a FPI framework. In general, good agreement is found between detailed chemistry computations and the proposed approach. Nonetheless, stretch effects were also present. However, once minimised, the source term correction approach shows a good performance. Results using the source term correction are found to be in good agreement with detailed chemistry solutions, which evidenced the capabilities of the technique. It ensures that only one progress-variable is sufficient to include differential diffusion effects in database cases.

Although not directly addressed, besides accuracy, a further consideration to be taken into account for the present approach is computational efficiency. Because differential diffusion effects are directly incorporated to the progress-variable transport equation, no additional parameter nor transport equation need to be solved. Furthermore, the size of the database is not increased with respect to the unity Lewis number case. Thus, memory usage is also not increased.

As a final note, although the present work is focused on premixed flames, the correction approach can be easily extended to non-premixed cases.

References

[1] N. Peters. Numerical and asymptotic analysis of systematically reduced reaction schemes for hydrocarbon flames. In *Proceedings of the Symposium Held at INRIA Sophia-Antipolis*, 1985.

[2] N. Peters and B. Rogg. *Reduced Kinetic Mechanisms for Applications in Combustion Systems, Lecture Notes in Physic.* Springer-Verlag, Berlin Heidelberg, 1992.

[3] U. Maas and S. Pope. Simplifying chemical kinetics: Intrinsic low-dimensional manifolds in composition space. *Combustion and Flame*, 88:239–264, 1992.

[4] U. Maas and S. Pope. Laminar flame calculations using simplified chemical kinetics based on intrinsic low-dimensional manifolds. *Proceedings of the Combustion Institute*, 25(1):1349–1356, 1994.

[5] U. Maas. Coupling of chemical reaction with flow and molecular transport. *Applications of Mathematics*, 40(3):249–266, 1995.

[6] D. Schmidt, J. Segatz, U. Riedel, J. Warnatz, and U. Maas. Simulation of laminar methane-air flames on automatically simplified chemical kinetics. *Combustion Science and Technology*, 113(1):03–16, 1996.

[7] O. Gicquel, N. Darabiha, and D. Thevenin. Laminar premixed hydrogen/air counter-flow flame simulations using flame prolongation of ILDM with differential diffusion. *Proceedings of the Combustion Institute*, 28:1901–1908, 2000.

[8] J. A. V. Oijen and L. P. H. de Goey. Modeling of premixed laminar flames using flamelet-generated manifolds. *Combustion Science and Technology*, 161(1):113–137, 1999.

[9] J. A. V. Oijen and L. P. H. de Goey. Modeling of premixed counter-flow flames using the flamelet-generated manifold method. *Combustion Theory and Modeling*, 6(3):463–478, 2002.

[10] J. D. Regele, E. Knudsen, H. Pitsch, and G. Blanquart. A two-equation model for non-unity lewis number differential diffusion in lean premixed laminar flames. *Combustion and Flame*, 160(2):240–250, 2013.

[11] R. Mercier, P. Auzillon, V. Moureau, N. Darabiha, O. Gicquel, D. Veynante, and B. Fiorina. LES modeling of the impact of heat losses and differential diffusion on turbulent stratified flame propagation: Application to the TU darmstadt stratified flame. *Flow, Turbulence and Combustion*, 93(2):349–381, 2014.

[12] A. S. Doost, A. Ketelheun, A. Sadiki, and J. Janicka. Differential diffusion effects in fgm context for premixed LES of hydrogen blended fuels. In *Proceedings of the European Combustion Meeting*, 2015.

[13] J. A. M. de Swart, R. J. M. Bastiaans, J. A. V. Oijen, L. P. H. de Goey, and R. C. Stewart. Inclusion of preferential diffusion in simulations of premixed combustion of hydrogen/methane mixtures with flamelet generated manifolds. *Flow, Turbulence and Combustion*, 85(3):473–511, 2010.

[14] A. Donini, R. J. M. Bastiaans, J. A. V. Oijen, and L. P. H. de Goey. Differential diffusion effects inclusion with flamelet generated manifold for the modeling of stratified premixed cooled flames. *Proceedings of the Combustion Institute*, 35(1):831–837, 2015.

[15] T. Poinsot and D. Veynante. *Theoretical and Numerical Combustion*. R.T. Edwards Inc., 2005.

[16] M. D. Smooke, J. A Miller, and R. J. Kee. Determination of adiabatic flame speeds by boundary value methods. *Combustion Science and Technology*, 34(1-6):79–90, 1983.

[17] B. Fiorina, R. Baron, O. Gicquel, D. Thevenin, S. Carpentier, and N. Darabiha. Modelling non-adiabatic partially premixed flames using flame-prolongation of ILDM. *Combustion Theory and Modelling*, 7:449–470, 2003.

[18] F. A. Lammers and L. P. H. de Goey. The influence of gas radiation on the temperature decrease above a burner with a flat porous inert surface. *Combustion and Flame*, 136(4):533–47, 2004.

[19] R. Hilbert, F. Tap, H. El-Rabii, and D. Thévenin. Impact of detailed chemistry and transport models on turbulent combustion simulations. *Progress in Energy and Combustion Science*, 30:61–117, 2004.

[20] C. T. Bowman, M. Frenklach, G. Smith, W. C. Gardiner, and et al. http://www.me.berkeley.edu/gri-mech/releases.html.

[21] O. Park, S. Peter, N. Liu, and N. E. Fokion. Combustion characteristics of alternative gaseous fuels. *Proceedings of the Combustion Institute*, 33:887–894, 2011.

[22] H. Erjiang, X.. Li, M. Xin, Y. Chen, Y. Cheng, Y. Xie, and Z. Huang. Laminar flame speeds and ignition delay times of methane–air mixtures at elevated temperatures and pressures. *Fuel*, 158:1–10, 2015.

[23] D. D. S. Liu and R. MacFarlane. Laminar burning velocities of hydrogen-air and hydrogen air-steam flames. *Combustion and Flame*, 49(1-3):59–71, 1983.

[24] L. M. T. Somers and L. P. H. De Goey. A numerical study of a premixed flame on a slit burner. *Combustion Science and Technology*, 108:121–132, 1995.

[25] M. D. Smooke, I. K. Puri, and K. Seshadri. A comparison between numerical calculations and experimental measurements of the structure of a counter-flow diffusion flame burning diluted methane in diluted air. *Proceedings of the Combustion Institute*, 21(1):1783–1792, 1988.

[26] O. Lehmkuhl, C.D. Pérez Segarra, R. Borrell, M. Soria, and A. Oliva. Termofluids: A new parallel unstructured CFD code for the simulation of turbulent industrial problems on low cost PC cluster. *Proceedings of the Parallel CFD Conference*, pages 1–8, Antalya, Turkey, 2007.

[27] J. Ventosa-Molina, J. Chiva, O. Lehmkuhl, J. Muela, C.D. Pérez-Segarra, and A. Oliva. Numerical analysis of conservative unstructured discretisations for low mach flows. *International Journal for Numerical Methods in Fluids*, In press, 2016.

[28] R. W. C. P. Verstappen and A. E. P. Veldman. Symmetry-preserving discretization of turbulent flow. *Journal of Computational Physics*, 187:343–368, 2003.

[29] J. D. Buckmaster. Two examples of stretched flame. *Q. Journal of Mechanics and Applied Mathematics*, 35(2):249–63, 1982.

[30] C. K Law, D. L. Zhu, and G. Yu. Propagation and extinction of stretched premixed flame. *Proceedings of the Combustion Institute*, 21(1):1419–1426, 1988.

[31] C. K. Law. Dynamics of stretched flame. *Proceedings of the Combustion Institute*, 22(1):1381–1402, 1989.

[32] M. Matalon and J. K. Bechtold. The dependence of the markstein length on stoichiometry. *Combustion and Flame*, 127:1906–1913, 2001.

[33] D. R. Dowdy, D. B. Smith, S. C. Taylor, and A. Williams. The use of expanding spherical flames to determine burning velocities and stretch effects in hydrogen/air mixtures. *Proceedings of the Combustion Institute*, 23(1):325–332, 1991.

[34] K. T. Aung, M. I. Hussan, and G. M. Faeth. Flame stretch interactions of laminar premixed hydrogen/air flames at normal temperature and pressure. *Combustion and Flame*, 109(1-2):1–24, 1997.

4

Analysis of partially premixed flames using flamelet models

Abstract. The present chapter is devoted to the study of partially premixed flames using flamelet models. The ability of premixed and non-premixed models are studied as single mode solutions for multi-regime flames. To check the capability and critical aspects of the flamelet database different types of flames are analyzed. To support the discussion of flamelet databases, finite rate chemistry solutions and classical diffusion flamelets approaches are also considered for all cases. A series of 3D jet coflow simulations are performed for mixture equivalence ratios of $\phi = \infty$, $\phi = 6.16$ and $\phi = 3.08$. Results obtained using flamelet databases, classical flamelet diffusion database and finite rate chemistry approaches are compared with experimental data. The results show good agreement in general with the experimental data and evidence the capabilities and limitation of each flamelet database approach as single mode solution of partially premixed flames.

4.1 Introduction

In the last decades, most studies reported in the literature have been concerned with experimental and numerical analysis of premixed and non-premixed flames. More recently, there has been increasing interest in the area of partially premixed combustion due to the wide range of their application, as in house-hold and industrial heating systems [1, 2]. The terminology of partially premixed flames (PPFs) or multi-regime flames indicates that in a flame some regions at some instants are burning like a premixed flame, while some other, or the same, regions at some instants are burning like a non-premixed flame. A PPF is a flame where in the fuel stream a mixture of fuel and oxidizer is present. Additionally, further oxidizer is available to provide for the complete combustion. One example of partial premixing is the base region of a lifted jet flame [3–8]. PPFs are present in many combustion applications: Bunsen burners, furnaces, gas- turbine combustors, gas-fired domestic appliances, internal combustion engines, etc.

The common use of PPFs in combustion applications, most of them under turbulent regimes, has motivated the interest scientific community in their mathematical modelling and numerical solution. A large variety of approaches exists to tackle their modeling. Among them, different combustion models are based on the laminar flamelet concept. This concept of flamelet-type combustion [7, 9–11] make particularly strict assumptions about how mixing processes and chemistry interact. On the one hand, mathematical models that rely on the non-premixed flamelet equations [12, 13] are strictly valid only in the non-premixed combustion regime. In this regime fuel and oxidizer enter reaction zones from different directions or streams. On the other hand, premixed modelling is required when fuel and oxidizer enter the reaction zone in a fully mixed state. Combustion models based on the premixed flamelet equations [14–16] are strictly valid only in premixed combustion regimes. In many reactive flows, the assumption of a single burning regime is valid and a traditional flamelet implementation may describe combustion accurately [9, 12]. In other flows, however, combustion occurs in multiple or mixed regimes in which a single regime assumption no longer holds. To study these kind of combustion flows in the context of mixed regimes, traditional models must be extended beyond single regime implementations.

Still, it is of interest to analyse the capacity of the single-regime flamelets in representing mixed-mode regimes. To this end, a jet flame is considered burning in different modes: from a pure diffusion flame to a premixed mode. The aim is to understand what are the capabilities and limitations of the single-mode flamelets. The traditional approach for locating the regime is the flame index [18-20]. In these approaches, the flame index is constructed by examining the alignment of gradients of fuel and oxidizer. A modified version of this approach to extend its applicability has also been addressed [5]. In a recent work of Domingo et al. [7], flame regime is defined using the flamelet transformations and by considering the relative magnitude

of a series of Damköhler numbers describing different physical processes. Through the aforementioned indicators, it is possible to identify which regions of the flame are burning in which mode and characterize the need for using multi-regime flamelets.

The object of this study is to use of computations of 3D partially premixed coflow flames to assess the features of PPFs and explore all characteristics of PPFs by finite chemistry and flamelet approach. Two particular questions motivate the study. First, study of PPFs using premixed and non-premixed flamelet databases and comparison with the finite rate chemistry solutions (detailed chemistry). Second, highlight the capabilities and shortcomings of single mode flame databases for solution of multi-regimes flame.

The outline of this chapter is as follows. The configuration of the geometry and case definition are provided in the second section. Section three covers the mathematical models, namely detailed chemistry and flamelet approaches. In the same section, the detail of tabulation technique and definition of the progress variable are also explained. Numerical simulations of all cases including results and discussions are provided in section four. Conclusions are drawn in the final section.

4.2 Case definition

The studied flame is a laminar CH_4/air flame in a coflow with a burner configuration as defined by Bennet et al. [2]. This flame has been analysed by many researchers experimentally and numerically [2, 17–20]. Furthermore, this flame configuration has been studied for different burning conditions, ranging from a pure diffusion case to almost premixed cases.

In the present work three flames are computationally simulated by considering different levels of premixing of the primary inlet. The first one represents a non-premixed flame, with an equivalence ratio of $\phi = \infty$. The other two are partially premixed with equivalence ratios $\phi = 6.16$ and $\phi = 3.08$. Equivalence ratios, inlet flow rates, and stoichiometric mixture fraction conditions are listed in Table 4.1. Primary air is oxygen-enriched (25% O_2 by volume) and secondary air is regular (20.9 % O_2). Methane and primary air flow rates in the inner jet are given by the three entries in the Q_{CH_4} and Q_{air} columns, respectively. Flow rates in the outer jet are defined in the last row of Table 4.1. At the first column of the table labels for each case are introduced to identify studied configuration.

The geometry of the case is described in Fig. 4.1. Fuel mixed with primary air flows from an un-cooled circular tube of inner radius, $r_i = 5.55$ mm, with a wall thickness of $w_i = 0.8$ mm. Air is injected from the annular region between this tube and a concentric $r_o = 47.6$ mm inner radius brass cylinder. The outer tube thickness is $w_o = 3.4$ mm. The axial boundaries are at z=0 and z=200 mm. For the formulation

Table 4.1: Flame parameters for computations

	ϕ	Q_{CH_4} (cm^3/min)	Q_{air} (cm^3/min)	V_z (cm/s)	Y_{CH_4}	Y_O	Y_{N_2}
	Inner jet						
NPMF	∞	330	0	5.67	1.0	0.0	0.0
PPF6	6.16	330	420	12.89	0.30226	0.19627	0.50147
PPF3	3.08	330	840	20.11	0.17803	0.23121	0.59076
	Outer jet						
	All	0	44000	10.48	0.0	0.232	0.768

of boundary conditions, the latter can be considered infinitely far from the flame. Neumann boundary conditions are applied at vertical walls and exit of burner. The inlets boundary conditions are defined in Sec. 4.4.1.

4.3 Mathematical models

4.3.1 Finite rate chemistry models

A three dimensional detailed model based on the full analysis of transport equations in physical space is used [21, 27]. For this study combustion process is described by the Navier-Stokes equations for low Mach number flows namely, continuity, and momentum along with species and energy equations. All the equations have already been described in Chapter 1, specifically Eqs. (1.22), (1.23), (1.33), (1.25).

4.3.2 Flamelet models

Two types of flamelet models are studied in this chapter. One of them is described the premixed combustion phenomenon. The second one is associated with non-premixed flames.

Diffusion flame The species and energy equations can be expressed in a flame reference space, where based on an asymptotic analysis, tangential gradients in comparison to normal terms are neglected. The mathematical model can be expressed as follows, considering a Fickian diffusion assumption for further detail on the derivation

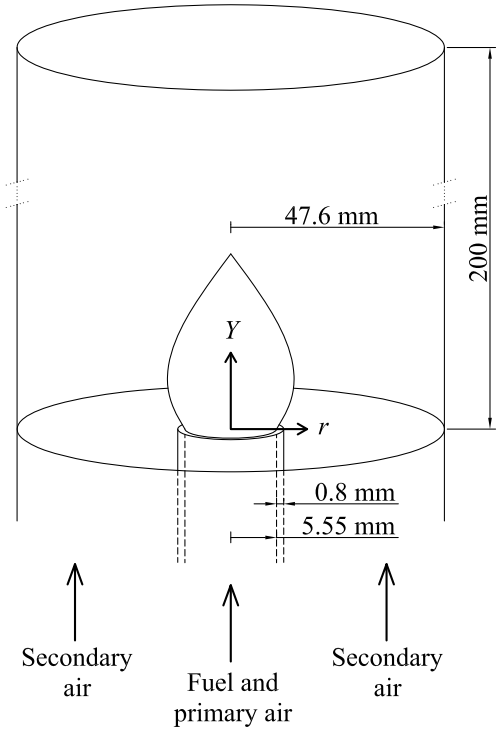

Figure 4.1: Schematic diagram of coflow burner.

refer to Ventosa-Molina [21]

$$\rho\frac{\partial Y_k}{\partial \tau} = \dot{\omega}_k + \frac{\rho\chi_Z}{2}\frac{Le_Z}{Le_k}\frac{\partial^2 Y_k}{\partial Z^2} + \frac{1}{4}\frac{\partial Y_k}{\partial Z}\left[2\rho\chi_Z\frac{\partial}{\partial Z}\left(\frac{Le_Z}{Le_k}\right) + \left(\frac{Le_Z}{Le_k} - 1\right)\left(\frac{\partial \rho\chi_Z}{\partial Z} + \frac{\chi_Z}{D_Z}\frac{\partial \rho D_Z}{\partial Z}\right)\right] \tag{4.1a}$$

$$\rho\frac{\partial T}{\partial \tau} = \frac{\rho\chi_Z}{2}Le_Z\frac{\partial^2 T}{\partial Z^2} - \frac{1}{c_p}\dot{q}^R - \frac{1}{c_p}\sum_{k=1}^{N_s}\dot{\omega}_k h_k + \frac{\rho\chi_Z}{2}\frac{Le_Z}{c_p}\frac{\partial c_p}{\partial Z}\frac{\partial T}{\partial Z} - \sum_{k=1}^{N_s}\frac{\rho\chi_Z}{2}\frac{Le_Z}{Le_k}\frac{\partial Y_k}{\partial Z}\left(1 - \frac{c_{p,k}}{c_p}\right)\frac{\partial T}{\partial Z} \tag{4.1b}$$

where Y_k, $\dot{w}_k$, h_k, $c_{p,k}$ and Le_k are the species mass fraction, reaction rate, enthalpy, heat capacity and Lewis number. T, ρ, Le_Z and κ denote the temperature, mixture

density, mixture fraction Lewis number, thermal conductivity. $\dot{q}^R$ represents radiative heat losses. $\chi_Z = 2D_Z\left(\frac{\partial Z}{\partial x_i}\frac{\partial Z}{\partial x_i}\right)$ is the scalar dissipation rate and D_Z is the mixture diffusivity. In flamelet Eq. (4.1), χ is the scalar dissipation rate, which introduces flow effects into flamelet space, and is defined as

$$\chi = 2D_z(\nabla Z.\nabla Z) \tag{4.2}$$

where D_z is the diffusion coefficient of the mixture fraction equation. To solve the diffusion flamelet equations in a preprocessing stage a functional form for χ as a function has to be prescribed [21]

$$\chi(Z) = a_\infty \frac{f(Z)}{f(Z_{st})} \tag{4.3}$$

where a_∞ is the nominal strain rate in counter flow configuration,

$$f(Z) = \frac{\Phi}{\pi} e^{(-2[erf^{-1}(2Z)]^2)}$$

and erf^{-1} is the inverse of complementary error function. Φ is a coefficient for variable density effects.

Solution to flamelet equations Eqs. (4.1) can be represented in the $T_{st} - \chi_{st}$ plane, depicting the S-shaped curve, as show in Fig. 4.2 for a methane/air flame.

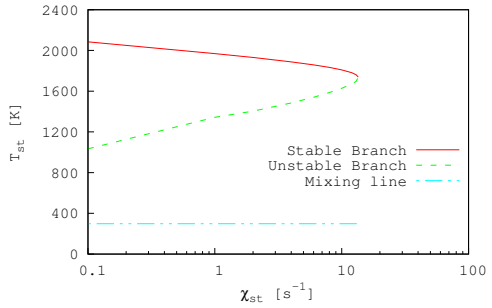

Figure 4.2: S-shaped curve for a methane/air flame.

Premixed flame The equations describing a premixed flame in a flamelet reference can be expressed as

$$\dot{m} = const = \rho_u S_L \tag{4.4a}$$

$$\dot{m}\frac{\partial Y_k}{\partial x} + \frac{\partial(\rho V^c Y_k)}{\partial x} = \frac{\partial}{\partial x}\left(\frac{\rho D_k}{W}\frac{\partial(WY_k)}{\partial x}\right) + \dot{\omega}_k \tag{4.4b}$$

$$\dot{m}\frac{\partial T}{\partial x} = \frac{\dot{\omega}'_T}{c_p} + \frac{1}{c_p}\frac{\partial}{\partial x}\left(\lambda\frac{\partial T}{\partial x}\right) + \frac{\rho}{c_p}\left(\sum_{k=1}^{N_s}\frac{c_{p,k}D_k}{W}\frac{\partial(WY_k)}{\partial x}\right)\frac{\partial T}{\partial x} \tag{4.4c}$$

V_j^c represents the correction velocity and W the mean molecular mass of the mixture. S_L is the laminar flame velocity and $\dot{m}$ is the mass flow rate. For more detail refer to Chapter 2.

In the context of tabulation techniques, the mixture fraction definition adopted for partially premixed methane/air flames is as described [21]

$$Z = \frac{\frac{Z_C}{\nu_C W_C} + \frac{Z_H}{\nu_H W_H} + \frac{2(Z_{O,2}-Z_O)}{\nu_O W_O}}{\frac{Z_{C,1}}{\nu_C W_C} + \frac{Z_{H,1}}{\nu_H W_H} - \frac{2Z_{O,1}}{\nu_O W_O} - \left(\frac{Z_{C,2}}{\nu_C W_C} + \frac{Z_{H,2}}{\nu_H W_H} - \frac{2Z_{O,2}}{\nu_O W_O}\right)} \tag{4.5a}$$

$$s = \frac{\nu_O W_O}{\nu_F W_F} \tag{4.5b}$$

where $Y_{F,1}$ is the fuel mass fraction at the fuel boundary and $Y_{O,2}$ is the oxidizer mass fraction at the oxidizer boundary and s is the mass stoichiometric coefficient. Further term Z_C, Z_H and Z_H can be defined as

$$Z_C = \sum_{k=1}^{N_s} a_{k,C}\Big(\frac{W_C}{W_k}\Big)Y_K, \quad Z_H = \sum_{k=1}^{N_s} a_{k,H}\Big(\frac{W_H}{W_k}\Big)Y_K, \quad Z_O = \sum_{k=1}^{N_s} a_{k,O}\Big(\frac{W_O}{W_k}\Big)Y_K$$

where $a_{k,p}$'s are the number of atoms of $p \in \{C, H, O\}$ in species k. The equivalence ratio of the mixture is defined as $\phi = s(Y_F/Y_O)$. Furthermore, the equivalence ratio of the premixed flame is conveniently expressed in terms of a mixture fraction Z using Eq. (4.5). The mixture fraction Z is defined to be unity in the pure fuel stream and zero in pure air stream.

4.3.3 Chemistry tabulation

The basis of chemistry tabulation technique has been mainly presented and defined in Chapter 3. It consists of relating all flame quantities (species mass fraction, temperature, source terms, etc.) to a set of parameters. In this chapter two look-up labels are used, a diffusion database build using diffusion flamelets (DF) and a database constructed using premixed flamelets (PM). In order to construct these databases, the set of 1D solutions are stored as function of (Y_c, Z) coordinates.

In the construction of the look-up table, the selection of Y_c needs careful attention. Y_c is usually defined as a linear combination of species mass fractions of the major species [22, 23]

$$Y_c = \sum_{k=1}^{N} a_k Y_k \tag{4.7}$$

where $a_k \in \mathbb{R}$ denotes a coefficient for the kth species and N number of species used in the progress-variable definition. The a_k values must ensure a unique representation of all flamelet solutions. For both databases CO_2, CO, H_2O and H_2 species are used in definition of progress variable with $a_k = 1$ such that

$$Y_c = Y_{CO_2} + Y_{CO} + Y_{H_2O} + Y_{H_2}. \tag{4.8}$$

As PM and DF databases consist of one-dimensional laminar flames, that are computed for a Z ranging from the lean $Z_L = 0.0$ to the rich $Z_R = 1$. However, for premixed databases, solutions range from a lean to a rich flammability limit. For example, for the combustion of pure methane with air, the lean flammability limit is $\phi = 0.4$, which corresponds to Z=0.022. The rich flammability limit for this case is $\phi = 2.4$, corresponding to Z=0.122. In other-words, premixed database is based on flames that lie $0.022 \leq Z \leq 0.122$. To complete the database, two further flamelet solutions are added: Z=0.0 and Z=1.0, which are extinct solutions. On other hand, the non-premixed naturally spans from Z=0.0 to Z=1.0. Both databases use 100 grid points for each parameter.

To utilize these databases during the CFD simulations, transport equations for Z and Y_c are solved together with continuity and momentum equations:

$$\frac{\partial \rho Y_c}{\partial t} + \frac{\partial}{\partial x_j}\left(\rho u_j Y_c\right) = \frac{\partial}{\partial x_j}\left(\rho D \frac{\partial Y_c}{\partial x_j}\right) + \dot{\omega}_c \tag{4.9a}$$

$$\frac{\partial \rho Z}{\partial t} + \frac{\partial}{\partial x_j}\left(\rho u_j Z\right) = \frac{\partial}{\partial x_j}\left(\rho D \frac{\partial Z}{\partial x_j}\right) + \dot{\omega}_c \tag{4.9b}$$

where $D = \frac{\lambda}{\rho c_p}$ and $\dot{\omega}_c$ are the progress-variable diffusivity and reaction rate, respectively. The latter terms are found in the look-up table in terms of Y_c and Z. The former equations implies the assumption of a unity Lewis number ($Le_k = 1$), as it is detailed in Chapter 3.

4.4 Numerical simulations

In order to analyse the behaviour of the flamelet databases or flamelet progress variable (FPV) solutions, numerical simulations of a 3-dimensional circular-coflow burner is performed. Its geometry is shown in Fig. 4.1. The case geometry corresponds to the one studied by Bennet et al. [2].

Inflow gases are a mixture of CH_4 and air. Fresh gases are at $T_0 = 300K$ and atmospheric pressure. Plug flow profiles are used for both inflow inlets using the velocity of Table 4.1. Two chemical mechanisms, namely Smooke [24] and GRI3.0 [25], are considered. The Smooke mechanism is a reduced chemical mechanism, which consists of 15 species and 46 reactions. GRI3.0 is detailed chemical mechanism and involves $N_s = 53$ species and 325 reactions.

Numerical computations are carried out using the general purpose unstructured and parallel object-oriented Computational Fluid Dynamics (CFD) code TermoFluids [26]. A finite-volume approach is used to solve the different transport equations. Temporal integration is performed using a 2nd order predictor-corrector scheme [27]. A symmetry-preserving scheme [28] is used to discretise the convective terms in the momentum equations. For the scalar equations, a upwind scheme is used. A second order central difference scheme is used to construct the discrete diffusive term for all transported quantities.

Mesh The computational domain is discretised using a cylindrical structured grid. Several zones with the different grid densities are defined to capture the flame front. The density of grid nodes is increased near to the inner tube exit where the flow of methane is higher. Away from it the density of mesh is gradually decreased. To ascertain that mesh independent results were obtained, simulations were run on the three meshes. The finest had three times the number of control volumes of the coarsest one. Specifically, it consists of 2.5×10^5 control volumes. Fig. 4.3 depicts the convergence of the temperature field as the mesh is refined. Note that the difference between the numerical and experimental results is due to the former not incorporating radiation effects. Tests correspond to a diffusion flame configuration. Simulations were run using a flamelet model with a diffusion database (DF). All further simulations have been run on the finest mesh.

4.4.1 Effect of the boundary conditions

In this section, two inflow boundary condition are considered for the scalar quantities of the fuel stream, namely Z and Y_c:

- Dirichlet $$\phi_{y=0} = \phi_B \tag{4.10a}$$
- Transport $$(\rho v\phi)_B = (\rho v\phi - \rho D\frac{\partial\phi}{\partial y})_{y=0} \tag{4.10b}$$

where 'B' denotes the value of the scalar upstream the fuel inlet and 'y=0' denotes the computational domain boundary. Three different combinations have been tested and results are presented in Fig. 4.4. BocoD results are associated with Dirichlet boundary conditions for both Y_c and Z. BocoC results are obtained considering Eq. (4.10) for Y_c and Eq. (4.10a) for Z. For BocoF results, the Eq. (4.10a) for Y_c and Eq. (4.10) for Z are used.

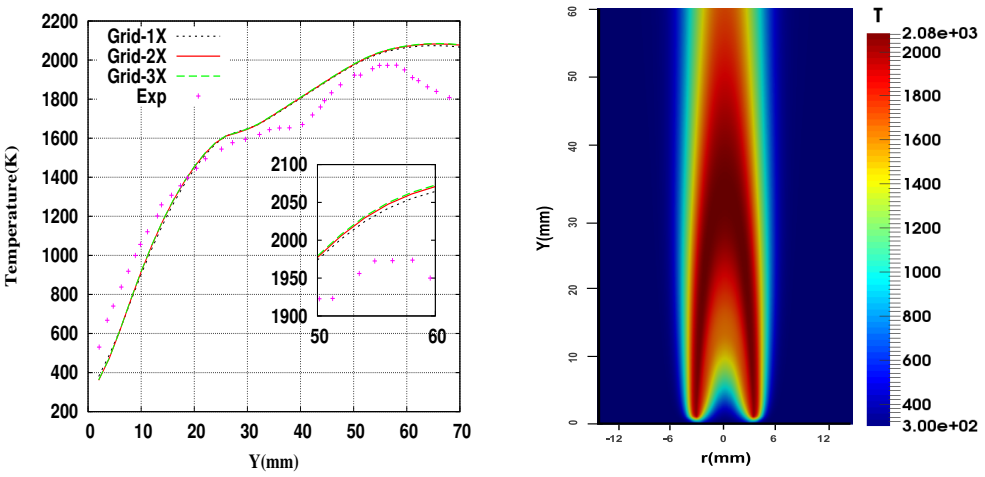

(a) (b)

Figure 4.3: Effect of grid refinement and Temperature color-levels. Simulations were performed at three grid refinement levels. In this figure, all results belong to NPMF case. Color-level figure is truncated.

Analysing the results in physical space two main aspects are of relevance:

- with 'BocoD' and 'BocoF' the flame is shifted downstream. The best match is achieved when using 'BocoC' set of boundary conditions. Note that radiation is not being considered. Hence, peak temperature value is over-predicted.
- Considering the O_2 profiles, near the inlet the profiles position is the same regardless of the boundary condition used. However, with 'BocoD' and 'BocoF' more O_2 has been consumed than with 'BocoC'. Downstream this results in 'BocoD' and 'BocoF' showing less agreement with the experimental data.

Then, if the profiles distributions are presented in non-dimensional space, where the peak temperature position is used as a reference, it can be seen that the profiles, in general, collapse to a single curve. Nonetheless, in physical space there are the reported differences. Hence, for the rest of the simulations the 'BocoC' set of boundary conditions are used.

4.4.2 Flame burning modes

Partially premixed flames can be regarded as a combination of premixed and non-premixed burning modes. Before proceeding to the simulation results, it is interesting to identify and visualize the burning regimes to support the results discussion. The

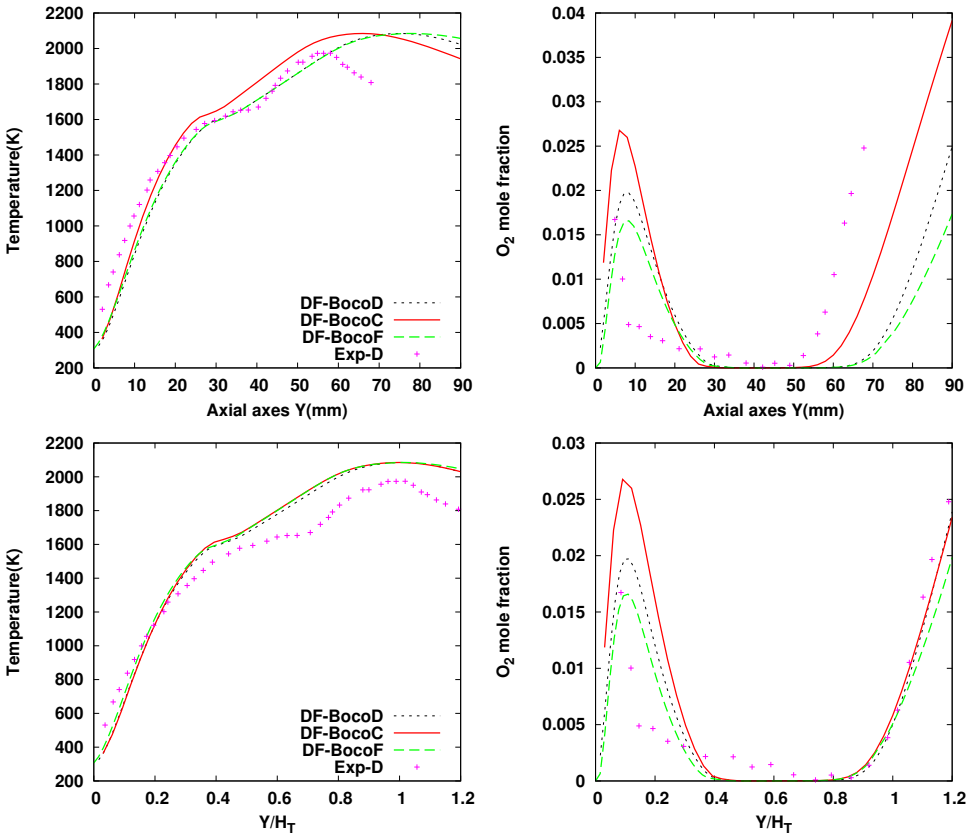

Figure 4.4: Solution dependencies on boundary conditions. Simulations were performed for NPMF case using a diffusion database (DF)

concept of the flame index was first introduced by Yamashita et al. [3] to analyse the jet diffusion flame stability. The burning index is determined by the alignment of fuel and oxidizer gradients. On the one hand, if both fuel and oxidizer come from the same stream, then burning mode is premixed. On the other hand, if the two of them enter the reaction zone from opposite sides, then it is non-premixed. This burning index can be calculated as follows

$$\alpha = \frac{\nabla Y_F . \nabla Y_O}{|\nabla Y_F . \nabla Y_O|}. \tag{4.11}$$

The value of flame index $\alpha = 1$ indicates a premixed burning mode and in the case of $\alpha = -1$ it represents the non-premixed. Fig. 4.5 shows the burning mode regions with different colours (red shows the premixed and blue represents non-premixed mode). These results are obtained by post-processing finite rate chemistry results. It can be seen that in case of NPMF, near the inlet the burning mode corresponds to diffusion, because of pure fuel intake. Oppositely, for the PPF3 case, a premixed mode is found near the inlet, as the oxidiser is also present in the fuel stream.

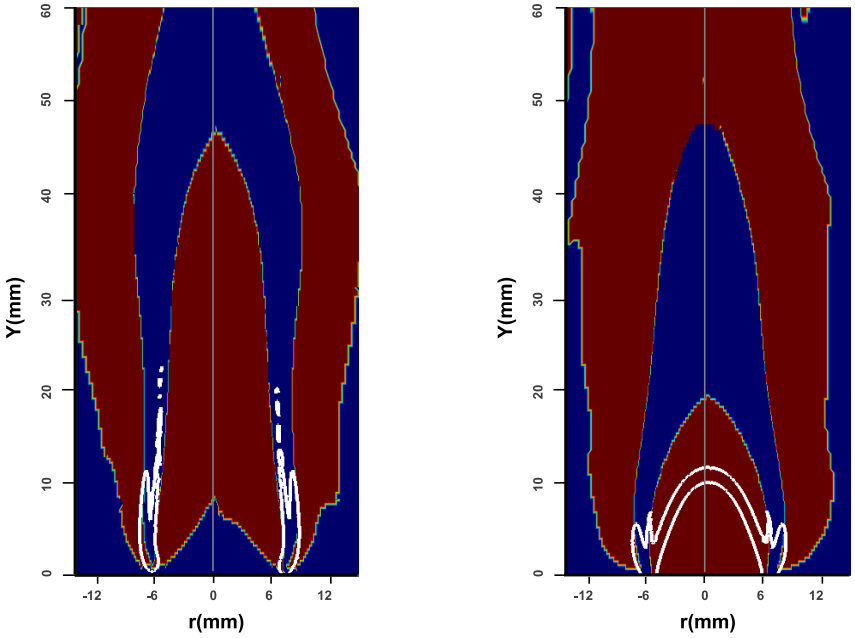

NPMF PPF3

Figure 4.5: Burning mode identification using finite rate chemistry simulation solutions. Red color represents the premixed mode and blue color shows non-premixed mode. Presented contour lines of heat release are taken at $5{\times}10^5$ $[\frac{W}{m^3}]$. Figures are truncated for best representation.

4.4.3 Flamelet modelling

Simulations results are classified into three cases, namely non-premixed flame (NPMF), partially premixed at ϕ=6.16 (PPF6) and partially premixed at ϕ=3.08 (PPF3). These cases are numerically studied using flamelet databases containing

flamelet solutions computed using the GRI3.0 chemical mechanism. Besides FPV solutions, finite rate (FR) chemistry simulations have also been performed using the Smooke chemical mechanism for all three cases.

Diffusion flamelet databases: full vs classical Fig. 4.6 depicts the comparison between diffusion database analysis of NPMF case. Two different simulations results are shown in Fig. 4.6. One is considering the classical approach (DF-C) and the other one using full set of diffusion flamelets. The diffusion flamelet database (DF) consists of three set of solutions which are represented in the S-shaped curve, see Fig. 4.2,: the ones which belong to the upper stable branch, the middle ones which correspond to the unstable branch and the bottom ones, corresponding to extinguished flamelets. Typically, considering only the stable branch solutions database is referred as the classical flamelet approach. Results are plotted in Fig. 4.6 in non-dimensional and dimensional space. Both approaches show the same trend as the experimental results. However, concerning the flame structure near the burner inlet, the full flamelet database solutions better capture the flame. Fig. 4.7 shows the flame is slightly uplifted from the base in case of experimental results. This similar behaviour can be seen in the FPV full database case. On the other hand the classical approach is not able to capture this intermediate states as the classical database only includes fully burning solutions. Still, the classical flamelet shows a significant agreement with the experimental data at the centerline and close to the fuel inlet, as can be seen in Fig. 4.6.

Concerning the partially premixed cases, the behaviour of both diffusion databases approaches is found to be similar. Temperature contour-levels are presented in Fig. 4.8 for the partially premixed case of $\phi = 3.08$. In the current study, the flame height is an important parameter for the comparison of numerically computed and experimentally measured results. Computed flame heights for all three cases are presented in Table 4.2. As the level of partial premixing is increased the smaller the amount of secondary oxygen that must diffuse inward to create a stoichiometric mixture and thus, the shorter the axial distance required for this necessary diffusion occurs [2]. In other words, it means that the flame height is reduced with increasing levels of the premixing. The computed results follow this trend as well.

Observing the results of the Table 4.2 it can be noticed that the classical flamelet consistently results in shorter flames than the full diffusion one. The reason for this is that the classical flamelet only includes fully burning flamelets, while the full database also contains flamelets at intermediate states.

Premixed and diffusion databases comparison In the following, numerical results obtained using the PM and DF databases are composed. Computed flame heights are presented in Table 4.3. It can be seen that flame heights in case of FPV modelling are quite better than the FR case. Specifically, FR solutions under-predict the flame

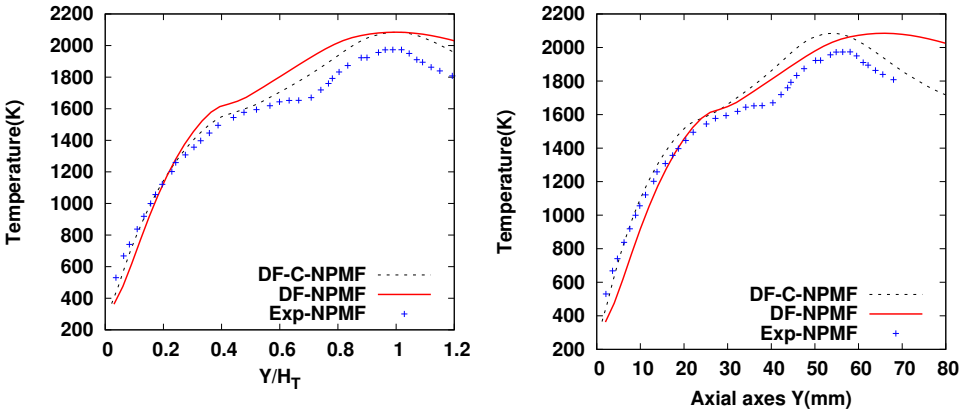

Figure 4.6: Temperature profile along axial axes (Y) of burner for NPMF. Left figure represents profiles as function of non-dimensional position ($\frac{Y}{H_T}$). Right figure shows in dimensional Y axes.

Table 4.2: Comparison of flame height using full and classical approaches

	$H_T(mm)$		
ϕ	Full	Classical	Exp.
∞	66	54	57
6.16	48	41	49
3.08	42	38	42

height for partially premixed flames. Comparing DF and PM results, it can be seen that PM database consistently results in shorter flame lengths.

Table 4.3: Comparison of flame height using FR, DF and PM approaches

	$H_T(mm)$			
ϕ	DF	PM	FR	Exp.
∞	66	56	60	57
6.16	48	44	42	49
3.08	42	40.8	32	42

Focusing on the comparison between modelling the cases using either a diffusion

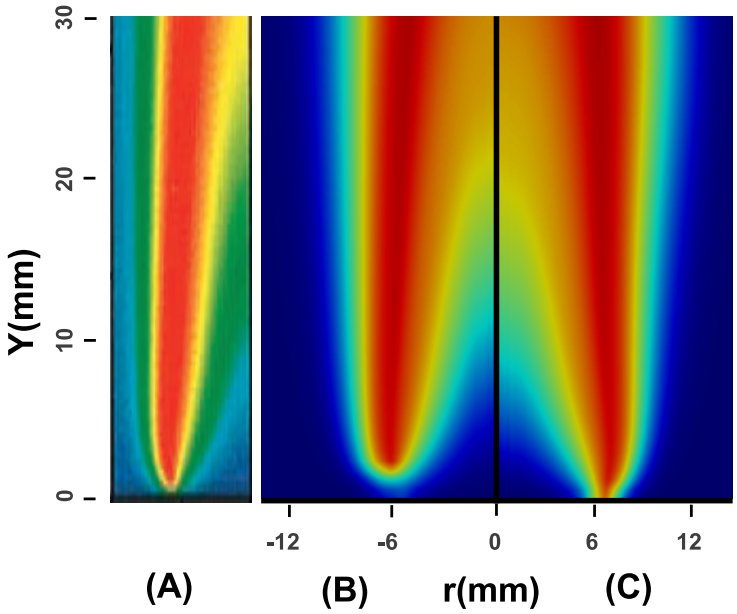

Figure 4.7: Contour-level representation of temperature for NPMF. Figure (A) shows reference solution [2], figure (B) belongs to full FPV and figure (C) associates with classical approach. Figures are truncated for best representation.

database or a premixed database, results along the axial axis for the three considered cases are presented in Fig. 4.9, Fig. 4.10 and Fig. 4.11, respectively. For a more detailed analysis of the flame structure, four major species CH_4, O_2, CO_2 and H_2O mole fraction profiles are presented. Concerning the FR solution, simulation results are overall in good agreement for all three cases. Still, differences can be observed when compared to the experimental results, which are attributed to the use of a reduced chemical mechanism. FR solutions as ϕ is decreased result in a poor agreement in the temperature profiles. FR main species are in general in good agreement, specially for CO_2. However, O_2 and H_2O show larger deviations.

Comparing the DF and PM results for the case of NPMF, as depicted in Fig. 4.9, it is observed that the DF results follow the same trends as the experimental results. However, the PM solution over-predict the temperature. Still, this does not come a surprise, as in this particular case, a non-premixed case is simulated using premixed flamelets. On the other hand, for partially premixed flames both DF and PM

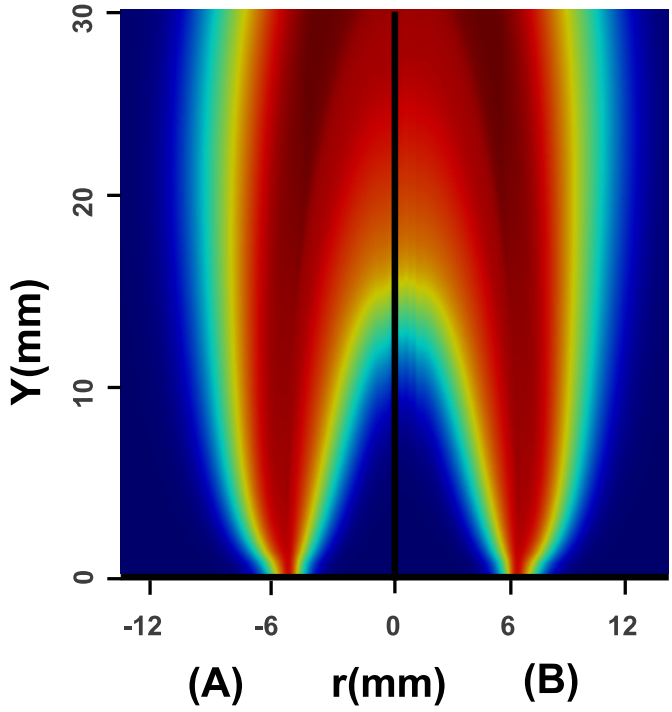

Figure 4.8: Contour-level representation of temperature for PPF3. Figure (A) belongs to full FPV and figure (B) associates with classical approach. Figures are truncated for best representation.

databases are fairly successful in reproducing the experimental results. Regarding the PM database as ϕ decreases, increase in premixing level, agreement with experimental data is increased. DF shows very good agreement for NPMF case. DF also shows good agreement for PPF6 and PPF3 regarding the temperature. However, species profiles show decreased agreement as ϕ decreases.

From the numerical analysis of the discussed flames, three main effects are observed. First, the maximum temperature of the flame is increased as increase in premixing. A similar trend is reported by other researchers [1, 2, 20]. It is observed that it is due to increasing strength of the inner flame front, leading to increased heat release near the axial axis. This behaviour is seen using both approaches as presented in Fig. 4.12.

Second, trend of partially premixed flame can be seen in the temperature profiles,

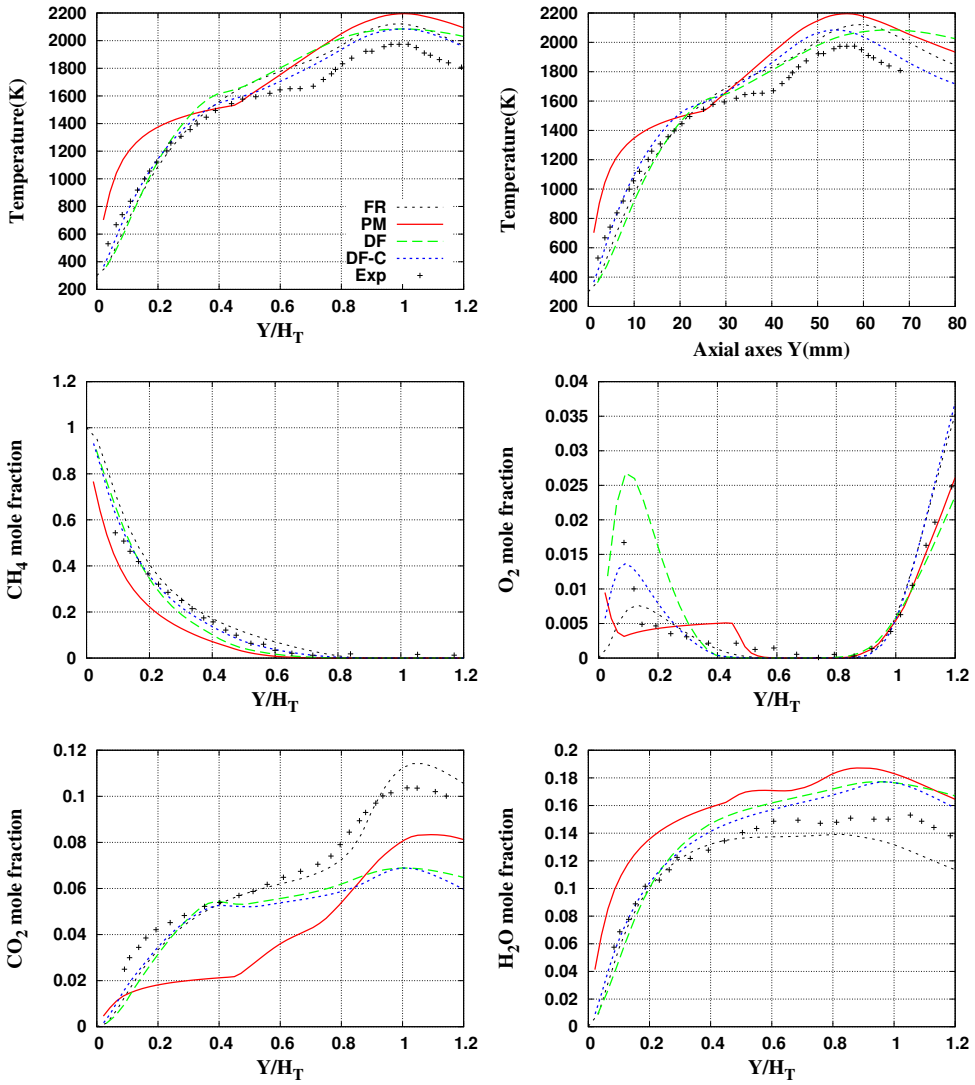

Figure 4.9: Temperature and mole fraction profile of CH_4, O_2, CO_2 and H_2O for NPMF. All profiles are presented as function of non-dimensional position ($\frac{Y}{H_T}$) except last one. Last right hand figure is presented temperature along Y axes.

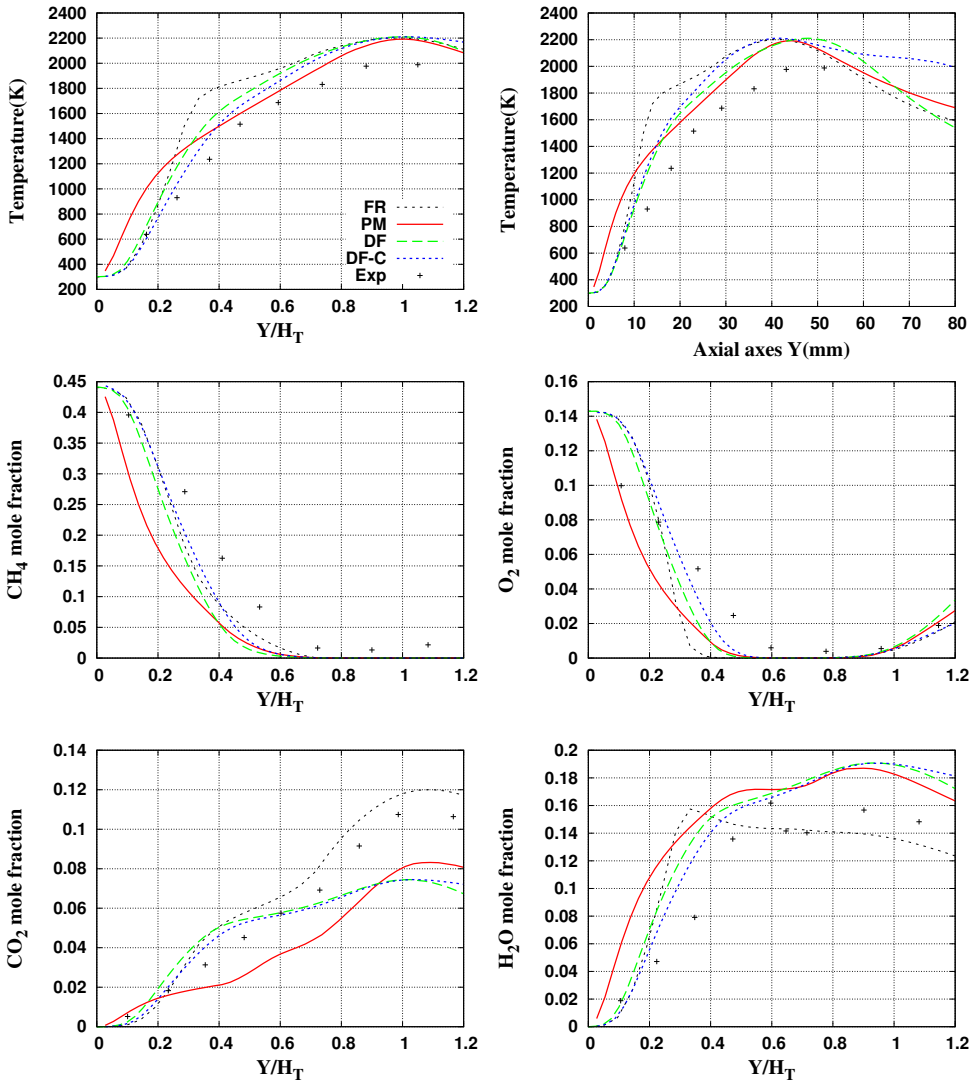

Figure 4.10: Temperature and mole fraction profile of CH_4, O_2, CO_2 and H_2O for PPF6. All profiles are presented as function of non-dimensional position ($\frac{Y}{H_T}$) except last one. Last right hand figure is presented temperature along Y axes.

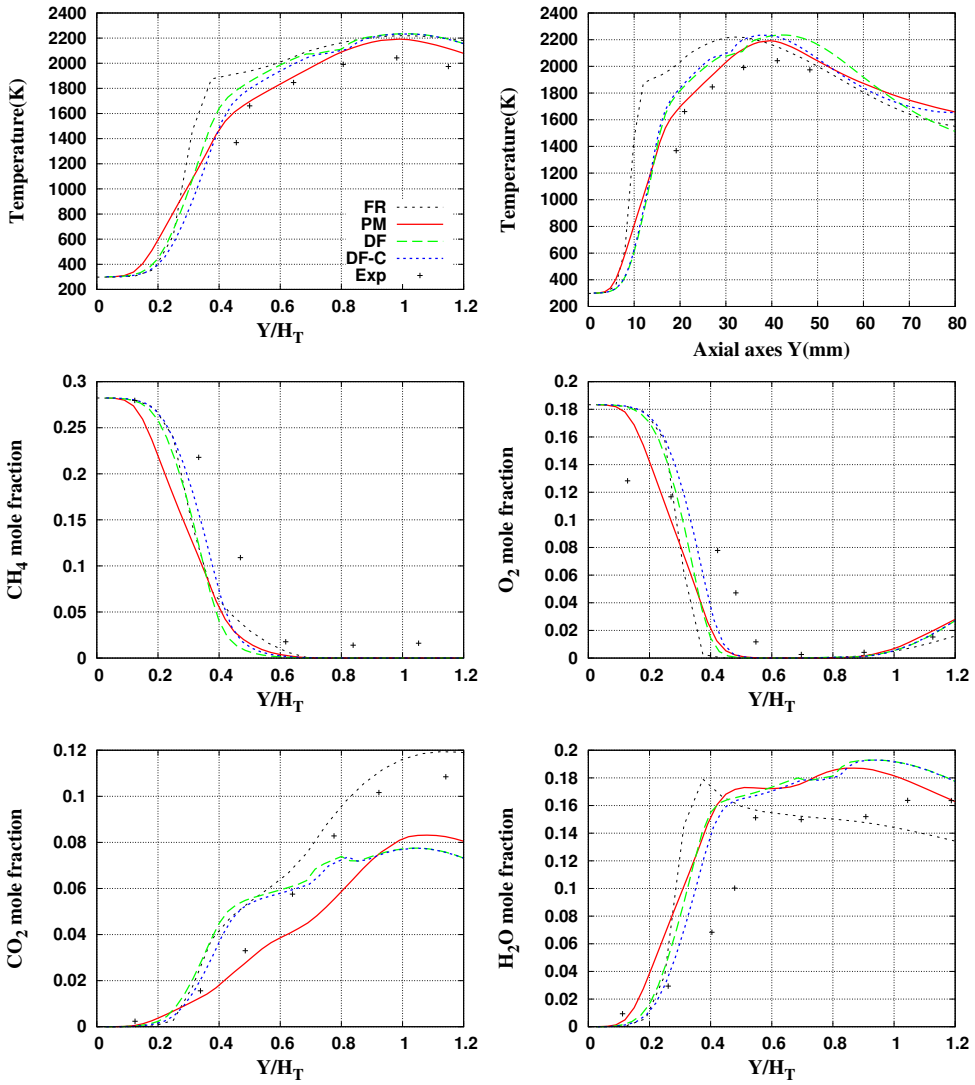

Figure 4.11: Temperature and mole fraction profile of CH_4, O_2, CO_2 and H_2O for PPF3. All profiles are presented as function of non-dimensional position ($\frac{Y}{H_T}$) except last one. Last right hand figure is presented temperature along Y axes.

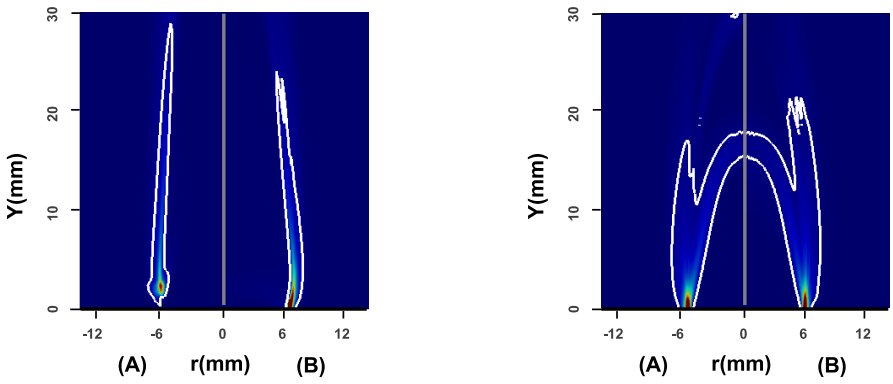

NPMF PPF3

Figure 4.12: Colour-level representation of reaction rate of progress variables. Minimum and maximum ranging (0-160)$[\frac{kg}{m^3.s}]$. Presented contour lines of reaction rate are taken at 2 $[\frac{kg}{m^3.s}]$. Figure (A) belongs to DF database and figure (B) associates with PM database. Figures are truncated for best representation.

which are presented in Fig. 4.13. There is a bump which appears due to the heat release in the inner flame front. This behaviour does not appear for NPMF. The strength of this bump in temperature is started when premixing increasing.

Third effect, at the region close to the fuel inlet, Y<15mm, the reduction in axial temperature is well predicted by the current simulations, and according to the experimental data shown in Fig. 4.13, except for the PM-NPMF one.

4.5 Conclusions

This study attempts to address a partially premixed flame in the context of flamelet modelling using single regime databases. A 3D jet coflow application has been studied. Finite rate chemistry and flamelet database approaches have been used for a partially premixed flame. Specifically, the work has been carried out to check capabilities of premixed and non-premixed flamelet databases methodologies as a single regime flamelet model.

On the basis of the current study, it shows the possibility to solve the multi-regime flames using single mode tabulated chemistry databases. Finite chemistry solution provides good estimations for diffusion flame. Lower agreement is found in the present simulations as the level of premixing is increased. This is attributed to

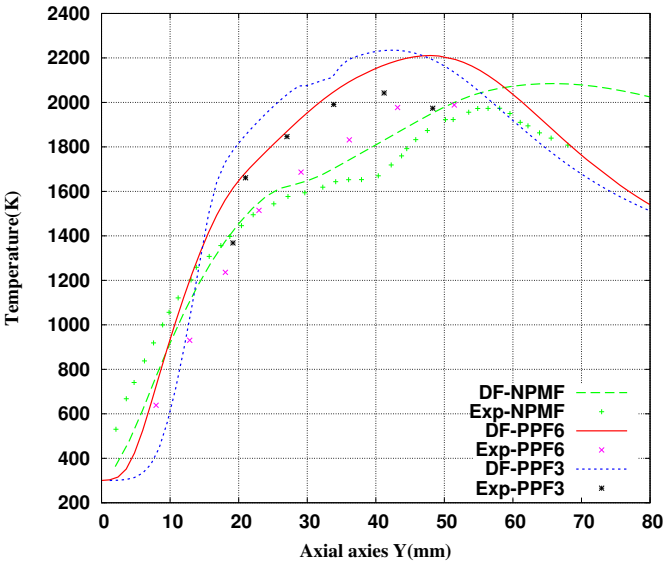

Figure 4.13: Temperature profile along axial axes.

the use of a reduced chemical mechanism. The use of detailed chemical scheme would be interesting for better estimation in case of partially premixed flames.

The classical diffusion database approach overall shows good agreement. However, it is not able to capture the characteristics of the flame base specially in the case of the full diffusion case. In the case of partially premixed flame, it provides good results. This approach can be used for the intermediate range of premixing.

Diffusion database resulted in good temperature as well as major species distributions when diffusion flame is studied. Premixed diffusion database performs well near high premixing region. Results also highlight the deviations between the experimental results when DF and PM databases are used near high premixing or low-level premixing limits, respectively.

As a final note, it has been shown the ability of single regime flamelets to solve partially premixed flames. Although they perform better in their corresponding mixing regions of applicability, they provide accurate-enough results away from them. Hence, diffusion databases are better suited for low-levels of premixing and premixed databases are better suited for higher ones.

References

[1] Q. V. Nguyen and R. W. Dibble. Raman-LIF measurements of temperature, major species, oh, and no in a methane-air bunsen flame. *Combustion and Flame*, 105:499–510, 1996.

[2] B. A. V. Bennett, C. S. McEnally, L. D. Pfefferle, and M. D. Smooke. Computational and experimental study of axisymmetric coflow partially premixed methane/air flames. *Combustion and Flame*, 123:522–546, 2000.

[3] H. Yamashita, M. Shimada, and T. Takeno. A numerical study on flame stability at the transition point of jet diffusion flames. *Proceedings of the Combustion Institute*, 26(1):27–34, 1996.

[4] Y. Mizobuchi, S. Tachibana, J. Shinjo, S. Ogawa, and T. Takeno. A numerical analysis on structure of turbulent hydrogen jet lifted flame. *Proceedings of the Combustion Institute*, 29:2009–15, 2002.

[5] K. J. Nogenmyr, J. Kiefer, Z. S. Li, X. S. Bai, and M. Aldén. Numerical computations and optical diagnostics of unsteady partially premixed methane/air flames. *Combustion and Flame*, 157:915–924, 2010.

[6] E. Mastorakos. Ignition of turbulent non-premixed flames. *Progress in Energy and Combustion Science*, 35:57–97, 2009.

[7] P. Domingo, L. Vervisch, and J. Reveillon. DNS analysis of partially premixed combustion in spray and gaseous turbulent flame-bases stabilized in hot air. *Combustion and Flame*, 140:172–195, 2005.

[8] A. R. Masri. Partial premixing and stratification in turbulent flames. *Proceedings of the Combustion Institute*, 35:1115–1136, 2015.

[9] N. Peters. *Turbulent Combustion*. Cambridge University Press, 2000.

[10] E. Knudsen and H. Pitsch. A general flamelet transformation useful for distinguishing between premixed and non-premixed modes of combustion. *Combustion and Flame*, 156(3):678–696, 2009.

[11] B. Fiorina, O. Gicquel, L. Vervisch, S. Carpentier, and N. Darabiha. Approximating the chemical structure of partially premixed and diffusion counterflow flames using FPI flamelet tabulation. *Combustion and Flame*, 140:147–160, 2005.

[12] H. Pitsch and H. Steiner. Large-eddy simulation of a turbulent piloted methane/air diffusion flame (Sandia flame D). *Physics of Fluids*, 12:2541–2554, 2000.

[13] C. D. Pierce and P Moin. Progress-variable approach for large-eddy simulation of non-premixed turbulent combustion. *Journal of Fluid Mechanics*, 504:73–97, 2004.

[14] V. Moureau, P. Minot, H. Pitsch, and C. Berat. A ghost-fluid method for large-eddy simulations of premixed combustion in complex geometries. *Journal of Computational Physics*, 221(2):600–614, 2007.

[15] J. A. Oijen van, R. J. M. Bastiaans, and L.P.H. Goey de. Low-dimensional manifolds in direct numerical simulations of premixed turbulent flames. *Proceedings of the Combustion Institute*, 31:1377–1384, 2007.

[16] K.-J Nogenmyr, C. Fureby, X. S. Bai, P. Petersson, R. Collin, and M. Linne. Large eddy simulation and laser diagnostic studies on a low swirl stratified premixed flame. *Combustion and Flame*, 155(3):357–368, 2008.

[17] K. Claramunt, R. Consul, C. D. Pérez-Segarra, and A. Oliva. Multidimensional mathematical modeling and numerical investigation of co-flow partially premixed methane/air laminar flames. *Combustion and Flame*, 137:444–457, 2004.

[18] R. Consul, C. D. Pérez-Segarra, K. Claramunt, and A. Oliva. Detailed numerical simulation of laminar flames by a parallel multiblock algorithm using loosely coupled computers. *Combustion Theoretical and Modelling*, 7(3):525–544, 2003.

[19] K. Claramunt, R. Consul, D. Carbonell, and C. D. Pérez-Segarra. Analysis of the laminar flamelet concept for nonpremixed laminar flames. *Combustion and Flame*, 145:845–862, 2006.

[20] A. Cuoci, Frassoldati, T. Faravelli, and E. Ranzi. laminarsmoke: numerical modeling of laminar reacting flows. In *http://www.opensmoke.polimi.it/*, 2013.

[21] J. Ventosa-Molina. *Numerical simulation of turbulent diffusion flames using flamelet models on unstructured meshes.* PhD thesis, Universitat Politécnica de Catalunya (UPC), Terrassa, Spain, 2015.

[22] B. Fiorina, R. Baron, O. Gicquel, D. Thevenin, S. Carpentier, and N. Darabiha. Modelling non-adiabatic partially premixed flames using flame-prolongation of ILDM. *Combustion Theory and Modelling*, 7:449–470, 2003.

[23] F. A. Lammers and L. P. H. de Goey. The influence of gas radiation on the temperature decrease above a burner with a flat porous inert surface. *Combustion and Flame*, 136(4):533–47, 2004.

[24] M. D. Smooke, I. K. Puri, and K. Seshadri. A comparison between numerical calculations and experimental measurements of the structure of a counter-flow diffusion flame burning diluted methane in diluted air. *Proceedings of the Combustion Institute*, 21(1):1783–1792, 1988.

[25] C. T. Bowman, M. Frenklach, G. Smith, W. C. Gardiner, and et al. http://www.me.berkeley.edu/gri-mech/releases.html.

[26] O. Lehmkuhl, C.D. Pérez Segarra, R. Borrell, M. Soria, and A. Oliva. Termofluids: A new parallel unstructured CFD code for the simulation of turbulent industrial problems on low cost PC cluster. *Proceedings of the Parallel CFD Conference*, pages 1–8, Antalya, Turkey, 2007.

[27] J. Ventosa-Molina, J. Chiva, O. Lehmkuhl, J. Muela, C. D. Pérez-Segarra, and A. Oliva. Numerical analysis of conservative unstructured discretisations for low mach flows. *International Journal for Numerical Methods in Fluids*, 2016.

[28] R. W. C. P. Verstappen and A. E. P. Veldman. Symmetry-preserving discretization of turbulent flow. *Journal of Computational Physics*, 187:343–368, 2003.

5

Conclusions

This thesis is a continuation of the research work carried out on combustion modelling during the last years at CTTC (heat and mass transfer technological center). At CTTC, our group already established the numerical platform for detailed chemistry simulation of laminar flames. These codes are being used for the design and analysis of industrial equipment systems and the understanding of and modelling of more complex flows. Furthermore, a framework for the alternative solutions of detailed chemistry solution, the flamelet model techniques, was also developed for diffusion flames. In the current study, has been developed a framework to provide the flamelet solution of premixed flames.

The thesis is organized in four chapters. In chapter 1, the mathematical fundamentals on reacting flows are posed. The formulations described all associated terms concerning reacting flows. The low-Mach Navier-Stokes equations are detailed along with the related detailed molecular fluxes formulations.

Chapter 2 addressed fundamental concepts of premixed flames, their structure, and numerical solution strategies. The main contribution of this thesis are described in Chapter 3 which is based on chapter 2. In this chapter, all work is related with the development of the numerical framework to solve one-dimensional laminar premixed flames. Two new ideas are implemented in numerical solution to solve the highly nonlinear stiff system of flamelet models: grid generation using a Gaussian function and the transformation of physical space into logical space. The numerical framework provides very good performance when using these two strategies. Results are excellently matched with experimental data as well as with existing numerical data of the scientific literature.

Chapter 3 accounts for one of the most relevant topics in flamelet solution techniques. In flamelet models, chemistry is precomputed and stored into a database. This chapter was based on the idea to include differential diffusion effects into flamelet models without increasing the computational cost. In this approach, chemistry is based on a database which associated with 1D flamelet solutions. To incorporate differential diffusion effect for flame solution require at least two flamelet equations which are associated with a database. In this context, many researchers proposed at least 2D

manifold (number of flamelet equations). In the current study, we introduce a new correction technique which provides a flame solution using only a 1D manifold. This technique is a new addition to flamelet solution techniques. 2D premixed adiabatic burner stabilized flame is studied with correction technique. Results of simulation are found in excellent agreement with the finite rate chemistry solutions, which evidence the worth of new technique.

Chapter 4 consist of the analysis of partially premixed flames. The study of partially premixed flames was conducted using the premixed and non-premixed databases. A 3D jet coflow case was studied. The main idea is to explore partially premixed flames using single mode flamelet databases. Besides the flamelet database solution, the partially premixed flame is also studied using classical flamelet database and finite rate chemistry approach. Three flames with different premixing equivalence ratios are studied. For finite chemistry solution the Smooke chemical scheme is used and for rest simulations Gri3.0. In this study, it is observed that the finite chemistry solution provide good agreements. However, it suffers disagreement for partially premixed flames. Differences are attributed to the use of a reduced chemical mechanism.

Regarding the premixed and non-premixed databases, it is observed that premixed database performs well near high mixing region, but lacks on lower premixing region. Particularly, in the case of diffusion flame, it is not able to capture the flame structure as well as temperature. On the other hand, the non-premixed database performs well for the diffusion case and lower mixing region but have discrepancies near high mixing region. Thus, it is concluded, as an option to solve partially premixed flame using single mode database, if the mixing is near to lower side then non-premixed flamelet database option is good otherwise on higher mixing side premixed one.

The main objective of the thesis is considered to have been achieved. Numerical infrastructure for premixed flame using the flamelet concept has been developed. Numerical experiences in the modelling of the flamelet technique have been acquired through the development of this thesis.

Future Work

As future work in laminar flame, and as a direct continuation of the research work presented in this thesis. Two main aspects are foreseen. First, a new proposed correction technique is based on databases which are consist of 1D unstretched flame solutions. Flame stretch and curvature effects play an important role in multi-dimensional flames, because they have a large influence on the mass burning rate. In next step, we will have to include the stretch effects into flamelet model to take into account multi-dimensional effects.

Second, as multi-regime flame is studied in this thesis using the single burning mode databases. In near future, we will address partially premixed flames using both

premixed and non-premixed databases by detecting the burning mode index.

6

Main publications in the context of this thesis

International Journal Papers:

- S. Ahmad, J. Ventosa-Molina, C. D. Pérez-Segarra, A. Oliva. 'A flamelet model based correction technique to integrate the differential diffusion effects by using one-dimensional manifold'. Submitted to Journal of Combustion and Flame, 2016.

International Conference Papers:

- S. Ahmad, J. Ventosa-Molina, C. D. Pérez-Segarra, A. Oliva. 'A progress-variable correction technique to integrate differential diffusion effects in flamelet model'. 8th European Combustion Meeting, Dubrovnik, Croatia, April, 2017.